
Masters Theses

Student Theses and Dissertations

Fall 2021

Multiple-site fatigue cracking methodology to assess structural integrity of aircraft riveted panels

Haroldo Chacon

Follow this and additional works at: https://scholarsmine.mst.edu/masters_theses



Part of the [Aerospace Engineering Commons](#)

Department:

Recommended Citation

Chacon, Haroldo, "Multiple-site fatigue cracking methodology to assess structural integrity of aircraft riveted panels" (2021). *Masters Theses*. 8012.

https://scholarsmine.mst.edu/masters_theses/8012

This thesis is brought to you by Scholars' Mine, a service of the Missouri S&T Library and Learning Resources. This work is protected by U. S. Copyright Law. Unauthorized use including reproduction for redistribution requires the permission of the copyright holder. For more information, please contact scholarsmine@mst.edu.

MULTIPLE-SITE FATIGUE CRACKING METHODOLOGY TO ASSESS
STRUCTURAL INTEGRITY OF AIRCRAFT RIVETED PANELS

by

HAROLDO CHACON

A THESIS

Presented to the Graduate Faculty of the
MISSOURI UNIVERSITY OF SCIENCE AND TECHNOLOGY

In Partial Fulfillment of the Requirements for the Degree
MASTER OF SCIENCE IN AEROSPACE ENGINEERING

2021

Approved by:

Dr. Lokeswarappa R. Dharani, Advisor
Dr. Brandon Chapman
Dr. K. Chandrashekhara

© 2021

Haroldo Chacon

All Rights Reserved

ABSTRACT

Multiple Site Damage (MSD) is the most common source of Widespread Fatigue Damage (WFD) affecting structural integrity of aging aircraft fleets. Therefore, an understanding of its progression, the development of methods to prevent the onset, and the maintenance procedures precluding WFD are important to improve aircraft fleet longevity. A reliable and efficient numerical methodology to perform detailed Multiple Site Damage assessment in riveted structural joints was developed. A probabilistic methodology was employed in conjunction with Monte Carlo simulation technique; the fatigue initiation life at every potential crack initiation site was determined and initial damage scenarios were generated. Probabilistic crack growth analyses were performed, thus accounting for multiple adjacent crack scenarios. Stress intensity factors for complex configurations were computed using compounding and superposition of classical and known solutions. The failure criterion employed was based on the first crack link-up where the plastic zone touch model was used. An automated tool to perform the MSD assessment was developed by using the Excel VBA code. The total time to crack initiation and total time to crack propagation obtained by numerical simulations agreed with the experimental results previously published. Statistical treatment was completed by using cumulative distribution function to establish maintenance action to preclude WFD. The results obtained from the MSD model were consistent with real aircraft maintenance intervals. The proposed methodology and the computer program developed were useful resources to predict MSD behavior and to establish maintenance actions to preclude its occurrence in real aircraft structures.

ACKNOWLEDGMENTS

I am especially grateful to my advisor, Dr. Lokeswarappa Dharani, for his support and supervision throughout this research. His knowledge profoundly inspired me during my master's degree journey, and his contributions left a significant academic impact on my life. Thank you to Dr. Brandon Chapman for providing significant contributions and constructive feedbacks, and Dr. K. Chandrashekhara who generously served as committee member. I acknowledge Dr. Abilio N. Garcia, who shared his PhD dissertation, which inspired me to study multiple-site damage. A special thanks to my mentor, Adrian Stanescu, for serving as my proctor, for all technical support, and professional opportunities. My sincere appreciation to the Boeing Company for generously funding my graduation degree and for all professional growth. A special acknowledge to Joe Cardinal and to the Southwest Research Institute for generously providing me NASGRO v9.2 which served as a baseline to validate part of the solutions applied in this work. Thanks to Andre Parsekian for all the support and fellowship. Thanks are due to Haroldo Costa who shared his experiences at the Missouri University of Science and Technology. I am eternally grateful to my parents, Maria A. Nere (in-memory) and Andre Chacon, in lovely memory of my grandparents, Eduardo Nere and Maria Aparecida, and my brother, Robson Chacon. Thanks for your guidance and support to complete my studies. I give special thanks to my wife, Rafaelle Schimith, and to my son, Jordan S. Chacon, for their love, for taking my dreams as part of their dreams, and for supporting me throughout all my endeavors. Finally, I thank God for all his kindness and blessings, and for providing me the required strength in times of difficulty and for all the opportunities I have been given.

TABLE OF CONTENTS

	Page
ABSTRACT.....	iii
ACKNOWLEDGMENTS	iv
LIST OF ILLUSTRATIONS.....	vii
LIST OF TABLES.....	x
NOMENCLATURE	xi
 SECTION	
1. INTRODUCTION.....	1
1.1. MULTIPLE-SITE CRACKING AND ITS CONTEXT AS RESEARCH TOPIC	1
1.2. RESEARCH PROJECT DESCRIPTION.....	4
1.3. THESIS OBJECTIVE.....	5
1.3.1. Academic Need	6
1.3.2. Industry Need.	7
2. LITERATURE REVIEW.....	8
2.1. HISTORICAL OVERVIEW OF MULTIPLE-SITE FATIGUE DAMAGE.....	8
2.2. EVOLUTION OF CERTIFICATION REQUIREMENTS	13
2.3. AGING AIRCRAFT REQUIREMENTS.....	19
2.4. REVIEW OF PREVIOUS PUBLISHED MSD METHODOLOGIES	22
2.4.1. Fatigue Initiation Life.....	23
2.4.2. Crack Propagation Life..	28
2.4.3. Failure Criterion	29

2.4.4. Summary of Published MSD Methodologies.....	30
2.5. THEORETICAL BACKGROUND.....	31
2.5.1. Stress-Life (S-N) Approach.....	31
2.5.2. Linear Elastic Fracture Mechanics.....	37
2.5.3. Fatigue Crack Growth.....	37
3. METHODOLOGY FOR ASSESSING STRUCTURAL INTEGRITY OF AIRCRAFT RIVETED PANELS IN THE PRESENCE OF MULTIPLE-SITE FATIGUE CRACKING.....	39
3.1.1. Fatigue Crack Initiation Life.....	39
3.1.2. Fatigue Crack Propagation Life.....	44
3.1.3. Failure Criterion.....	66
4. RESULTS AND DISCUSSIONS.....	69
5. CONCLUSIONS AND FUTURE WORK.....	96
5.1. CONCLUSIONS.....	96
5.2. RECOMMENDATIONS FOR FUTURE WORK.....	97
BIBLIOGRAPHY.....	100
VITA.....	106

LIST OF ILLUSTRATIONS

	Page
Figure 1-1 B737-200 N73711 Aloha Airlines Fuselage Damage Detail [2].	1
Figure 1-2 Effect of MSD on Residual Strength Capability [4].	2
Figure 1-3 B737-300 N632SW Southwest Airlines Fuselage Damage [5].	3
Figure 1-4 Detail of Fuselage Skin Damage on N632SW [5].	3
Figure 2-1 B737-200 N73711 Aloha Airlines Fuselage Damage Detail [18].	8
Figure 2-2 Aloha Airlines B737-200 Lap Joint Construction Detail [2].	11
Figure 2-3 Knife Edge Effect Found in Aloha Airlines Riveted Lap Joint [1].	11
Figure 2-4 Design Recommendation to Avoid Knife Edge Effect [19].	12
Figure 2-5 Difference between MSD and MED [3].	12
Figure 2-6 Manufacturing Flaw – Wing Pivot Fitting of a Crashed F-111[2].	14
Figure 2-7 Horizontal Stabilizer Spar Chord Fracture Surface [21].	16
Figure 2-8 Residual Strength in the Presence of MSD and Monitoring Period [3].	20
Figure 2-9 S-N Curve and Best Fit for Steel AISI 1090.	33
Figure 2-10 Constant Amplitude Loading [45].	34
Figure 2-11 Scatter Factor of the S-N Curve [49].	36
Figure 2-12 Typical Crack Growth Curve [48].	38
Figure 3-1 Critical Rivet Row and ‘Potential Crack Initiation Sites [54].	40
Figure 3-2 Numerically Generated Random Numbers – Gaussian distribution.	41
Figure 3-3 Fatigue Initiation Life Calculation Process.	43
Figure 3-4 Randomized Fatigue Life [6].	43

Figure 3-5 Lead and Opposite Crack Sizes.....	45
Figure 3-6 MSD Model Initial Crack Sizes.	46
Figure 3-7 Corner Crack at a Hole [59].....	48
Figure 3-8 Two Unsymmetrical Cracks Emanating from a Hole.	50
Figure 3-9 Concentrated Loads at Crack Plane [62].....	52
Figure 3-10 Two-Unequal Cracks – Income/By-Pass Stresses and Pin Load.	53
Figure 3-11 Two-Unequal Cracks - Remote Stress and Pin Load.....	53
Figure 3-12 NASSIF Solution TC23 Input Data.	54
Figure 3-13 NASSIF Solution TC23 Output Data.....	54
Figure 3-14 Comparison of Stress Intensity Factors.....	55
Figure 3-15 Cracks near a Circular Hole, Remote Stress Tip A [65].....	57
Figure 3-16 Cracks near a Circular Hole, Remote Stress Tip B [65].	58
Figure 3-17 Two Unequal Cracks Subjected to Remote Stress.....	59
Figure 3-18 SIF for Two Unequal Cracks Subjected to Remote Stress Tip A [65].	61
Figure 3-19 SIF for Two Unequal Cracks Subjected to Remote Stress Tip B [65].....	62
Figure 3-20 SIF for Two Unequal Cracks Subjected to Remote Stress Tip C [65].....	62
Figure 3-21 SIF for Two Unequal Cracks Subjected to Remote Stress Tip D [65].	63
Figure 3-22 Plastic Zone Touch or Link-Up Model Suggested by Swift [4].	67
Figure 3-23 Example of Lead Crack Propagation after Link-Up [16].....	68
Figure 4-1 Analyzed Lap Joint.	69
Figure 4-2 2024-T3 Mean Life ($\log N_f$) for Fatigue Crack Initiation.....	70
Figure 4-3 2024-T3 Standard Deviation ($\log N_f$) for Crack Initiation.....	71
Figure 4-4 Local Stresses as a Function of PCIS [6].....	72

Figure 4-5 7,200 Pairs of Random Numbers Generated for the MSD Model.....	74
Figure 4-6 Mean Fatigue Life (TTCI) Convergence Check – 400 MCS.....	76
Figure 4-7 Mean Fatigue Life (TTCI) – 400 MCS for a Local Stress of 396 MPa.....	77
Figure 4-8 Standard Deviation (TTCI) Convergence Check – 400 MCS.....	77
Figure 4-9 Distribution of Total Lives Compared with Fatigue Test Data.....	78
Figure 4-10 Fatigue Life (TTCI+TTCP) Convergence Check – 400 MCS.....	80
Figure 4-11 Experimental Results – Crack Propagation Test – Lap Joint #2 [26].....	82
Figure 4-12 Crack Growth Analysis Compared to Experimental Data.....	83
Figure 4-13 Widespread Fatigue Damage (WFD) – Cumulative Density Function.....	84
Figure 4-14 Distribution of Total Lives Compared with Fatigue Test Data.....	88
Figure 4-15 Fatigue Life (TTCI+TTCP) Convergence Check – 400 MCS.....	88
Figure 4-16 Crack Growth Analysis Compared to Experimental Data.....	90
Figure 4-17 Distribution of Total Lives – 400 MCS.....	91
Figure 4-18 Fatigue Life (TTCI+TTCP) Convergence Check – 400 MCS.....	92
Figure 4-19 Distribution of Total Lives – 600 MCS.....	92
Figure 4-20 Fatigue Life (TTCI+TTCP) Convergence Check – 600 MCS.....	93
Figure 4-21 Distribution of Total Lives – 800 MCS.....	93
Figure 4-22 Fatigue Life (TTCI+TTCP) Convergence Check –800 MCS.....	94

LIST OF TABLES

	Page
Table 3-1 Initial Flaw Sizes – Definitions of USAF MIL-A-83444 [2].	44
Table 4-1 MSD Model Input Data.	73
Table 4-2 Example of Damage Scenarios Generated via MSD Model.	75
Table 4-3 Experimental Fatigue Test Data Presented by Garcia [6].	79
Table 4-4 Initial Crack Length - Lap Joint Specimen #2 [26].	81
Table 4-5 Limit of Validity (LOV) for Airbus Models [68].	85
Table 4-6 Limit of Validity (LOV) of 4 Different Manufacturers [68].	86
Table 4-7 MSD Model Input Data – 400 MCS 120 MPa.	87
Table 4-8 MSD Model Input Data 400 MCS 122 MPa.	91
Table 4-9 Influence of Number of MC Simulation on WFD Parameters.	95

NOMENCLATURE

Symbol	Description
A	S-N curve material constant
a	Crack half-length
a	S-N standard deviation constant
a	Corner crack length - thickness direction
AAWG	Airworthiness Assurance Working Group
AC	Avsitory Circular
ARAC	Aviation Rulemaking Advisory Committee
ASIP	Aircraft Structural Integrity Program
a'	Equivalent crack length
a ₁	Lead crack length
a ₂	Opposite crack length
a _{MSD}	MSD crack length
A _{net}	Net section area
a/t	Back face correction factor
α	Randon number
B	Basquin coefficient
b	S-N standard deviation constant
b	Eccentricity associated with fastener load application point
b	Distance from crack tip of size a ₂ to central crack a ₁
BOAC	British Overseas Airways

C	Crack growth constant (Paris equation)
c	S-N standard deviation constant
c	Corner crack length - width direction
CAR	Civil Air Regulations
CFR	Code of Federal Regulation
CTOA	Crack Tip Opening Angle
CTOD	Crack Tip Opening Displacement
D	Fastener diameter
D	Cumulative Damage - Miner's Rule
dA	Difference in crack area
da/dN	Crack growth rate
DAH	Design Approval Holder
DBEM	Dual Boundary Element Method
Di	Cumulative damage associated with i^{th} PCIS
dII	Difference in potential energy
E	Modulus of Elasticity
EIFS	Equivalent Initial Flaw Size
ESDU	Engineering Science Data Unit
FAA	Federal Aviation Administration
FAR	Federal Aviation Regulation
f_b	Bowie correction factor
FCIL	Fatigue Crack Initiation Life
FCGL	Fatigue Crack Growth Life

FCPL	Fatigue Crack Propagation Life
FCS	Fatigue Critical Structure
FCAS	Fatigue Critical Alternation Structure
FEA	Finite Element Analysis
FEAM	Finite Element Alternating Method
FEM	Finite Element Method
F_{int}	Interacting factor between two unequal cracks
f_w	Finite width correction factor
FQI	Fatigue Quality Index
FSFT	Full Scale Fatigue Test
$f_{(x)}$	Gaussian distribution probability density function
G	Crack driving force
GFEA	Global Finite Element Analysis
GDP	Gross Domestic Product
h	Integration interval
ICA	Instruction for Continued Airworthiness
ISP	Inspection Start Point
I_{WFD}	Recurring inspection dedicated to WFD
K	Stress intensity factor
K_{eff}	Effective stress intensity factor
K_c	Fracture toughness
K_r	Resultant compounded stress intensity factor
K_0	Stress intensity factor emanating from a hole

K_0'	Stress intensity for an equivalent crack in the absence of all boundaries
LEFM	Linear Elastic Fracture Mechanics
LOV	Limit of Validity
m	Crack growth curve slope (Paris constant)
MCS	Monte Carlo Simulation
M_e	Boundary correction factor
MED	Multiple Element Damage
MRO	Maintenance Repair and Overhaul
MSD	Multiple Site Damage
M_1	Front face correction factor
NASA	National Aeronautics and Space Administration
NDI	Non Destructive Inspection
N_f	Number of cycles to nucleate a crack
NTSB	National Transport Safety Board
N_0	Number of cycles required to growth a crack of length a_0
OEM	Original Equipament Manufactures
P	Fastener load
p	S-N curve exponent
POD	Probability of Detection
PCIS	Potential Crack Initiation Site
PZT	Plastic Zone Touch
Q	Constant which accounts for a/c ratio
R	Stress ratio

RFL	Randomized Fatigue Life
r_p	Plastic zone in front of crack tip
S	Applied stress
SIF	Stress Intensity Factor
S_{lim}	Fatigue endurance limit
SMAAC	Structural Maintenance for Aging Aircraft Program
SMP	Structural Modification Point
S-N	Stress-Life Method
STC	Supplemental Type Certificate
S_0	Remote tensile stress
S_3	Bearing stress
t	Thickness
TCP	Time to Crack Propagation
TTCI	Total Time to Crack Initiation
TTCP	Total Time to Crack Propagation
USAF	United States Air Force
VBA	Visual Basic for Applications
VCCT	Virtual Crack Closure Technique
y_1, y_2	Transformed random numbers
W	Panel width
WFD	Widespread Fatigue Damage
$WFD_{(avg)}$	WFD average behavior
Z	Westergaard stress function

1. INTRODUCTION

1.1. MULTIPLE-SITE CRACKING AND ITS CONTEXT AS RESEARCH TOPIC

Multiple Site Damage (MSD) was recognized as a threat to structural integrity and airworthiness of aging aircraft because of the near-catastrophic accident involving an aged B737-200, registry N73711, Aloha Airlines flight 243 from Hilo to Honolulu on April 28th, 1988 (Figure 1-1). The aircraft suffered a sudden decompression event at 24,000 feet (Flight Level 240) due to unstable fuselage failure attributed to the growth and link-up of collinear cracks that nucleated at a lap joint adjacent rivet holes, as concluded in [1].



Figure 1-1 B737-200 N73711 Aloha Airlines Fuselage Damage Detail [2].

MSD is a source of Widespread Fatigue Damage (WFD) and is characterized by the simultaneous presence of fatigue cracks within the same structural elements [3]. This type of damage can rapidly decrease the residual strength below the certification levels compared to a single lead crack case, as shown in Figure 1-2 according to Swift [4].

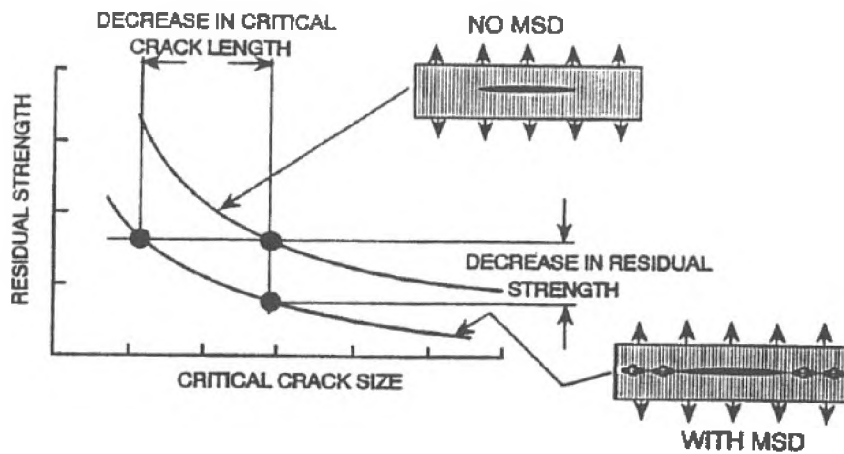


Figure 1-2 Effect of MSD on Residual Strength Capability [4].

On April 1st, 2011, a B737-300 operating Southwest flight 812 experienced rapid decompression in-flight due to fuselage failure [5]. A portion of the fuselage crown skin flapped during the flight and crack propagation was arrested on adjacent frames. The crew was able to manage an emergency descent, and they safely landed the aircraft without significant injuries (Figure 1-3 and Figure 1-4).



Figure 1-3 B737-300 N632SW Southwest Airlines Fuselage Damage [5].

NTSB determined that the probable cause of this incident was the incorrect installation of the upper skin fuselage lap joint during production, thus leading to multiple-site fatigue cracking in service [5]. The crack propagation was contained by fuselage frames that functioned as crack arresters.

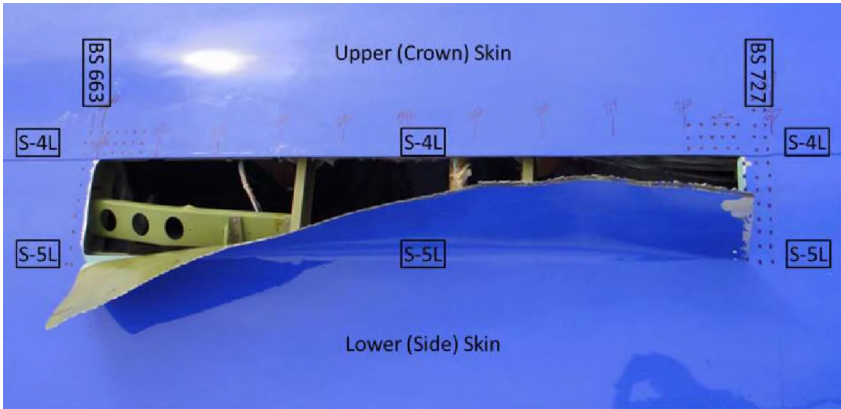


Figure 1-4 Detail of Fuselage Skin Damage on N632SW [5].

More than 20 years after the Aloha Airlines flight 123 accident and Southwest Airlines flight 812, the research performed emphasized the importance of the MSD assessment in the context of aircraft structural integrity. The need to understand, predict its average behavior, and prevent its onset was important, with special emphasis on the design of future aircraft structures and safe operation of existing aging aircraft fleets.

1.2. RESEARCH PROJECT DESCRIPTION

To investigate the MSD problem in aeronautical riveted panels, a probabilistic model to assess it was presented and discussed in this research. Due to the stochastic characteristic of fatigue crack nucleation and propagation lives, 400 simulations were required to accurately predict the onset of MSD. The Monte Carlo simulation technique was employed to predict both crack initiations and propagation lives.

An extensive literature review was carried out concerning how to predict and preclude the MSD onset as well as, how to determine the maintenance actions required to avoid WFD failure. This can be summarized by the determination of Inspection Start Point (ISP) and Structural Modification Point (SMP). Researchers' methodologies were presented and discussed from the past 30 years; their contributions to practical engineering standpoint, as well as, limitations were synthesized within the scope of this thesis. The previous researchers formed the theoretical background for supporting this work.

The proposed methodology encompassed three distinct phases:

- Crack initiation life (probabilistic fatigue approach).
- Crack growth life: considering multiple collinear cracks scenarios.
- Failure criterion: crack link-up.

Based on numerical results (crack initiation + crack propagation lives), cumulative probability function was used to determine maintenance actions required to prevent WFD, herein defined as ISP, SMP, and recurring inspection intervals $I_{(WFD)}$.

Results obtained via numerical simulation were compared to fatigue experimental data from previously published literature.

1.3. THESIS OBJECTIVE

Considering Multiple-Site Fatigue Damage phenomena's close relationship to aircraft safety and continued airworthiness, to accurately and efficiently predicting the onset of the MSD and assessing its subsequent crack propagation phase that accounts for multiple collinear crack interactions play a fundamental role in aging aircraft operations.

Although researchers have addressed the topic of WFD over the past three decades [4, 6-14], they applied complex and time consuming computational tools such as J-Integral, VCCT, CTOD, and CTOA via Finite Element Analysis (FEA), or Dual Boundary Element techniques to compute complex stress intensity factors solutions. When applying such techniques in association with Monte Carlo simulation, which is usually required to account for the stochastic nature of fatigue crack initiation phenomena, the methodology becomes cumbersome, if not impossible, due to the high number of simulations to accurately predict fatigue life scatter behavior.

This work is intended to develop a relatively simple, reliable, and easy to implement numerical methodology to assess the MSD problem in riveted aeronautical structures by applying probabilistic fatigue method and classical fracture mechanics solutions. Simulation results, both crack initiation and crack propagation phases, were statistically

treated by using cumulative probability function to establish maintenance actions required, precluding WFD.

The objectives of this research encompassed academic interest and industry need, as described in the following sections:

1.3.1. Academic Need. The MSD problem was a focal point for many researchers, but most of the proposed methodologies came from the aerospace industry, as presented in [15]; therefore, the solutions were not available for public use. Based on an initial bibliographic review, limited research was performed addressing the topic of MSD and none of them at Missouri University of Science and Technology.

Federal agencies, such as NASA [12, 13] and FAA [16], have conducted valuable research in this field; however, most of them used complex numerical methods, such as CTOD via FEA, to compute stress intensity factor solutions for complex geometries, like adjacent collinear cracks on stiffened panels, thus making its implementation considerably involved and costly from a computational standpoint.

This study was intended to benefit students and researchers by offering accessible material and results to implement new methodologies, to perform trade studies, and to investigate the MSD phenomena. This study offered improvements for calculating MSD average behavior and its parameters (ISP, SMP and Inspection Interval), thus contributing to the safe operation of aging aircraft. A detailed comparison between results obtained using the proposed MSD methodology and fatigue experimental data published in the literature, with the aim to verify methodology accuracy compared to experimental results and propose future improvements is presented. Topics to be investigated in future academic research were presented and discussed in the final section of this thesis.

1.3.2. Industry Need. Civil aeronautical regulations require aircraft manufactures to conduct Full Scale Fatigue Tests (FSFT) to demonstrate the aircraft structure will be free from WFD up to the Limit of Validity (LOV), according to [17]. However, when an airplane enters into service, the structure is susceptible to cracks due to corrosion, to fatigue due to variable amplitude load application inherent to its normal operation, and to accidental damage due to airport service handling. Therefore, structural repairs are made on original Primary Structural Elements (PSE). Structural repairs can effect original Fatigue Critical Structures (FCS) or create Fatigue Critical Alternation Structure (FCAS). Regulatory authorities also require WFD assessment to be performed for repair and alterations on WFD susceptible structures. The list of WFD susceptible structures was presented and discussed in Section 2. It was concluded that performing fatigue tests for each repair made on an aircraft structure was impractical due to associated costs and elapsed time; therefore, it is important to find a reliable method to accurately predict the MSD behavior of such structures by defining appropriate, cost efficient, and supplemental inspections.

The primary objective of this research was to present a relatively simple methodology implementation, compared to tools such as FEA, to accurately and efficiently predict MSD onset and its subsequent crack propagation. The proposed methodology might be used by general aeronautical industry, including Maintenance Repair and Overhaul (MROs), Supplemental Type Certificate (STC) holders to determine maintenance actions that preclude WFD due to MSD phenomena.

2. LITERATURE REVIEW

2.1. HISTORICAL OVERVIEW OF MULTIPLE-SITE FATIGUE DAMAGE

Multiple-site fatigue damage (MSD) became a worldwide concern and got the attention of the aerospace industry, aviation regulatory agencies, researchers, and academic institutes on April 28th, 1988, when an Aloha Airlines aged B737-200 operating Flight 243 from Hilo to Honolulu, Hawaii suffered a sudden decompression event at 24,000 feet due to major fuselage failure. The flight crew successfully managed the situation by performing an emergency descent (Figure 2-1) and safely landed at Kahului Airport on Maui. One flight attendant perished during this incident, as described in [1].



Figure 2-1 B737-200 N73711 Aloha Airlines Fuselage Damage Detail [18].

The aircraft with tail number N73711 was built in 1969, as line number 152, and had nearly 90,000 flight cycles (second highest number of cycles across B737 worldwide

fleet) at the time of the incident, as described in the National Transport Safety Board (NTSB) report [1]. Aloha Airlines operated short Hawaiian Islands routes that exposed its airplanes to an aggressive corrosive environment, and the plane accumulated cycles at a faster rate than other 737 operators. After a detailed aircraft accident investigation was conducted by the NTSB, it was concluded that the contributing factors to the incident were associated with multiple fatigue cracks initiated at a fuselage lap joint and the inability of Aloha Airlines, maintenance program to detect disbonding and fatigue cracking before reaching critical crack length [1].

Typical modern aircraft fuselage construction (semi-monocoque) is made of skins, stringers and frames [19]. Skin panels are joined in the longitudinal direction using lap joint construction, which is characterized by overlapping upper and lower panels, typically using three rows of fasteners. On early B737 line numbers (1 through 291), the fuselage lap joints were cold bonded using an epoxy impregnated woven cloth. In addition to that, the joints were mechanically fastened using three rows of countersink rivets (see Figure 2-2). The cold-bonding manufacturing process was originally intended to provide better structural efficiency compared to classic mechanically fastened joints. The fuselage hoop load was transferred through the combination of bonded joint and rivets, instead of fasteners only, allowing the use of relatively thin skin panels (0.036 inches), thereby reducing the overall weight and cost. However, early production history using cold-bonded lap joints revealed difficulties associated with skin panel cleaning processes, as described in [1,2]; expected quality thin surface oxide for a bonding layer was not achieved. The bond quality was degraded when condensation was not properly removed from the cloth before assembling. These production difficulties led to non-uniform bonds with

environmental durability below the desired level; this increased susceptibility to corrosion and caused areas of the lap joint not to bond. During the normal operation of the aircraft, moisture is expected, especially in the Aloha Airlines environment. Moisture can enter into the joint through areas of disbond and corrosion can occur. The combination of moisture and corrosion could also contribute to further disbonding of the lap joints. These conditions yielded a bonded joint with a hoop load that was not transferred through the bond layer, but through three rows of countersink rivets. The cold-bond construction optimized the skin panel thickness to 0.036 inches, and the countersink depth went through the entire sheet, creating a knife edge condition (see Figure 2-3), thereby, fatigue life of the structure was decreased. According to Niu [19], the skin thickness must be equal to or greater than 1.5 times the countersink depth in critical fatigue areas to avoid knife edge effects (see Figure 2-4).

The service difficulty report described random cracking at fuselage lap joints of the B-737s that occurred as the aircraft accumulated flight cycles, and it was associated with the joint bond process and operational environment [1]. Similar structural details (fastener holes) operating under same stress level in the presence of high stress concentration factor due to countersunk rivets with knife edge effect and the environmental aspects contributed to collinear cracks nucleation and link-up. This situation caused a major lead crack that rapidly grew to the point where the structure no longer withstood operational flight loads; this resulted in unstable crack growth and the departure of approximately 18 feet of forward fuselage (Section 43) during flight. This phenomena became known as widespread fatigue damage (WFD).

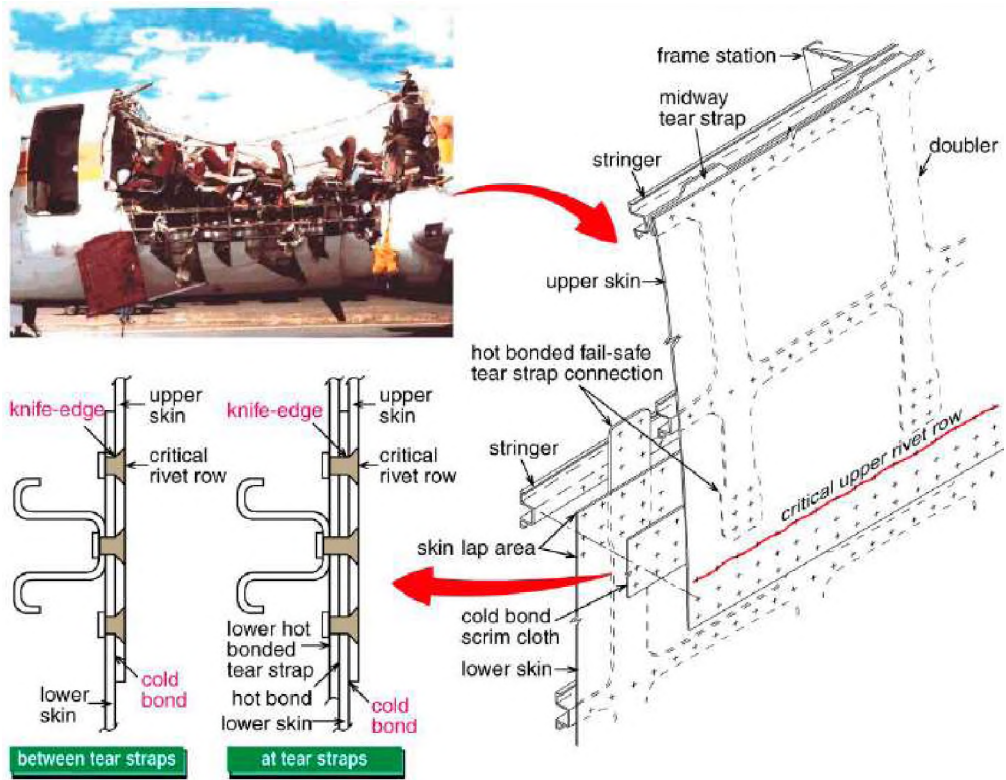


Figure 2-2 Aloha Airlines B737-200 Lap Joint Construction Detail [2].

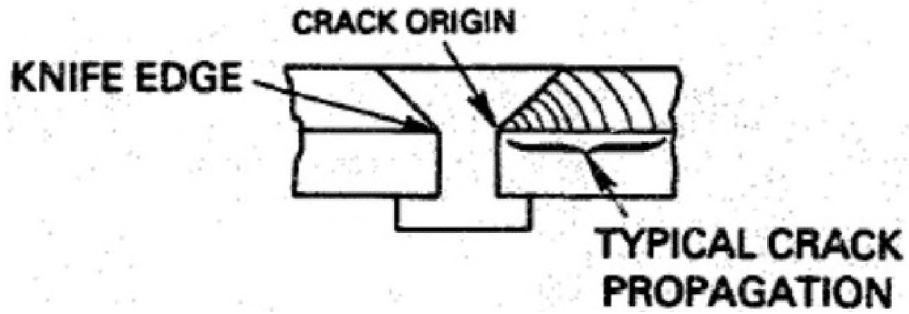


Figure 2-3 Knife Edge Effect Found in Aloha Airlines Riveted Lap Joint [1].

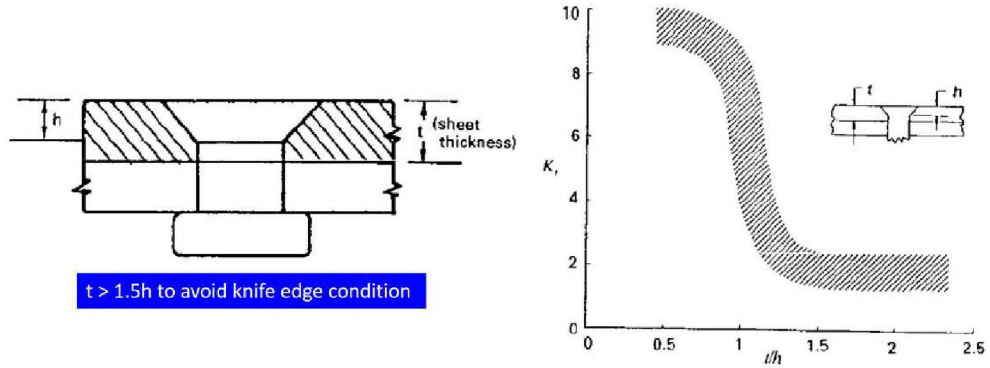


Figure 2-4 Design Recommendation to Avoid Knife Edge Effect [19].

Widespread fatigue damage (WFD) is characterized by simultaneous presence of fatigue cracks at multiple locations that are of sufficient density and size such that the structure no longer provides adequate residual strength, as defined in [3].

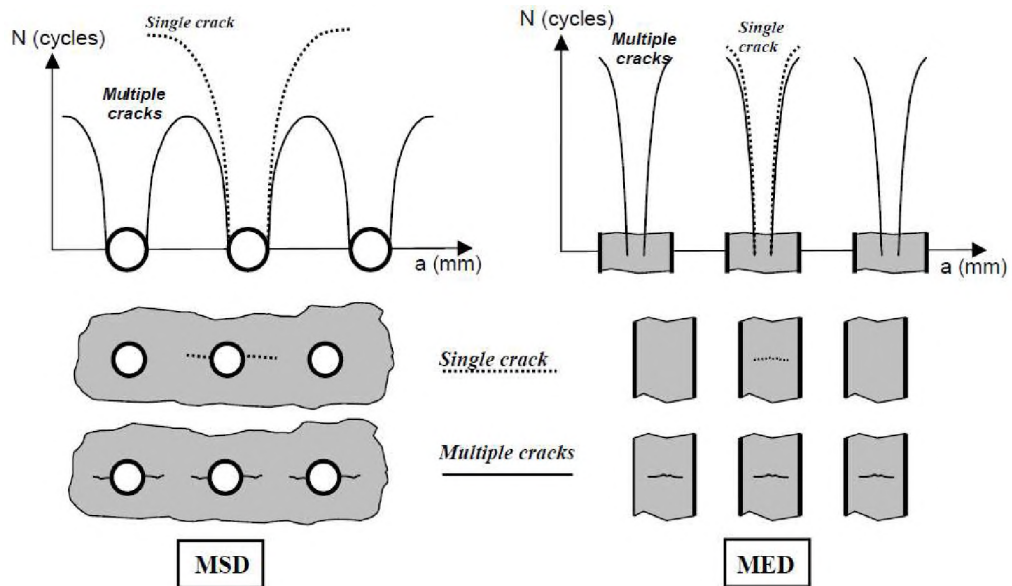


Figure 2-5 Difference between MSD and MED [3].

Sources of WFD are described by multiple-side damage (MSD), which consists of multiple cracks that nucleates from multiple adjacent structural details operating under same stress level and similar fatigue qualities interacting with each other, in addition to multiple element damage (MED), characterized by similar structural elements operating under the same stress levels, according to [3]. The difference between MSD and MED is illustrated in Figure 2-5.

2.2. EVOLUTION OF CERTIFICATION REQUIREMENTS

This section presented the chronologic sequence and evolution of fatigue and damage tolerance requirements for the past 60 years. These airworthiness standards were applied to the development and certification of transport category airplanes, aimed to prevent catastrophic failure from fatigue cracking, corrosion, and accidental damage.

Airworthiness standards evolved mostly due to the lessons learned from aircraft accident investigations, service experiences, industry and certifying agencies, research on fatigue and crack growth, and advances in non-destruction inspection (NDI) methods, and the development of new materials associated with better design construction and manufacturing processes.

The first notable modification regarding fatigue and damage tolerance certification requirements occurred in 1956, with the update of the Civil Air Regulations (CAR) 4b.270; this revision introduced the concept of fail-safe design as an option for the safe-life requirement, as described in [3]. Before 1956, commercial airplanes were designed and certified based on safe-life approaches [3].

In a fail-safe design approach, the structure is required to withstand design limit load conditions assuming a complete failure scenario of the primary structural member. The design arrangement requires multiple load paths and redundant structures intended to carry the redistributed load from the failed primary element [3]. The inspection requirements were based in the detection of a broken element, also called obvious damage.

The safety level introduced by adopting the fail-safe approach was closely related to the lessons learned from the well-known De-Havilland Comet I aircraft accidents.

British Overseas Airways Corporation (BOAC) registrations, G-ALYP, and G-ALYY were lost in 1954 due to fuselage structure catastrophic failures associated with fatigue cracks that nucleated at stress concentration points and propagated before being found and repaired, as described by Wanhill and Molent [2].

Although redundant structural elements provide an extra layer of safety to the design of aircraft structures, the fail-safe philosophy proved to be inadequate to provide the required safety level when an F-111 fighter jet with just 107 flight hours suffered a catastrophic accident on December 22, 1969 [2].

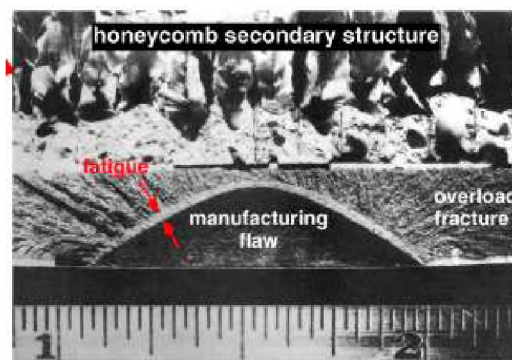


Figure 2-6 Manufacturing Flaw – Wing Pivot Fitting of a Crashed F-111[2].

The accident was attributed to an initial flaw from the manufacturing process of the wing pivot-fitting, as shown in Figure 2-6, and associated with the inability to detect the crack before reaching its critical length.

This accident motivated the United States Air Force (USAF) to develop the damage tolerance methodology, and the MIL-A-83444 standard was introduced in July 1974 [20]. The damage tolerance approach essentially involves the application of Linear Elastic Fracture Mechanics (LEFM) concepts and crack growth analysis to establish aircraft maintenance plans.

The milestone USAF achieved demonstrated the need to review transport category airworthiness standard requirements. It was clear that only focusing on fatigue life assessment and fail-safe design approaches did not provide the highest level of safety. The need to review and leverage the airworthiness standard levels became more obvious when the fatal accident involving model B707-300 Dan Air registration G-BEBP that happened in May 1977 near Lusaka Airport.

The evidences from the investigation demonstrated that fatigue cracking was associated with unanticipated local high stresses and loads acting on the horizontal stabilizer which were generated by the speed brake deployment after landing, according to Wanhill and Molent [2].

The accident investigation board concluded the accident was caused by loss of pitch control following the separation of the horizontal stabilizer and elevators, resulting from fatigue and improper failsafe design of the rear spar [21] as shown in Figure 2-7.



Figure 2-7 Horizontal Stabilizer Spar Chord Fracture Surface [21].

The Lusaka event got the attention of the Federal Aviation Administration (FAA), and they urgently adopted damage tolerance approaches; as a response, FAR 25.571 Amendment 25.45 titled “Damage Tolerance and Fatigue Evaluation of Structure” was released in 1978. The primary objective of the damage tolerance assessment was to provide an inspection program for each Principal Structural Element (PSE) by defining inspection thresholds and repetitive intervals, such as cracking due to fatigue, corrosion, or accidental

damage, thus insuring they do not propagate to critical size prior to being detected and repaired as discussed by Swift [22].

After the Flight 243 event, it was clear that there was a weak link in the airworthiness system, yet classical damage tolerance approaches were used to determine residual strength capabilities and to establish inspection thresholds and repetitive intervals via single crack growth scenario assessments. The traditional damage tolerance methodology was not adequate to provide the required safety level in areas susceptible to widespread fatigue damage. The need to address the effect of MSD and MED in such areas where these phenomena were expected to occur was evident, with special emphasis on the aircraft structure design phase to establish adequate inspection intervals, as required by current damage tolerance requirements and to support maintenance plans that are part of Instructions for Continued Airworthiness (ICA).

Based on new findings, the Aviation Rulemaking Advisory Committee (ARAC) proposed that an independent group be formed to address the need for specific regulations and maintenance tasks to preclude widespread fatigue damage in commercial aviation fleets [15].

As a result of this recommendation, an organization named Airworthiness Assurance Task Force, today known as Airworthiness Assurance Working Group (AAWG), was formed in June of 1988 by aircraft manufactures, operators, and regulatory agencies across the United States and Europe [15]. In 1993, the AAWG released its first report with recommendations and conclusions from preliminary research work, most notably all commercial jet transport aircraft models certified pre-amendment 45 had some sources of WFD. The AAWG report [15] released in 1999 contained recommended actions

for aircraft manufactures and operators to preclude MSD onset in aircraft structures as following:

- Develop and release guidance material (Advice Circular) and review/create regulatory requirements to preclude WFD in the fleet.
- Review structural areas susceptible to WFD.
- Establish WFD average behavior (point in time when 50% of entire fleet is expected to develop WFD due to MSD/MED).
- Calculate parameters to preclude WFD, Inspection Starting Point (SMP) and Structural Modification Point (SMP).
- Implement (if required) maintenance actions to preclude WFD.
- Perform additional research programs to better understand residual strength of aircraft structures in the presence of MSD/MED.

In 2010, the Federal Aviation Administration (FAA) created the Aging Airplane Program: Widespread Fatigue Damage Final Rule. This was the last and most significant change to structural requirements. In November 2010, the FAA released Amendment 25-132, revising 14CFR 25.751 [17] and adding 26.21 [23].

Along all recommended actions to reduce the probability of WFD occurrence, a list of candidate structures prone to develop this type of damage was published in the advisory material in 2011. The WFD susceptible structures list was the starting point to perform WFD in real aircraft structures. A unique list must be developed for a particular aircraft type certificate, based on service experience, teardown inspection history, or structural details and elements rationale that repeated over larges areas, which presented similar fatigue qualities, operating under the same stress levels [3].

2.3. AGING AIRCRAFT REQUIREMENTS

The new regulation from the Aging Airplane Program requires aircraft Design Approval Holders (DAH) to establish the Limit of Validity (LOV) of the engineering data that supports structural maintenance programs. Limit of Validity represents the maximum number of flight cycles, flight hours, or both to demonstrate that an airplane is free from widespread fatigue damage. To support the establishment of LOV, thereby showing compliance, DAH must prepare substantiating data for presentation to the regulatory agency. Data is composed of test evidence and analyses at minimum, if it is available, the survey from service experience and teardown inspection results from aged aircraft, should be included, demonstrating that WFD is unlikely to occur up to LOV [3].

As described in the Advisory Circular (AC) 120-104-1C published in January 2011, the establishment of LOV included the following tasks: Definition of candidate LOV, preparation of WFD susceptible structures list, performance of the WFD assessment for susceptible structures, and completion of the LOV. No aircraft may to operate beyond the LOV, except when additional substantiating data is presented demonstrating that WFD will not occur up to the claimed extended LOV [3].

The contents of this thesis were related to the task of performing WFD assessments of susceptible structures, yielding detailed explanations concerning this important task.

The following are the definitions of technical terminology applied to the study of WFD, according to AC 120-104 [3]:

Widespread Fatigue Damage (WFD): characterized by the simultaneous presence of fatigue cracks at multiple structural locations that are of sufficient size and density for the structure to no longer meet the residual strength requirements.

Multiple Site Damage (MSD): source of widespread fatigue damage characterized by the simultaneous presence of fatigue cracks in the same structural elements.

WFD (average behavior): the point in time when, without intervention, 50% of the entire fleet is expected to develop WFD for a particular structure according to Figure 2-8.

Inspection Start Point (ISP): the point in time when supplemental inspections of a fleet are initiated to preclude WFD, due to a specific probability of having a MSD/MED condition.

Structural Modification Point (SMP): the point in time when a structural component must be modified to preclude WFD.

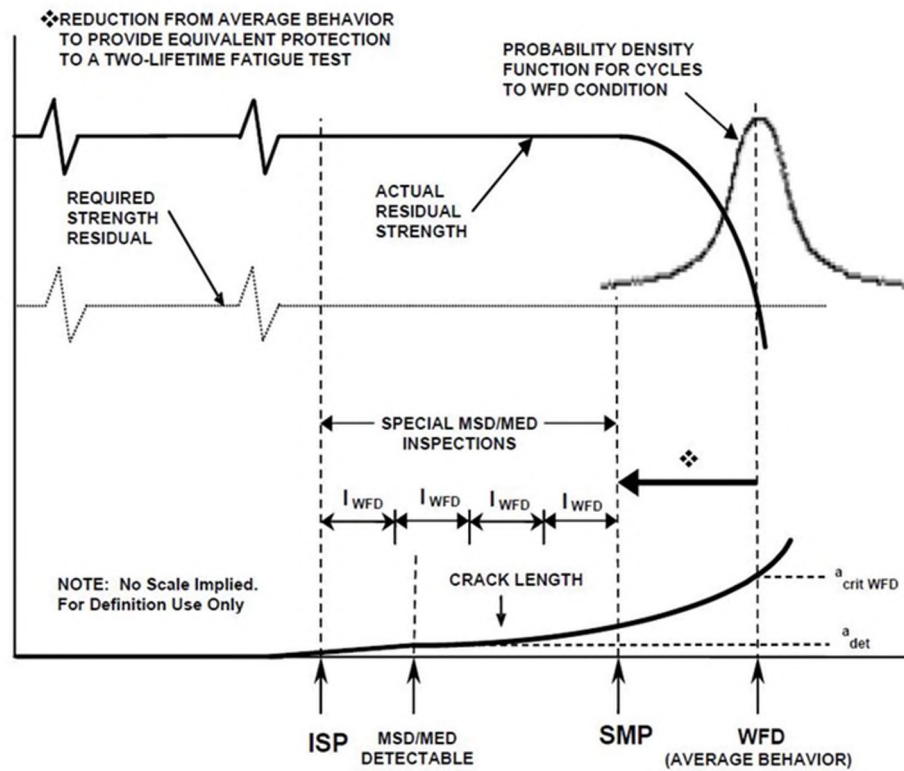


Figure 2-8 Residual Strength in the Presence of MSD and Monitoring Period [3].

Aircraft structures are susceptible to fatigue damage, which is characterized by the gradual degradation of a material susceptible to the application of cyclic loads. This degradation, or loss of strength, is a by-product of operational environment and material allowable, and can be statistically quantified at the end of the process; that is typically defined at the point in time when a particular structure susceptible to WFD is no longer able to withstand required residual strength loads, or simply static limit load condition [8].

There is always a possibility WFD can occur due to the numerous associated aspects no matter how small the probability is. Therefore, the most effective and practical way to mitigate its occurrence is by modifying or replacing susceptible structures at pre-determined and analytically derived times [4, 6]. For the purpose of a WFD assessment, this time is defined as SMP. Figure 2-8 schematically presents how maintenance actions and monitoring periods precluding WFD are established [3]. The determination of ISP, SMP, and I_{WFD} , herein defined as repetitive inspection interval, are the main reasons for the development of MSD assessment methodologies, as discussed by Garcia [6].

As shown in Figure 2-8, the inspection window or monitoring period starts at the point of MSD crack nucleation, also called ISP, and extends up to where 50% of the entire fleet is expected to experience WFD providing no action is taken. This point is also called $WFD_{(avg)}$. The repetitive inspection interval (I_{WFD}) is determined by employing safety factors during the monitoring period and providing opportunities to detect a MSD crack [3]. The methodology presented in Section 3 described the numerical procedures and steps followed to determine $WFD_{(avg)}$, ISP, and SMP.

2.4. REVIEW OF PREVIOUS PUBLISHED MSD METHODOLOGIES

Schijve [8, 24] and Swift [4, 7 and 25] provided significant contributions to this field; Swift brought attention to the importance of MSD in 1987 [7], even before the Aloha Airlines accident. Swift alerted the industry to the fact that traditional residual strength analysis considering a single lead crack may be inadequate in the presence of a MSD scenario, where small cracks can be initiated at both sides of each hole in a row of fasteners. He also pointed out that MSD cannot be ignored due to its catastrophic consequences [7]. Swift discussed topics that are challenging, even 34 years later, such as the difficulty of inspecting small cracks buried under rivet heads, using NDI techniques, and economical aspects associated with small intervals of inspections to establish maintenance plan for MSD. Schijve discussed how a small MSD crack can reduce the load for unstable crack extension, the importance of including crack arrest features while designing aircraft structures, and the difficulty to obtain relevant stress intensity factors [8]. He significantly contributed to the study of fatigue in riveted lap joints and stress intensity factor (SIF) determination.

Both Swift and Schijve agreed that MSD represents major threats to airworthiness of ageing aircraft, as reported by [9, 26]. Another point of agreement in the structures community is that MSD assessment should be performed using a probabilistic approach, with special emphasis on the application of Monte Carlo simulation (MCS) to account for the stochastic behaviors of fatigue crack initiation phenomena [6, 27, 28 and 29].

For the past twenty years, the USAF used probabilistic risk assessment methodology to determine the onset of WFD, as discussed by Lincoln [30]. The onset of WFD cracking was established as the point in time when damage tolerance or fail-safe

capability of the structure was degraded to a point where the probability of failure was reduced below a pre-established threshold. The assessment was performed by determining the probability distributions of crack length at a reference time, which was based on the results of a teardown inspection; the cumulative probability distribution of stress, using stress exceedance method; the probability of crack growth; and finally, the probability of detection (POD), according to [30].

Based on an extensive review of MSD assessment, it was concluded that there were three distinguished phases: fatigue crack nucleation, crack propagation, and failure criterion [6, 9, 31 and 32]. The following sections discussed published methodologies and the assumptions used to perform the MSD assessment based on the three phases.

2.4.1. Fatigue Initiation Life. Regarding the fatigue crack initiation phase, the Monte Carlo simulation technique was broadly employed [6, 9, 11, 27, 28, and 33-35] to calculate fatigue initiation life at fastener holes, and to generate large numbers of MSD scenarios to execute the subsequent phase, crack propagation assuming collinear cracks scenarios.

The initial stage consisted of sorting random numbers for each Potential Crack Initiation Site (PCIS) at basically 2 per fastener at 90° and 270° positions. The next step was to assume a statistical distribution based on fatigue test results to calculate the fatigue initiation life for each PCIS. From all studied works, lognormal distribution [6, 9, 28, 33, and 35] and Weibull distribution were predominantly used.

When a random number assuming zero mean and standard deviation equal to one $\{0,1\}$, is randomly placed in each PCIS [6, 28] and when calculating the fatigue life for a pre-defined number of fasteners, one unique damage scenario is created by running the

Monte Carlo simulation. Typically, a high number of Monte Carlo simulations (> 200), should be performed to achieve convergence for the fatigue initiation life. Convergence is typically checked by comparing the mean fatigue life for crack initiation, and its associated standard deviation, obtained via experimental data, against numerical results using the MCS [6].

Garcia and Irwin [9], found good correlation by performing 400 simulations, while Liao used 10,000 MCS in [35]. They used lognormal distribution to calculate fatigue initiation life, where they used values from previous work done by Santgerma [10], assuming $\log(\mu) = 5.637$, where μ is the mean fatigue initiation life, and $\log(\sigma) = 0.20$, where σ is the standard deviation associated with μ . Numerical results enclosed both fatigue crack initiation and propagation phases compared to 6 points from experimental work.

Bradfield and Garcia [33] discussed previously published work including fatigue lives of aeronautical riveted joints ranged between 40,000 to 200,000 cycles, $\log(\mu)$ from 4.6 to 5.3 and $\log(\sigma)$ from 0.01 to 0.24. Mean life and standard deviation values agreed with the numbers found by Santgerma.

Akpan [36] applied fuzzy and probabilistic random variables to characterize the MSD problem. Mean life (μ) and standard deviation (σ) results were compared considering Gumbel, Normal, Lognormal, and Weibull's distributions.

Another point of discussion, observed in the work of previous authors, was the number of fasteners considered during the Monte Carlo simulation, [9] used 9 fastener holes, [27] used 8 fasteners, and Kebir [28] used 14 holes.

An initial crack size of 1.5 mm was assumed by Garcia and Irving [9] for each randomly selected PCIS, and continuous damage assumption, proposed by Gallagher, Giessler and Berens [37], was assumed after link-up by setting a crack of 0.127 mm on the opposite hole.

The Equivalent Initial Flaw Size (EIFS) technique was employed to perform the Monte Carlo simulation [31, 27, and 35]. The concept was to generate equivalent initial crack sizes for placement in each nucleation site based on a known distributions of cracks, usually from teardown inspections of retired aircraft.

Bradfield and Garcia employed the Monte Carlo simulation in a more general sense to establish fatigue life of structural repairs. They suggested the application of a probabilistic model, rather than traditional deterministic approach, which applied pre-defined scatter factors [33].

Wang [26] applied the Monte Carlo simulation (1,000 simulations) in association with EIFS distribution to investigate the degradation in residual strength due to MSD.

Liao [11] applied Monte Carlo simulation using two random variables, squeeze force and friction coefficient, to predict fatigue life distributions. The Strain-Life approach was used to predict fatigue life, different from most authors, such as Garcia [6], Santgerma [10], Horst and Schmidt [38], Kebir, Roelandt and Gaudin [28], Grandt and Wang [27], and Dai, Creager, Odian and Safarian [39], who applied the Stress-Life, except [40] who also applied the Strain-Life approach for the fatigue initiation prediction.

Liao applied Gumbel distribution for the squeezing force, and normal distribution was chosen to represent the friction coefficient distribution. Lognormal distribution was

used to represent the stochastic behavior of fatigue life, in accordance with other researchers [6, 10 and 28].

Garcia and Mello [29] presented a probabilistic model to investigate the MSD problem in real aircraft structures. Monte Carlo simulation was performed using lognormal distribution for fatigue initiation life. For the crack propagation phase, both deterministic and probabilistic approaches were employed. Results from the numerical simulation were compared to fatigue data from riveted flat panels and to teardown inspections from an aged aircraft.

Sanches, de Jesus, Correia, Silva and Fernandes [40], presented a probabilistic approach to assess the fatigue of riveted joints using the Monte Carlo Simulation. Similarly to Liao [11], the Strain-Life approach was selected to predict fatigue initiation life. Crack growth life was predicted using Paris Law, with SIF predicted using FEM. A discussion was carried out accounting the probabilistic nature of MSD models inputs, such as clamping, friction coefficient, initial crack size, and crack growth properties, and they explored the influence on the MSD results.

An approach similar to Garcia and Mello [6, 29] was presented in Kebir, Roelandt and Gaudin [28], where it was discussed the application of MCS associated with DBEM. The only difference was that the crack growth phase was performed using a deterministic approach, instead of a probabilistic model. An automated tool was used to account for crack initiation, propagation, and final failure. Initial crack scenarios were randomly placed in each fastener at critical locations (2 per fastener hole), and crack growth was computed for each scenario.

For the fatigue initiation life, it was assumed that mean life and standard deviation for applied stress was known. An equation to calculate fatigue mean life and standard deviation as a function of applied remote stress for Aluminum 2024-T3 was presented. The fatigue life was distributed for each fastener fatigue critical location, assuming a lognormal distribution, using random numbers. Miner's rule was used to identify the first crack across all fasteners for each simulation, defining the initial crack scenarios. The numerical results from 200 MCS agreed with experimental data that showed the effectiveness of the proposed methodology [28].

Lazzeri [32] discussed numerical results obtained using computer code developed as part of the Structural Maintenance for Ageing Aircraft (SMAAC) program. He discussed deterministic versus probabilistic approaches applied to aircraft structures designs. The study presented the importance of considering stochastic behavior when assessing small undetectable cracks that can nucleate and grow at adjacent rivet holes. The stochastic nature of fatigue phenomena was accounted for during the crack initiation phase by applying EIFS method, and crack growth phase was considered by means of Paris and Forman Laws, as well as fracture toughness. Monte Carlo technique was implemented to perform the required high order simulations. Stress intensity factors were computed using the compounding method, where simple and known solutions were used to depict complex crack configurations, and the Swift Plastic Zone Touch (PZT) model was selected as the failure criterion. The computer program was validated with good agreement by comparing numerical versus experimental data.

2.4.2. Crack Propagation Life. A primary challenge to performing the MSD crack propagation phase was the determination of stress intensity factors that accounted for multiple crack scenarios. This was enhanced when collinear cracks of different sizes interacted with multiple boundaries, where a boundary had a pin-loaded fastener hole, free edge, stringer, or another crack. The difficulty was caused by how a particular Stress Intensity Factor (SIF) in one crack tip, e.g. lead crack, impacted the adjacent small cracks and vice versa. Considering this determination was required for each Monte Carlo Simulation to define initial scenarios, the computational workload was important, as discussed by Garcia [6].

Garcia provided recommendations for future work, where he concluded that it was possible to perform crack growth analysis for just 400 of scenarios in 2 to 4 weeks by using FEM or Dual Boundary Element Method (DBEM) due to computational workload. He also suggested the development of an in-house computer code by employing the compounding method to quantify the stress intensity factors and perform crack growth assessments. It was clear that using FEA or DBEM in association with high numbers of Monte Carlo simulations to predict MSD was not a recommended approach from a practical engineering standpoint. A vast model's diversity was employed within different proposed methodologies. Most significantly were the DBEM models [6, 9].

Garcia and Irwin [9] treated the crack propagation phase with a probabilistic model by using random variables to calculate the MSD parameters. They pointed out that accurate and computational economical methods should be used to calculate SIF for a MSD scenario, whereas DBFEM was chosen in their research [6, 9]

The use of Finite Element Alternating Method (FEAM) provided good quantitative estimates of SIF. Global FEA (GFEA) of multi-bay panels with cracks provided the information about realistic load flow pattern. A hierarchical model containing the cracked portion of the panel was isolated with corresponding stresses. After obtaining stress fields at crack locations, cracks were erased through alternating methods, by using analytical solutions for an infinite plate with pressurized cracks to accurately determine stresses at the crack tips. This sequential combination of FEM provided an efficient computational tool for calculating SIFs, as described by Park [41].

Kebir [28] treated the fatigue initiation phase using a probabilistic approach; applying the MCS technique, and crack propagation was performed using a deterministic approach. Similar to Garcia [6], he used DBFE to compute SIF. The Paris equation in conjunction with K_{eff} was used to compute crack growth. Failure mode was based on the Swift PZT model.

2.4.3. Failure Criterion. The presence of MSD cracks can rapidly reduce the residual strength capabilities of riveted panels, as described by [7, 12, 27, and 36]. A widely used model [9, 27, and 28] to predict residual strength in the presence of MSD is the Plastic Zone Touch (PZT), as suggested by Swift [42].

Bakuckas presented a summary of techniques employed to perform residual strength in the presence of MSD, such as Crack Tip Opening Angle (CTOA) and T-Integral [31]. One powerful approach to determine the residual strength of a panel that contains MSD cracks was presented by Newman [13] using the Crack Tip Opening Angle (CTOA). During an airframe structural integrity program (ASIP) conducted by National Aeronautics

and Space Administration (NASA) in partnership with FAA, residual strength of stiffened panels were predicted by numerical simulations and they correlated with experimental data.

The CTOA was introduced by Wells, as discussed by Ma, Lam, Kokaly, and Kobayashi [43], and according to Newman [13], this fracture criterion was experimentally checked as a valid criterion for Mode I crack opening in thin plates. This criterion was applicable for predicting the link-up of a lead crack with small MSD adjacent cracks. NASA's Langley Center also concluded that the ductile tearing was an important parameter for evaluation that could not be predicted by LEFM and J-Integral scope. For this evaluation, the elastic-plastic crack growth simulation criterion was efficient. The stable tearing is an intrinsic characteristic of the elastic-plastic materials due to plastic deformation during the unloading phase.

CTOA defined the displacement field in the crack tip, and its basic concept was that an opening angle remains constant during stable crack propagation. The use of a CTOA approach became an alternative criterion to J-Integral, and it was extensively used in the research of ductile fractures during the 80s and 90s, according to Ciliato [44].

The extensive contributions from the AAWG, which performed research on the WFD topic the past 30 years, must be noted. MSD assessment methodologies developed by three Original Equipment Manufacturers (OEM) and one United States airline were presented in the final report [15].

2.4.4. Summary of Published MSD Methodologies. The dominance of fatigue crack initiation life (FCIL) compared to fatigue crack growth life (FCGL) was mentioned by Garcia and Santgerma [9, 10], Proppe [14] and Klebir [28]. Across all developed models, the majority applied lognormal distributions to represent the fatigue life. Different

from the majority of works that presented numerical simulation versus test results, Wang [26] and Garcia [6] were the few authors who presented parametric studies and discussed the influence of parameters, such as rivet type, squeeze force, clamp-up, and its influence on fatigue life under MSD scenario.

2.5. THEORETICAL BACKGROUND

In this section, the theoretical background supporting fatigue and crack growth assessments of riveted structures was presented. Although different approaches to predict fatigue crack nucleation and crack growth phases of real structures were available in the literature, there was emphasis on Stress-Life (S-N) and Linear Elastic Fracture Mechanics (LEFM), respectively.

2.5.1. Stress-Life (S-N) Approach. Mechanical components, machines, vehicles and, engineering structures are subjected to repetitive loads in service where stresses well below the ultimate strength of the material can contribute to the development of microscopic defects, such as slip bands and dislocations. These microscopic defects accumulate damage through the time, and the defects develop into macroscopic surface fatigue cracks.

Fatigue is defined as the progressive process of damage accumulation and failure due to cyclic loading, according to Dowling [45]. The fatigue study started with W. A. J. Albert who published the first fatigue-test results known in 1837, according to Schutz [46]. Albert constructed a test machine to investigate strength of conveyor chains that failed in the mines of Clausthal, Germany. However, he did not use the term fatigue, which was first introduced by the Frenchmen J.V Poncelet in 1839 [45].

The first notary and scientific contribution to fatigue behavior of materials came in 1860 when August Wohler published the results of fatigue tests performed with railway axles. In 1870, he presented a final report containing Wohler Laws that stated: "Material can be induced to fail by many repetitions of stresses, all of which are lower than the static strength" as presented in [46:pg. 265].

Wohler presented his fatigue test results in the form of tables, Spangenberg plotted in the form of curves that became known as Wohler or S-N curves in 1936, as described in [46]. Wohler also drew conclusions about stress amplitude and the influence of mean stress in fatigue life. Wohler's work encompassed the development of fatigue test machines, measurement of service loads, calculation of respective stresses, design of finite life components, account for the fatigue scatter factor, and assessment of crack propagation. His conclusions and contributions are applied to the design and analysis of engineering structures in the modern industry.

In 1910, Basquin [47] plotted the Wohler's curve in the form of log-log and used the power-law equation to best fit test data. The equation describes the maximum alternate stress (σ_a), which can be applied as a function of number of cycles (N_f):

$$\sigma_a = A(N_f)^B \quad (1)$$

where A and B are fitting constants determined via S-N curve, as illustrated in Figure 2-9. Constant A represents the point where the best fit line reaches the ordinate axis, and B is the curve slope. If a test coupon, or a real scale component is subjected to a sufficient stress level, σ_{a1} , due to cyclic loading, at a certain point N_1 , fatigue crack is expected to nucleate; by continuing load application, the crack propagates until reaching final failure at N_{f1} cycles. When different stress level σ_{a2} is applied, where $\sigma_{a2} > \sigma_{a1}$ is applied, the specimen

fails at a lower number of cycles N_{f2} . Although, if lower stress $\sigma_{a3} < \sigma_{a2}$ is applied, a higher number of cycles $N_{f3} > N_{f2}$ is expected. By plotting the alternate stresses versus number of cycles in a log-log scale, the S-N curve can be built as shown:

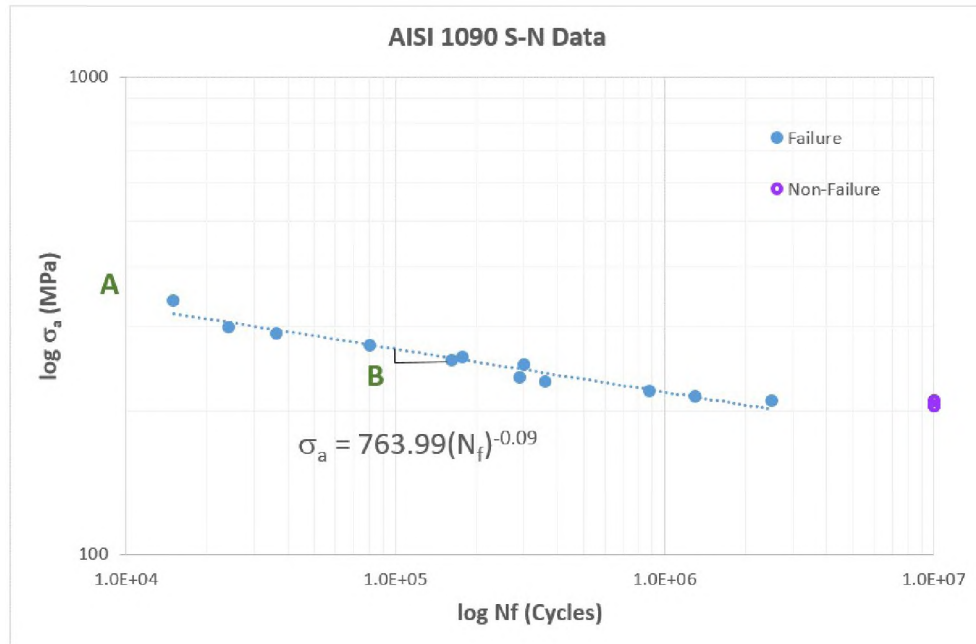


Figure 2-9 S-N Curve and Best Fit for Steel AISI 1090.

From the point where S-N constants were found using experimental data, the number of cycles to nucleate a crack can be determined using Equation 1. Note that S-N curves are usually determined by using data from completely reversed fatigue tests; however, engineering structures are often subjected to different stressing, typically non-zero mean or zero to tension. As discussed by Dowling, engineering practical applications and fatigue tests are subjected to cycling between maximum and minimum stress levels.

When the stress levels also called stress history are constant, it is called constant amplitude loading, as described in Figure 2-10.

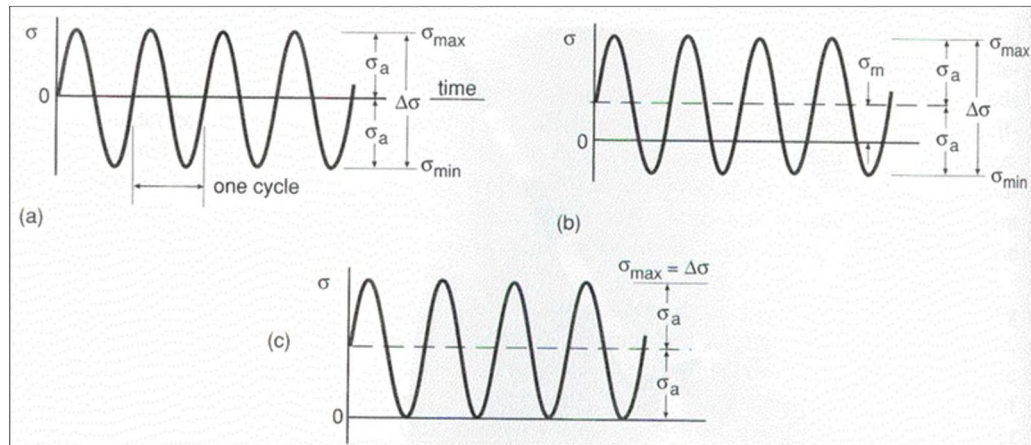


Figure 2-10 Constant Amplitude Loading [45].

Figure 2-10 illustrates three typical constant amplitude cycles. Case (a) shows zero mean cycling ($\sigma_m = 0$), also called completely reversed stress cycle. Case (b) has tensile mean stress ($\sigma_m > 0$), and case (c) is defined as zero to tension stress history ($\sigma_{min} = 0$). From Figure 2-10 it is possible to define important terms applied to the study of fatigue, especially stress-life approach; σ_{max} is the maximum stress level, σ_{min} is the minimum stress level. The difference between σ_{max} and σ_{min} is defined as stress range $\Delta\sigma$. The stress amplitude, or alternating stress σ_a , is defined as half of the stress range, and the mean stress σ_m is the average between maximum and minimum stresses, thereby the following equations can be written [45]:

$$\Delta\sigma = \sigma_{max} - \sigma_{min} \quad (2)$$

$$\sigma_a = \frac{\Delta\sigma}{2} = \frac{\sigma_{\max} - \sigma_{\min}}{2} \quad (3)$$

$$\sigma_m = \frac{\sigma_{\max} + \sigma_{\min}}{2} \quad (4)$$

The stress ratio R is defined as the ratio between minimum stress and maximum stress. Experimental fatigue tests are usually performed using $R = -1$ or $R = 0$, and the respective S-N curves significantly vary for different stress ratios, as presented by Dowling [45]:

$$R = \frac{\sigma_{\min}}{\sigma_{\max}} \quad (5)$$

when S-N curve yields $R = -1$, it means that a completely reversed cycle was applied, and for $R = 0$, a zero-to tension stress cycling was used to obtain the experimental results. It was important to observe that real components were subjected to a completely different stress ratio in service when compared to the stress ratio used to obtain the S-N curve. In this circumstance, equivalent stress models, such as the Goodman diagram, Gerber parabola, and Walker equation must be applied to account for the mean stress effect on SN curve. The influence of mean stress and the respective equivalent stress models were extensively discussed in classical textbooks such as [45, 48]; therefore further details were not included.

Stress history or spectra was described by using complex or random distributions; in this case, it was called variable amplitude loading, which is often found in aircraft structures, such as wing and empennage.

Failures associated with metal fatigue represent engineering concern regarding safety and cost. According to Dowling [45], the annual of fatigue failures in the US economy yielded approximately 3% of the gross domestic product (GDP).

One aspect to consider during fatigue design is the scatter factor associated with fatigue cracks. When different specimens, same geometry, same material, and same applied load are experimentally tested, each specimen presents a different fatigue life, as presented in Figure 2-11, that can be approximated as a normal distribution, as discussed by Bruhn [49].

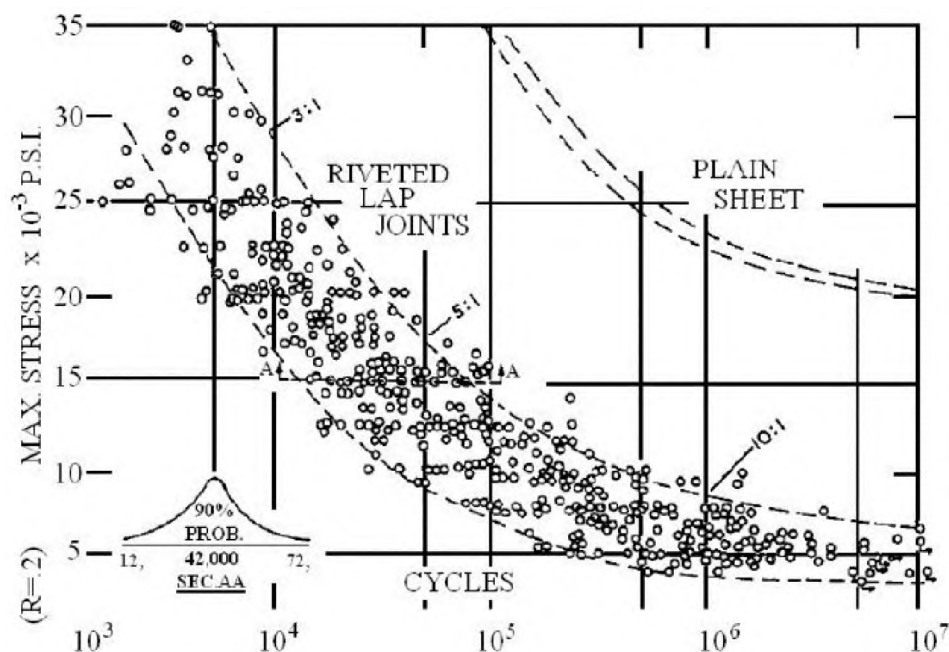


Figure 2-11 Scatter Factor of the S-N Curve [49].

The S-N curve scatter behavior plays a fundamental role on the MSD assessment of riveted lap joint structures, and usually it is accounted for by S-N mean life and the associated standard deviation [6].

2.5.2. Linear Elastic Fracture Mechanics. Griffith was the first to investigate the effect of cracks on the strength of solids, and he proposed an energy criterion for fracture in 1921 [50]. However, a practical criteria from the engineering standpoint was only developed in 1956 when Irwin developed the energy release rate approach, defined as the rate of change in potential energy with the crack area [51].

$$G = - \frac{d\Pi}{dA} \quad (6)$$

where Π is the potential energy of a cracked body, defined as the difference between the strain energy U and the work done by the external forces F , and A is the crack area. The energy release rate of an infinite plate containing a central crack of length $2a$ subjected to remote tensile stress is given by the following expression [51]:

$$G = \frac{\pi\sigma^2 a}{E} \quad (7)$$

where σ is the remote tensile stress, a is the half-crack length and E is the Young Modulus. According to Perez [52], elastic solid bodies containing cracks can be characterized by defining the state of stress near the crack tip. Westergaard, Irwin, and Williams were among the first to present closed form solutions for stresses in an elastic cracked body, as discussed by [51]. The concept of stress intensity factor, defined as the amplitude of the singularity in front of the crack tip, was introduced [51].

2.5.3. Fatigue Crack Growth. The first model to predict the crack growth behavior was presented by Paul Paris in the early 1960s [53], he defined the cyclic crack growth rate da/dN as a linear function (power law) of the stress intensity factor range ΔK as described below, and discussed by [45]: where C is a material constant, and m is the slope of the da/dN versus ΔK curve:

$$\frac{da}{dN} = C(\Delta K)^m \quad (8)$$

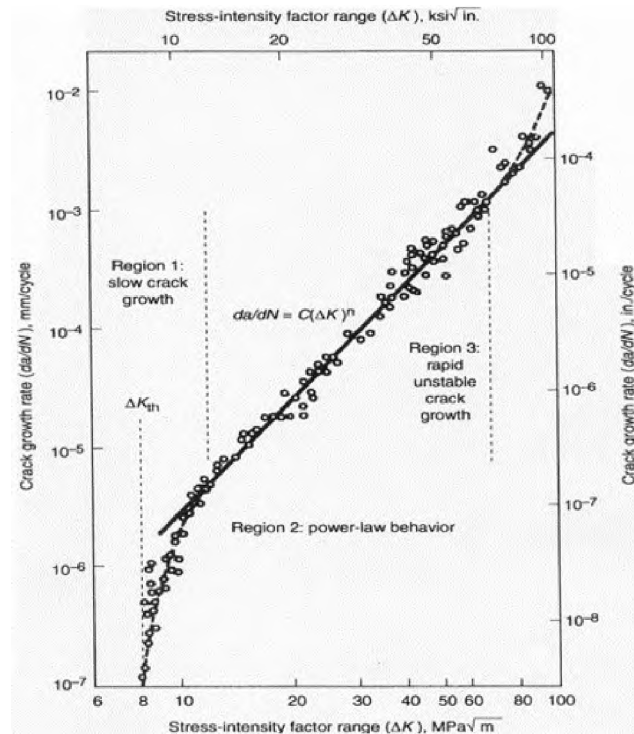


Figure 2-12 Typical Crack Growth Curve [48].

Below a certain ΔK value, crack growth is not expected to occur. This is called threshold region, also designated as Region I, and the respective stress intensity factor range is called $\Delta K_{threshold}$. There is a region where the crack growth behavior can be approximated by a linear relation (power law), as proposed by Paris. This is called linear region or Region II. The third and last region is defined by the instability, when the ΔK reaches the fracture toughness K_{Ic} and unstable crack growth occurs as described in Figure 2-12.

3. METHODOLOGY FOR ASSESSING STRUCTURAL INTEGRITY OF AIRCRAFT RIVETED PANELS IN THE PRESENCE OF MULTIPLE-SITE FATIGUE CRACKING

This section described the details of probabilistic methodology to perform MSD assessment by using Monte Carlo simulation technique to determine WFD parameters, such as $WFD_{(avg)}$, ISP, SMP, and I_{WFD} . As discussed in Section 2, the MSD numerical methodology is divided in to three distinguished phases: Fatigue Crack Initiation Life (FCIL), Fatigue Crack Propagation Life (FCPL), and Final Failure. An automated tool was developed using Excel® VBA code to perform numerical tasks required to run up to 2,500 Monte Carlo simulations. Program details, such as input and output data, were presented in Section 4.

3.1.1. Fatigue Crack Initiation Life. A typical riveted lap joint configuration with 3 rows of fasteners that were equally spaced in longitudinal and transversal directions, then subjected to remote stress ($R=0$, typically found in pressurized fuselage structures) was considered. In aircraft riveted lap joint structures, cracks are expected to nucleate at holes located in the critical end fastener row of the external (i.e., outer) joint member, also called critical rows, because fasteners for these rows transfer a considerable percentage of the total income load (typically 35% for 3 rows of fasteners [19]). In addition, for fuselage riveted lap joints, the external joint member local stresses are greater due to the presences of the countersinks for flush rivet installation. Therefore, only external rows of fasteners were considered during MSD modelling in this study.

The number of considered fasteners was widely discussed in Section 2. The methodology used considered up to 20 fasteners, which are typically found in a one-bay

fuselage panel, although they can be expanded to account for higher numbers if required. For each fastener considered in the numerical MSD assessment, there were 2 positions: Potential Crack Initiation Sites (PCIS), where cracks are likely to nucleate at 90° and 270° clockwise, see Figure 3-1.

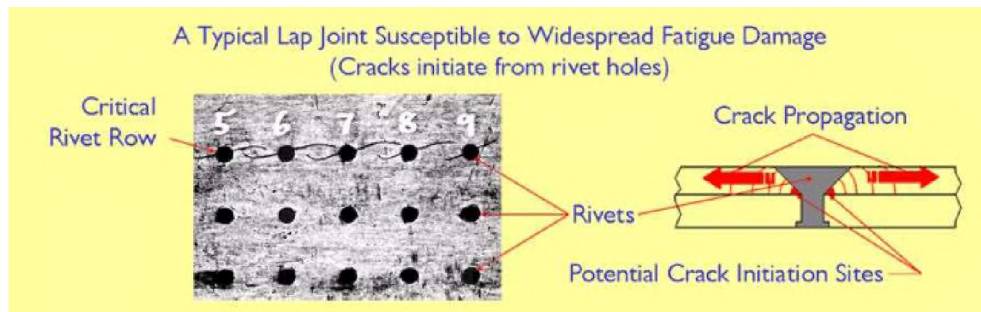


Figure 3-1 Critical Rivet Row and ‘Potential Crack Initiation Sites’ [54].

A lognormal distribution was assumed to represent the probabilistic nature of fatigue initiation life N_0 , defined as the number of cycles to nucleate a detectable crack of size a_0 . This was performed by applying equation [9]:

$$\log(N_0) = \mu + \alpha\sigma \quad (9)$$

Where N_0 is the fatigue initiation life, defined as the number of cycles required to nucleate a crack of a_0 size (log-scale), μ is the mean fatigue life based on S-N curve (log-scale), α is randomly distributed number with zero mean and standard deviation equal to one $\{N(0,1)\}$, and σ is the fatigue life standard deviation based on S-N curve (log-scale).

Normally distributed random numbers $\{N(0,1)\}$ are generated using the Box-Muller transformation described in [55]. The method produced a pair of Gaussian random

numbers from a pair of independent random variables. Let x_1 and x_2 be a pair of random independent numbers in the interval $\{0, 1\}$. A transformed pair of random numbers following Gaussian distribution, y_1 , and y_2 can be determined using the following expressions:

$$y_1 = \sqrt{-2\ln x_1} \cos(2\pi x_2) \quad (10)$$

$$y_2 = \sqrt{-2\ln x_1} \sin(2\pi x_2) \quad (11)$$

An algorithm using Excel[®] VBA was created to generate up to 100,000 pairs of random numbers to be used in Monte Carlo simulation. Figure 3-2 shows an example of 20,000 pairs of random numbers generated via VBA code and its comparison with theoretical normal distribution probability density function given by:

$$f(x) = \frac{1}{\sigma\sqrt{2\pi}} e^{-\frac{1}{2}\left(\frac{x-\mu}{\sigma}\right)^2} \quad (12)$$

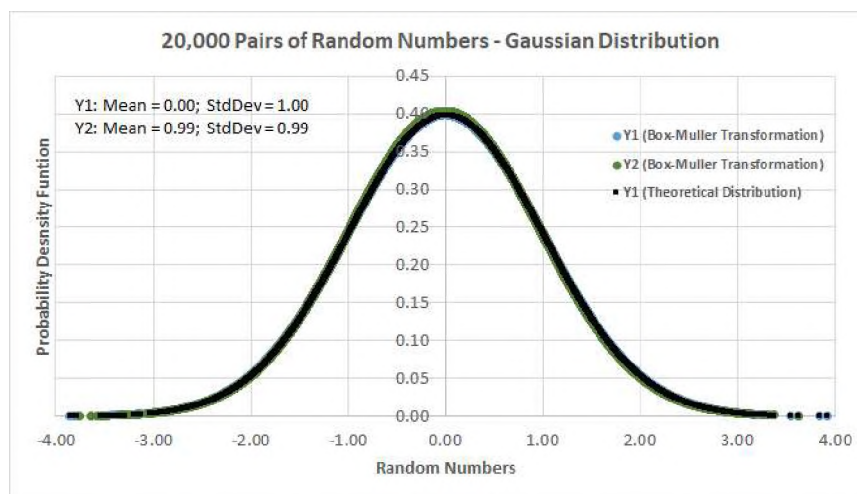


Figure 3-2 Numerically Generated Random Numbers – Gaussian distribution.

The mean fatigue life μ and the respective standard deviation σ are typically obtained from the S-N curve of single lap joint coupons. Garcia presented a model to calculate mean and standard deviation based on applied local elastic stress. For a typical fuselage lap joint made of Al2024-T3 Clad, $t = 1.6$ mm, $\sigma_u = 448$ MPa and $\sigma_y = 331$ MPa, the mean and standard deviation are given by [6]:

$$\mu = \log \left[10^5 \left(\frac{S-11.5}{494.5-11.5} \right)^{-6.2} \right] \quad (13)$$

$$\sigma = \frac{14018}{S^2} + \frac{2.76}{S} + 0.11 \quad , \quad (14)$$

where S is the maximum local stress for each PCIS in [MPa].

Kebir, Roelandt and Gaudin [28] used a similar model to perform probabilistic MSD assessment by applying Monte Carlo simulation. Mean and standard deviation are calculated using Equations 7 and 8:

$$\mu = \log 10^5 \left(\frac{S-S_{lim}}{FQI-S_{lim}} \right)^p \quad (15)$$

$$\sigma = \frac{a}{S^2} + \frac{b}{S} + c \quad , \quad (16)$$

where S_{lim} is the endurance limit in MPa, FQI is the ‘Fatigue Quality Index’, defined as the fatigue limit for a life of 10^5 cycles in MPa, p is the S-N curve exponent and S is the applied remote stress MPa. Constants a , b and c have no physical meaning and were determined via test data best fit. Therefore a randomized fatigue initiation life ‘ N_o ’ can be calculated by sorting-out generated ‘ α ’ numbers and solving Equation 1 for each PCIS. Figure 3-3 illustrates the numerical simulation process for a lap joint containing k fasteners.

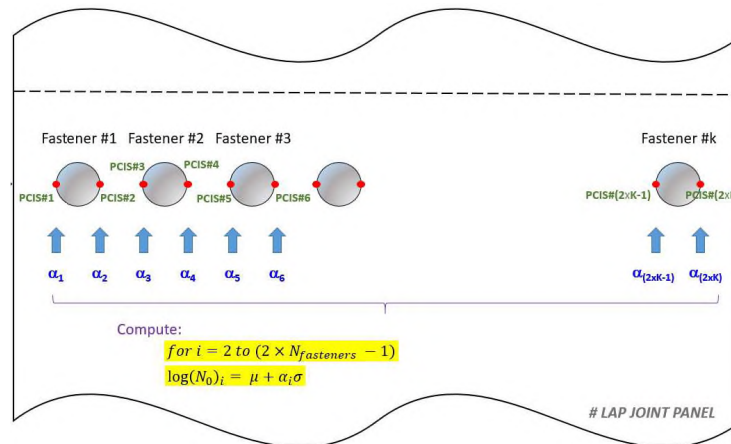


Figure 3-3 Fatigue Initiation Life Calculation Process.

By analyzing Equation 1, it was concluded that when $\alpha = 0$, the equation predicts N_0 equal to μ , which simply means 50% S-N curve or fatigue mean life. When α is different than zero, the fatigue scatter is taken into consideration. Garcia defined the concept of Randomized Fatigue Life (RFL) in his work [6].

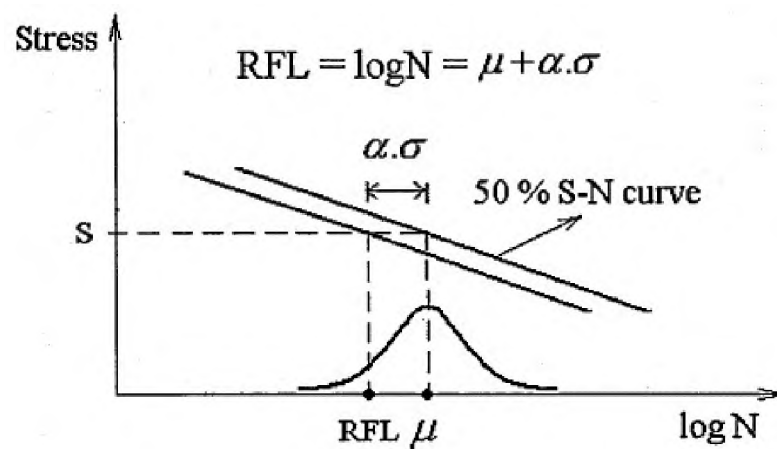
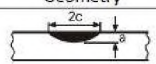

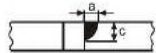
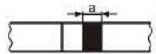


Figure 3-4 Randomized Fatigue Life [6].

By applying random numbers α , normally distributed $\{N(0, 1)\}$, the predicted life RFL (log-scale) is shifted to the left or to the right from central point (50% S-N curve - mean value), accounting for the stochastic nature of fatigue crack initiation, as presented in Figure 3-4. By employing the probabilistic model across lap joint critical rivet rows containing k fasteners, one can find the PCIS that developed the first crack the one presenting shorted life across all PCISs. Therefore one particular damage scenario was created. This step was repeated as many times as required to find convergence creating different numbers of initial damage scenarios to be used in the fatigue crack propagation life phase.

3.1.2. Fatigue Crack Propagation Life. The crack propagation phase was performed for each damage scenario generated from the previous phase (fatigue crack life initiation). For each PCIS (j), where $j=2$ to $(2 \times N_{\text{fasteners}}-1)$, with damage equal to one, an initial crack size of 1.27 mm was assumed. This initial size was in agreement with recommendations from USAF MIL-A-83444 [56] as defined in Table 3-1.

Table 3-1 Initial Flaw Sizes – Definitions of USAF MIL-A-83444 [2].

Types of flaw		Aspect ratio (a/c)	Flaw size a (mm) to be assumed immediately after inspection		
			Pre-service inspection with high standard NDI	In-service inspection with special NDI	
Description	Geometry		Fail-Safe	Slow flaw growth	
Surface flaw		1.0 0.2	1.27	3.18	6.35
Through crack			2.54	6.35	12.7
Corner flaw at a hole		1.0 0.2	0.51	1.27	6.35 mm beyond fastener head or nut
Through crack at a hole			0.51	1.27	6.35 mm beyond fastener head or nut

The computational algorithm did not start cracks at PCIS at $j=1$ or at $j=2 \times N_{\text{fasteners}}$ because it would lead to a single crack propagating toward the panel edge, and not uphold MSD scenario. Single lead cracks were covered by traditional damage tolerance assessment and were not part of this study.

At the same fastener hole where the first crack (lead crack) appeared when $D(j)=1$, an initial crack size of 0.127 mm was assumed at opposite PCIS; either $(j-1)$ or $(j+1)$ as shown in Figure 3-5.

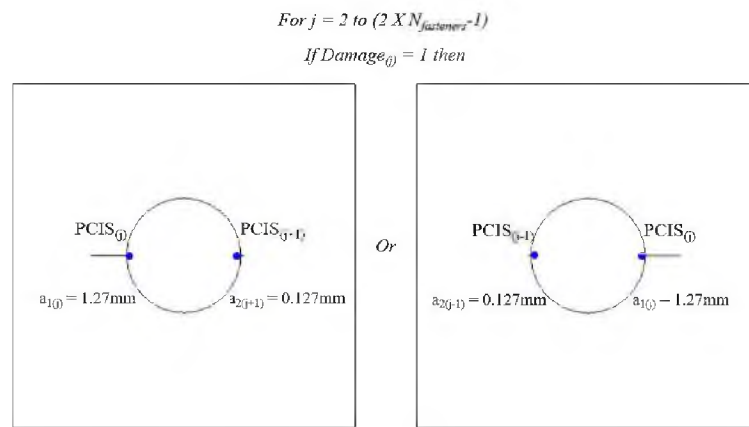


Figure 3-5 Lead and Opposite Crack Sizes.

The two adjacent fastener holes were assigned with two symmetrical cracks of 0.127mm (continuous damage) for each PIC, according to Figure 3-6. This approach was conservative and it was meant to cover PCIS which have cumulative damage close to one. This assumption simplifies computation workload avoiding cumulative damage reassessment.

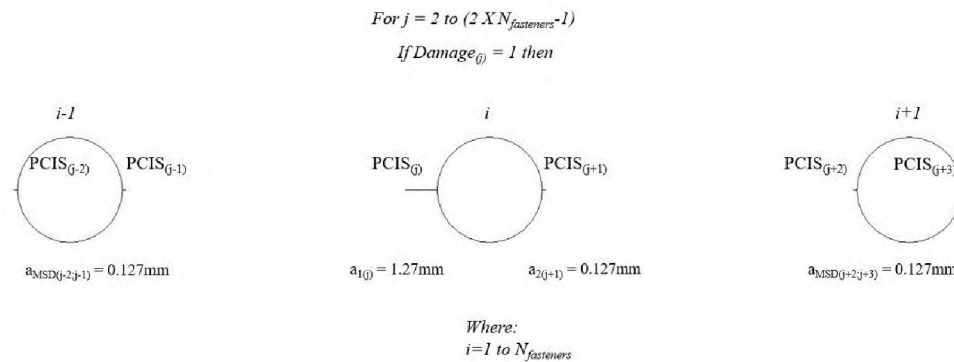


Figure 3-6 MSD Model Initial Crack Sizes.

After initial crack sizes were defined, the next step was to compute the stress intensity factors (SIF) for each crack tip within the model. This was performed using a compounding technique.

The compounding method was first discussed by Rook and Cartwright in 1974 as an efficient method to calculate SIF of complex crack configurations, instead of traditional theoretical or experimental approaches, which are often time consuming and costly [57]. The compounding method has been extensively used to compute SIF of complex configurations, such as MSD, based on well-known and simple SIF solutions [28, 38 and 58].

The basic idea was to account for the influence of different boundaries and the influence on crack of interest. Boundaries can be fastener holes, stringers, free edges or other cracks. ESDU [58] presented a systematic step-by-step procedure on how to employ a compounding method to compute SIF in complex solutions.

The procedure used in this work assumed a crack crossed a boundary; therefore, ancillary configurations were required to obtain the final stress intensity factor. From the

point where the influence of all boundaries were established, the compounding equation (Equation 17) was used [58]:

$$K_r = K_0' \left[1 + \sum_{n=2}^{n=N} \left(\frac{K_n'}{K_0'} - 1 \right) \right] \quad (17)$$

where K_r is the resultant compounded stress intensity factor, K_0' is the stress intensity factor for the equivalent crack in the absence of all boundaries, and K_n' is the stress intensity factor due to the effect of the n^{th} boundary acting on the equivalent crack, n denotes the n^{th} boundary, and N is the total number of boundaries.

The first consuming task, was to replace the original configuration with an equivalent configuration that had the same stress intensity factor. For the scope of the MSD model presented in this thesis, the original configuration constituted two-unsymmetrical cracks emanating from a pin-loaded fastener hole, while the equivalent configuration had a central crack of $2a$ in an infinite plate subjected to remote stress. The equivalent configuration SIF is also known as SIF in the absence of all boundaries K_0 , as described in ESDU [58].

The computation of SIF for cracks emanating from fastener holes have been topics of research over the past 50 years, significant and notable contributions were given by Schijve [24], Newman [59] and Rooke [60].

Newman's work [59] described a method to compute SIF for either one crack or two-symmetrical cracks emanating from a fastener hole in a finite width plate subjected to remote tension (Figure 3-7). Equation 18 was used in this work to compute SIF for the lead crack and opposite cracks, considering b equal to one, with one crack tip. Note the equation

is valid for both corner and through thickness phases. The same equation was employed to calculate SIF for MSD cracks and used on adjacent holes as described in Figure 3-6.

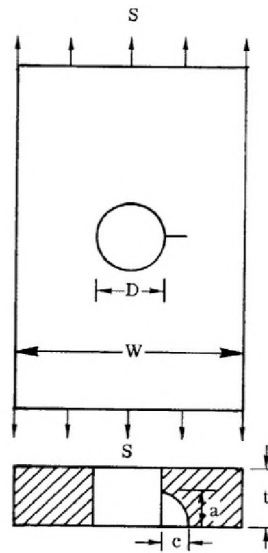


Figure 3-7 Corner Crack at a Hole [59].

The stress intensity factor can be calculated using Equation 18:

$$K_I = \sigma \sqrt{\pi \frac{a}{Q}} M_e f_b \sqrt{\sec \frac{\pi D}{2W}} \quad (18)$$

where $b = 1$ for a single corner crack, and $b = 2$ for two symmetrical corner cracks, described further below. The term Q is defined by Equation 19 for $a/c < 1.0$:

$$Q = 1 + 1.47 \left(\frac{a}{c} \right)^{1.64} \quad (19)$$

The boundary correction factor M_e is given by:

$$M_e = \left[M_1 + \left(\sqrt{Q \frac{c}{a} - M_1} \right) \left(\frac{a}{t} \right)^p \right] f_w \quad , \quad (20)$$

where p is defined as:

$$p = 2 + 8 \left(\frac{a}{c} \right)^3 \quad . \quad (21)$$

The terms M_1 and a/t are defined as front-face correction and back-face correction, respectively. M_1 for the range $(0.02 \leq a/c \leq 1.0)$ is given by Equation 22:

$$M_1 = 1.13 - 0.1 \frac{a}{c} \quad . \quad (22)$$

The finite width correcting factor is given by:

$$f_w = \sqrt{\sec \left(\frac{\pi}{2} \frac{D+bc}{W-2c+bc} \sqrt{\frac{a}{t}} \right)} \quad . \quad (23)$$

The term f_b in Equation 10 is known as the Bowie correction factor, applied to the thickness cracks emanating from a hole, while the secant term accounted for the interaction between the circular hole and the finite width, according to [59].

The Bowie correction factor (f_b) is given by the polynomial functions described below, where $b = 1$ is applied for a single crack, and $b = 2$ is used for two symmetrical cracks:

$$f_1 = 0.707 - 0.18\lambda + 6.55\lambda^2 - 10.54\lambda^3 + 6.85\lambda^4 \quad ; \quad (24)$$

$$f_2 = 1.0 - 0.15\lambda + 3.46\lambda^2 - 4.47\lambda^3 + 3.52\lambda^4 \quad (25)$$

where:

$$\lambda = \frac{1}{1 + \frac{2c}{D}} \quad . \quad (26)$$

The influence of the opposite, or the secondary crack was studied and discussed by Rooke and Tweed [61], and it was employed with the MSD model by computing the interacting factors. The interacting factors were also employed by Schijve [24], Wang [26], and Dai, Creager, Odian and Safarian [39].

The interacting factor simply compares the SIF for two cracks and for a single crack. Rooke and Tweed [61] described that individual crack lengths were not the most important parameter, but the total length from tip to tip (a_1+D+a_2), instead.

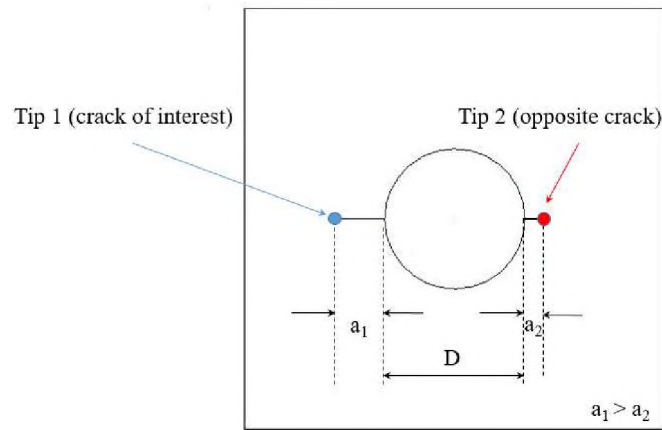


Figure 3-8 Two Unsymmetrical Cracks Emanating from a Hole.

The stress intensity factor at crack tip 1 (Figure 3-8) can be determined, thus accounting for the influence of the opposite crack, tip 2, as follows:

$$F_{\text{int}} = \frac{K_2}{K_1} = \frac{\sigma\sqrt{\pi a_2}}{\sigma\sqrt{\pi a_1}} = \sqrt{\frac{a_1+D+a_2}{a_1+D}} \quad (27)$$

Equation 27 can be simplified to:

$$F_{\text{int}} = \sqrt{1 + \frac{a_2}{a_1 + D}} \quad . \quad (28)$$

Therefore, the SIF at crack tip 1, considering the effect of crack tip 2, can be expressed as:

$$K_1 = K_0 F_{\text{int}} \quad , \quad (29)$$

where K_0 is the stress intensity factor of a single crack emanating from a hole, which can be calculated using Newman's solution in Equation 10.

Fastener load can vary along each fastener hole across the critical row, as discussed by Niu [19] and Swift [25]. There are broad range of methods for determining load transfer in lap joints, such as FEM or analytical approaches. An analytical approach, called severity factor, was discussed in detail by Niu [19]. This concept requires detailed analysis of load distribution on each fastener within the joint, and it accounts for fastener type, method of installation, interference, hole preparation, design detail, and the stress concentration factors associated with local load transfer and bypass load. Detailed analysis procedure was discussed in [19], and it was not included in the scope of this work; therefore, the pin-load was assumed to be input data for the MSD model.

The stress intensity factor for a pin-loaded fastener was computed by employing the superposition method as described by Schijve [62]. The fastener load applied to a circular hole was approximated as a concentrated force in a single point. For an infinite plate containing a central crack, subjected to two loads oriented in opposite directions on the crack plane, the exact solution was available was obtained by classical linear elastic fracture mechanics, as described by Schijve [62].

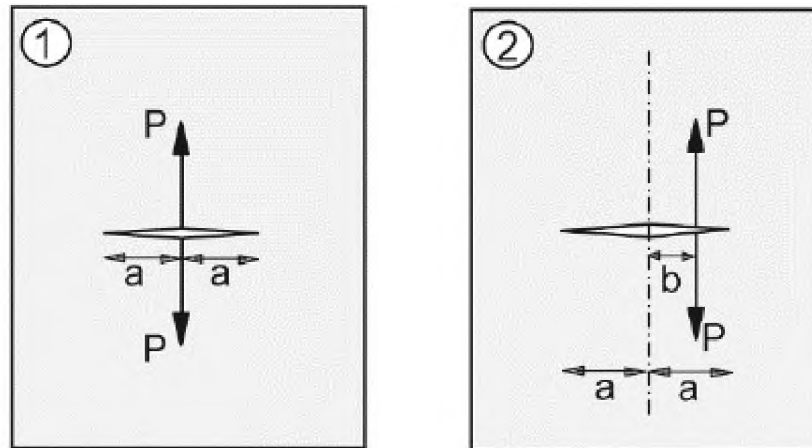


Figure 3-9 Concentrated Loads at Crack Plane [62].

Case 2 considered the effect of eccentricity, when the loads were not applied in the crack center (see Figure 3-9). The closed form, exact solution was described in [62]:

$$K = \frac{P}{\sqrt{\pi a}} \sqrt{\frac{a+b}{a-b}}, \quad (30)$$

where P is the fastener load per unit thickness (N/mm), crack half-length is defined by a , and b denotes for the eccentricity. However, to correctly compute the stress intensity factor for two cracks emanating from a pin-loaded hole subjected to income and by-pass stresses (Figure 3-10), the superposition method was applied as follows:

The income stress was (S_0+S_3) , S_0 denoted the by-pass stress and S_3 yielded the bearing stress, defined as P/D . By employing the superposition method, the final SIF, $K_{(1)}$ was obtained by adding the solutions from case A and case B. Case A was solved by applying Equations 18 and 28. However, the Case B SIF solution was not available and the superposition of known solutions was required.

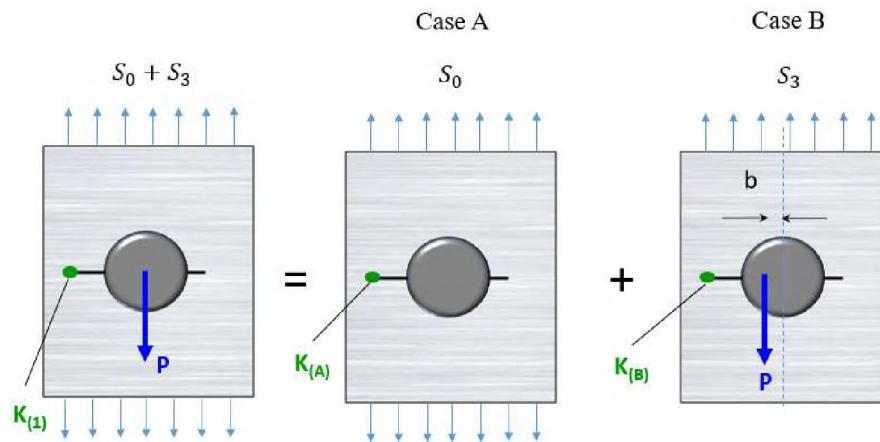


Figure 3-10 Two-Unequal Cracks – Income/By-Pass Stresses and Pin Load.

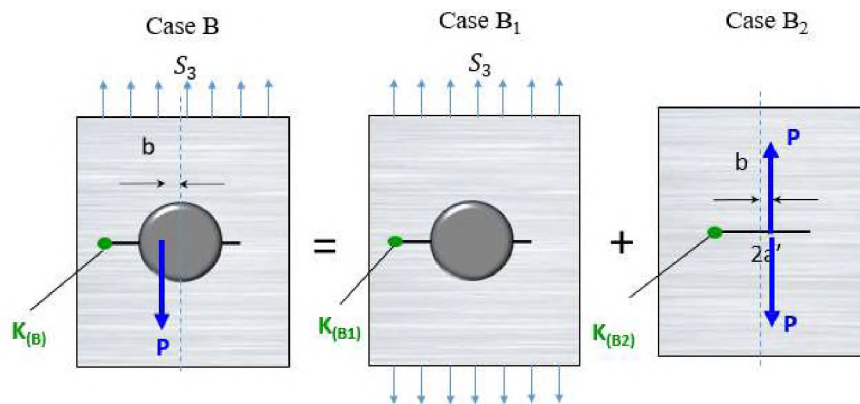


Figure 3-11 Two-Unequal Cracks - Remote Stress and Pin Load.

As shown in Figure 3-11, the solution for Case B was found by superposing solutions B1 and B2 that were solved by employing Equations 18 and 30, respectively. The proposed solutions, Equations 18 to 30, to compute the stress intensity factors of two unequal cracks were compared against NASGRO® 9.2 program [63]. The NASSIF module was employed by using through crack solution TC23. A lead crack of 1.6 mm and an

opposite crack of 0.53 mm were assumed, tensile remote stress of 80 MPa and bearing stress of 140 MPa were used. The input data were shown in Figure 3-12.

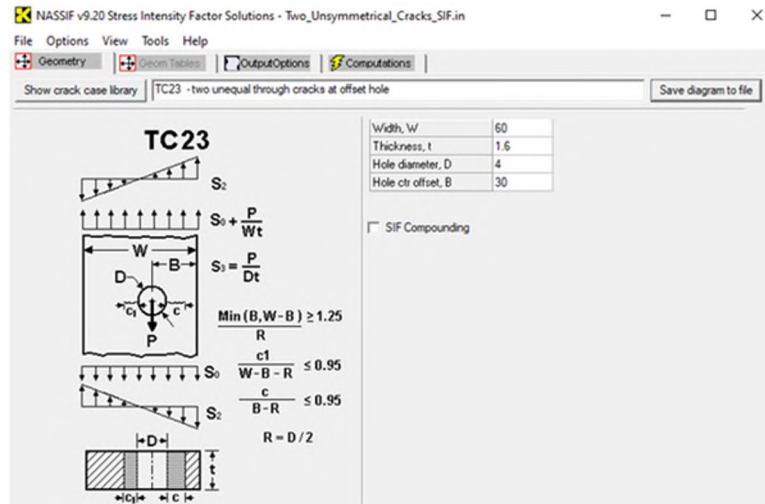


Figure 3-12 NASSIF Solution TC23 Input Data.

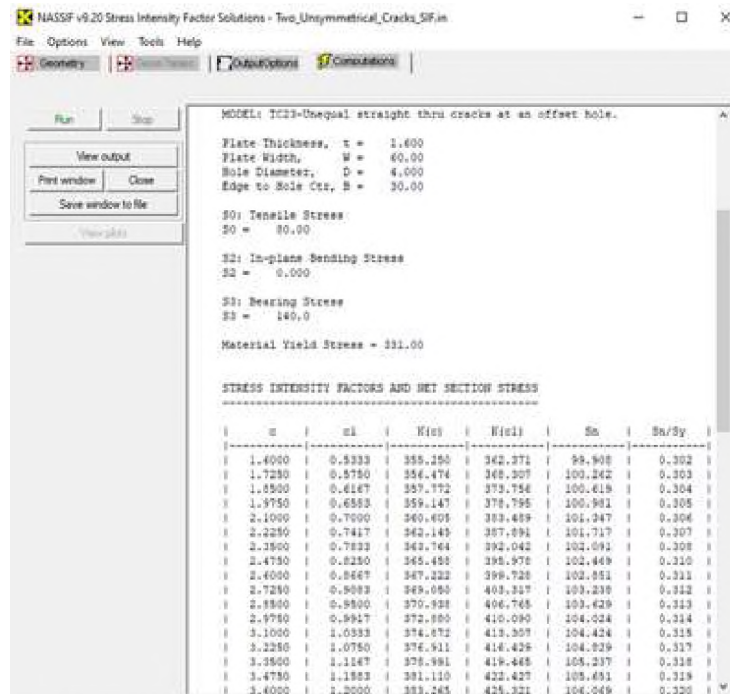


Figure 3-13 NASSIF Solution TC23 Output Data.

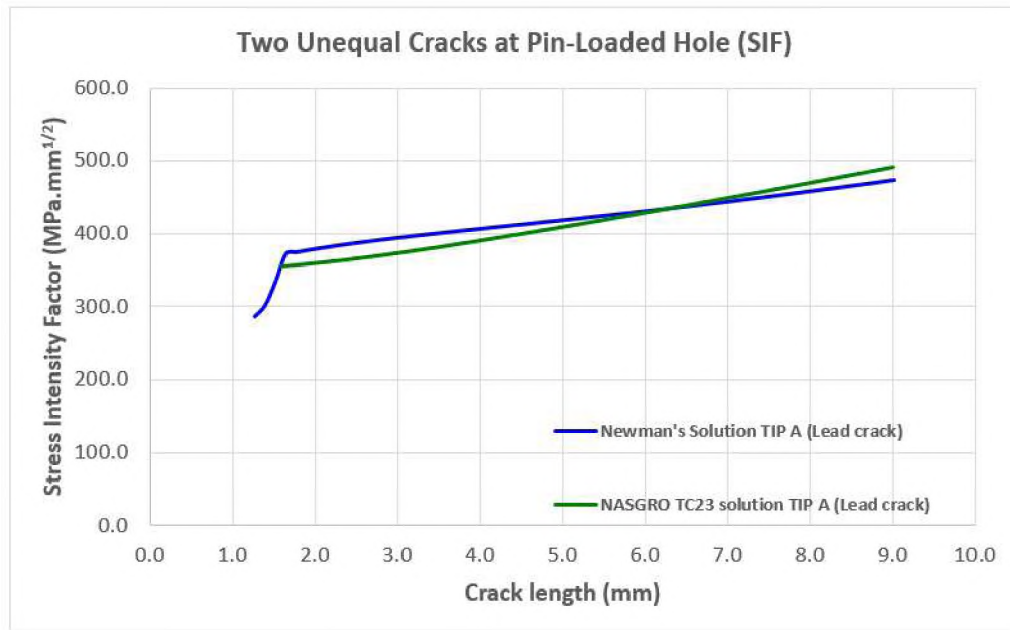


Figure 3-14 Comparison of Stress Intensity Factors.

Figure 3-14 presented the comparison of proposed SIF solution, two unequal cracks emanating from a pin-loaded hole, by employing Newman [59] and Rooke [61] solutions against NASGRO TC23 solution [64] presented in Figure 3-13.

The difference in curve slopes observed at crack lengths from 1.27 mm to 1.60 mm is attributed to the fact that Newman's solution accounted for corner and through-thickness cracks, while solution TC23 is valid to through-thickness only. It was concluded that proposed solutions correlated with NASGRO NASSIF solution, and therefore it was considered validated.

After determining the original configuration SIF for two unequal cracks emanating from fastener hole with pin-load, as shown in Equation 31, the ancillary crack can be easily found by equating the stress intensity factor with the infinite plate and central crack one:

$$\sigma \sqrt{\pi \frac{a}{Q}} M_e f_b \sqrt{\sec \frac{\pi D}{2W}} \cdot F_{int} + \left(\frac{S_3 \sqrt{\pi \frac{a}{Q}} M_e f_b \sqrt{\sec \frac{\pi D}{2W}} \cdot F_{int} + \frac{P}{\sqrt{\pi a}} \sqrt{\frac{a+b}{a-b}}}{2} \right) \quad (31)$$

$$K = \sigma \sqrt{\pi a'} \quad (32)$$

Equating 31 and 32, the ancillary crack size a' was found:

$$a' = \frac{\left[\sigma \sqrt{\pi \frac{a}{Q}} M_e f_b \sqrt{\sec \frac{\pi D}{2W}} \cdot F_{int} + \left(\frac{S_3 \sqrt{\pi \frac{a}{Q}} M_e f_b \sqrt{\sec \frac{\pi D}{2W}} \cdot F_{int} + \frac{P}{\sqrt{\pi a}} \sqrt{\frac{a+b}{a-b}}}{2} \right) \right]^2}{\pi \sigma^2}$$

The ancillary crack was the baseline for the compounding method, and it was placed into known configurations to compute geometrical correction factors for all boundaries. Classical textbook SIFs solutions used in the MSD model were presented by Rooke and Cartwright [65] and were presented in Figure 3-15 thru Figure 3-21. Crack configurations considered in the MSD model included: central crack with adjacent hole placed to the right subjected to remote tensile stress, central crack with adjacent hole placed to the left subjected to remote tensile stress, two unsymmetrical collinear cracks with applied remote tensile stress, and finally, a finite plate with eccentric crack, accounting therefore for the edge effect. Stress intensity factors were calculated for each crack tip used in the MSD model, which included lead crack, opposite crack and MSD adjacent cracks. Polynomial functions were generated applying linear regression to implement SIF solutions using VBA automated routine.

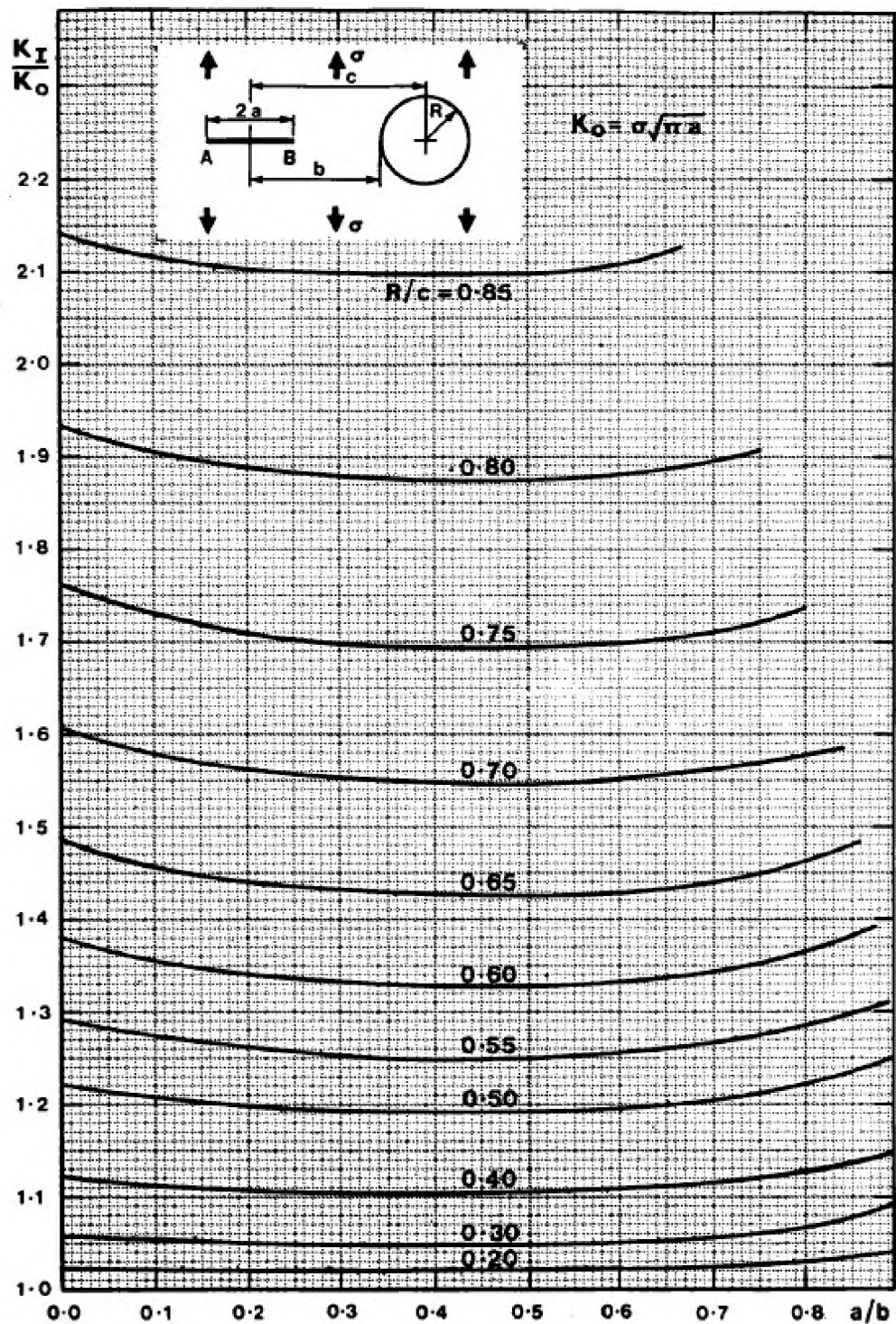


Figure 3-15 Cracks near a Circular Hole, Remote Stress Tip A [65].

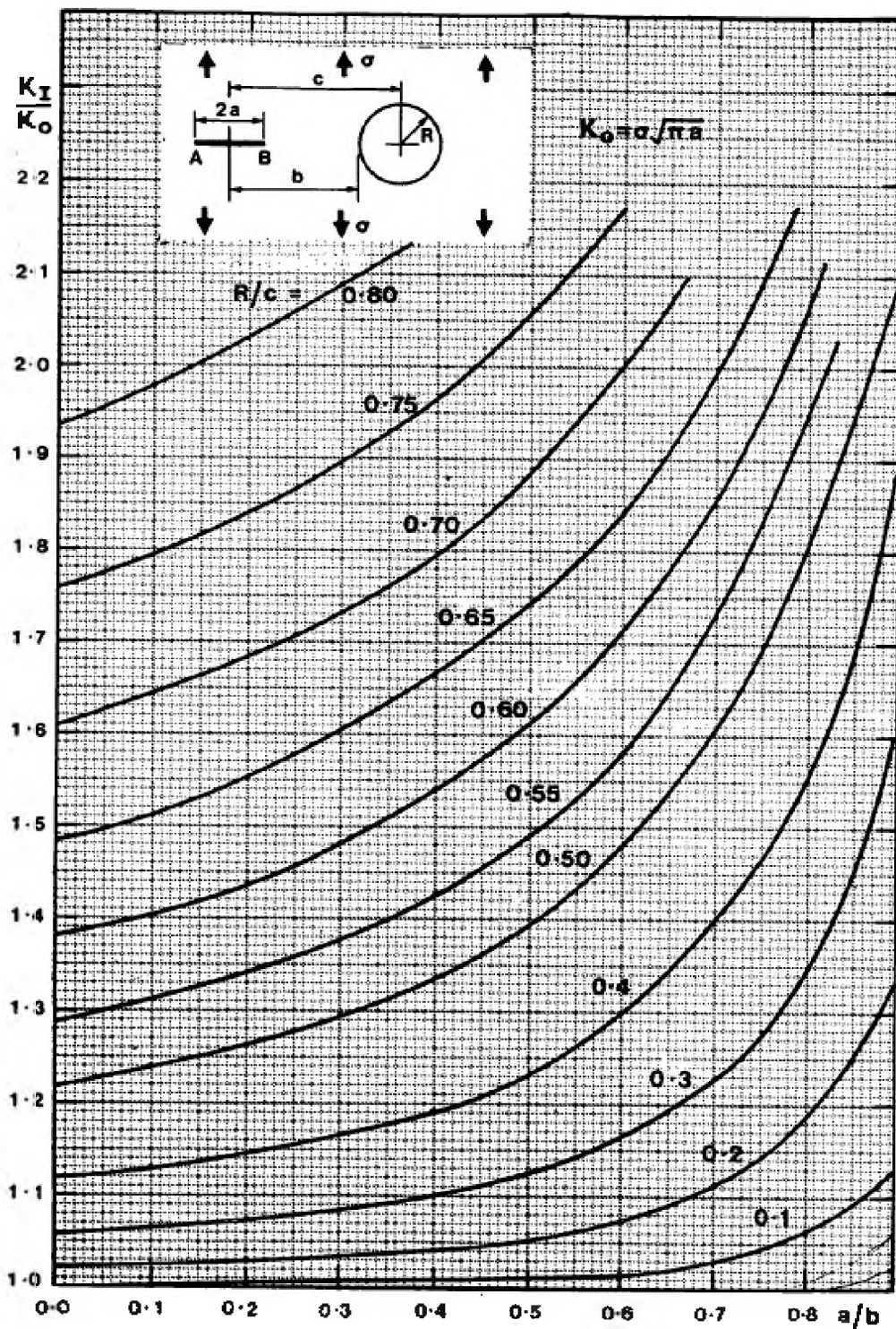


Figure 3-16 Cracks near a Circular Hole, Remote Stress Tip B [65].

According to Rooke and Cartwright [65], the stress intensity factors for two unequal collinear cracks subjected to remote stress (Figure 3-17) can be expressed in terms of the coordinates of the crack tips. Placing the coordinate system origin at Tip B, the coordinates of the remaining tips are calculated as follows:

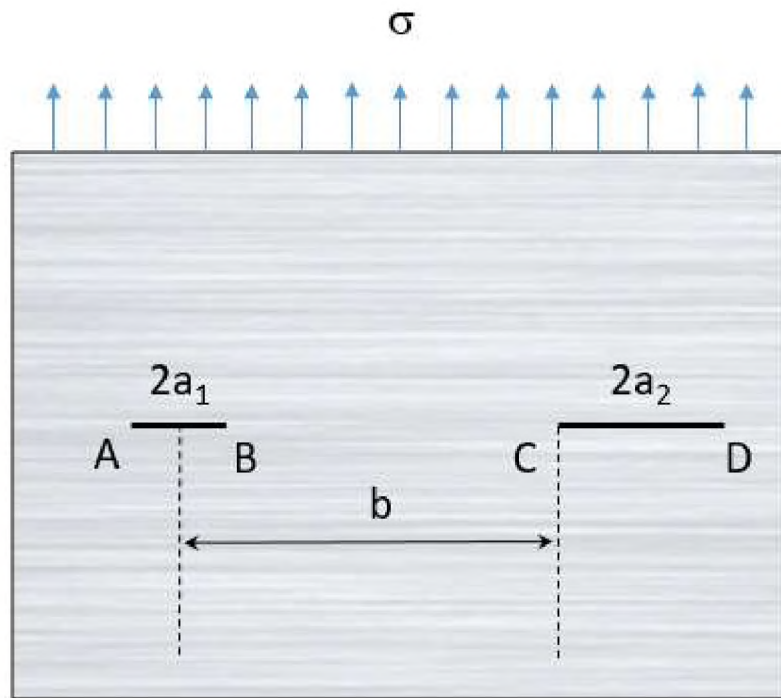


Figure 3-17 Two Unequal Cracks Subjected to Remote Stress.

$$x_A = \frac{2a_1}{b} \quad (33)$$

$$x_C = \frac{1-a_1}{b} \quad (34)$$

$$x_D = \frac{1-a_1}{b} + \frac{2a_2}{b} \quad (35)$$

The stress intensity factors for each crack tip are determined using the following tips. Crack Tip A is:

$$\frac{K_I}{K_0} = \sqrt{\frac{2\pi b}{a_1} \left[\frac{x_A^2 - C_1 x_A + C_2}{x_A(x_A + x_C)(x_A + x_D)} \right]} \quad (36)$$

Crack Tip B is:

$$\frac{K_I}{K_0} = - \sqrt{\frac{2\pi b}{a_1} \left[\frac{C_2}{\sqrt{x_A x_C x_D}} \right]} \quad (37)$$

Crack Tip C is:

$$\frac{K_I}{K_0} = - \sqrt{\frac{2\pi b}{a_2} \left[\frac{x_C^2 + C_1 x_C + C_2}{\sqrt{x_C(x_A + x_C)(x_D - x_C)}} \right]} \quad (38)$$

Crack Tip D is:

$$\frac{K_I}{K_0} = - \sqrt{\frac{2\pi b}{a_2} \left[\frac{x_D^2 + C_1 x_D + C_2}{\sqrt{x_D(x_D + x_A)(x_D - x_C)}} \right]} \quad (39)$$

The constants C_1 and C_2 are determined using:

$$C_1 = \frac{(x_A - x_D)K(k) - 2x_A\Pi(n,k) + 2x_D\Pi(m,k) + (x_A + x_D)[J(n,k) - J(m,k)]}{K(k) - \Pi(n,k) - \Pi(m,k)} \quad (40)$$

$$C_2 = \frac{C_1}{K(k)} [x_A K(k) - (x_A - x_D)\Pi(n,k)] - \frac{1}{K(k)} [x_A^2 K(k) - 2x_A(x_A + x_D)\Pi(n,k) + (x_A + x_D)^2 J(n,k)] \quad (41)$$

where $K(k)$ is the elliptic integral of first kind, and $\Pi(n,k)$ and $\Pi(m,k)$ are elliptic integrals of the third kind. J is defined as:

$$J_{(t,k)} = \int_0^{\frac{\pi}{2}} \frac{d\phi}{(1+t\sin^2\phi)^2 \sqrt{1-k^2\sin^2\phi}}, \quad (42)$$

where the parameters n, m and k are given by:

$$n = \frac{x_D - x_C}{x_A + x_C} \quad (43)$$

$$m = \frac{x_A}{x_D} \quad (44)$$

$$k^2 = mn \quad (45)$$

The plots of SIF for crack tips A, B, C and D are shown in Figure 3-18 to Figure 3-21.

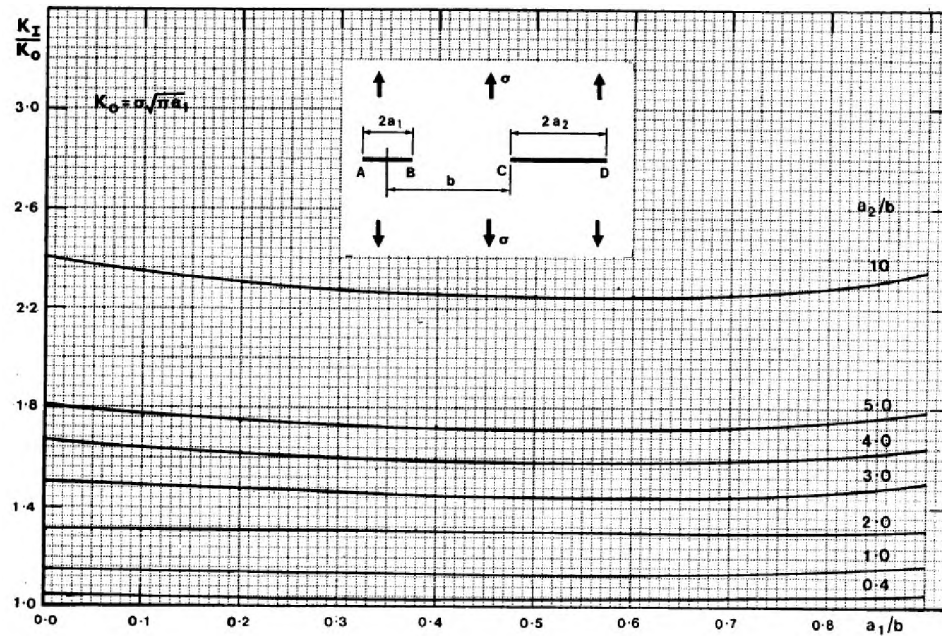


Figure 3-18 SIF for Two Unequal Cracks Subjected to Remote Stress Tip A [65].

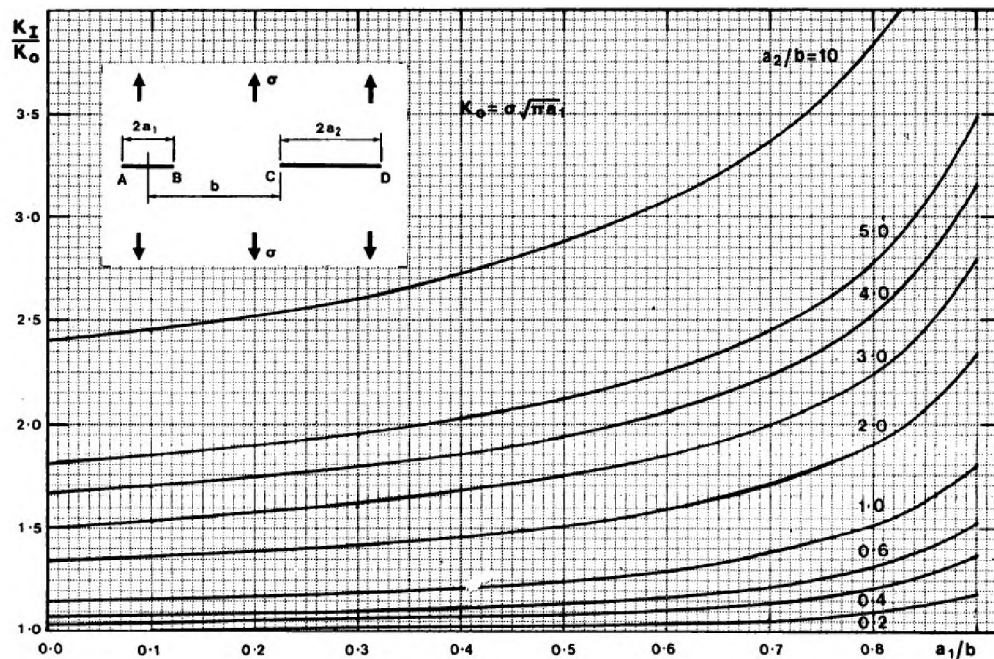


Figure 3-19 SIF for Two Unequal Cracks Subjected to Remote Stress Tip B [65].

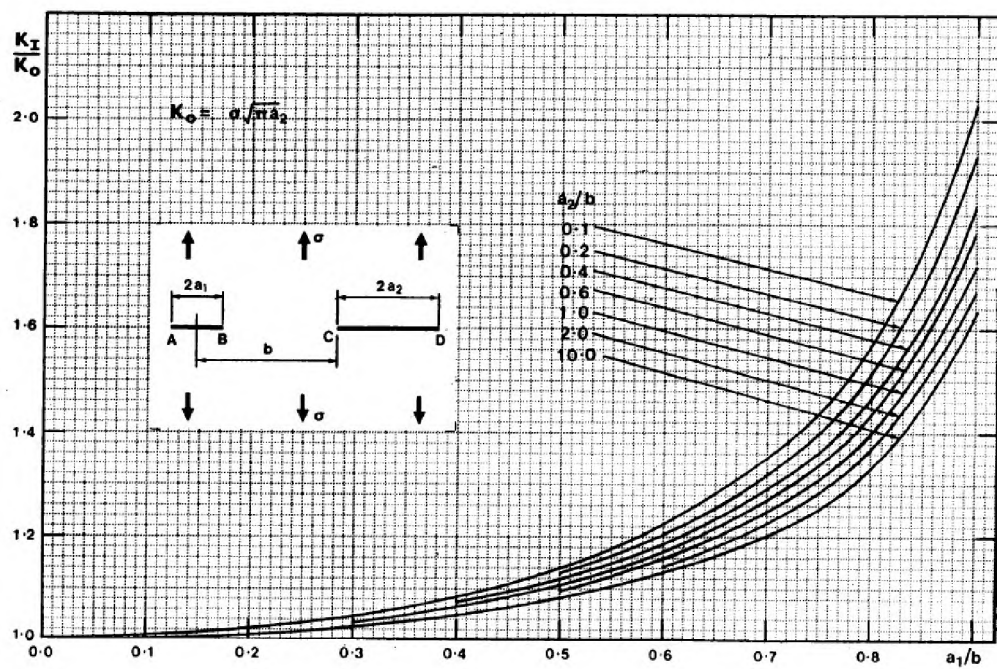


Figure 3-20 SIF for Two Unequal Cracks Subjected to Remote Stress Tip C [65].

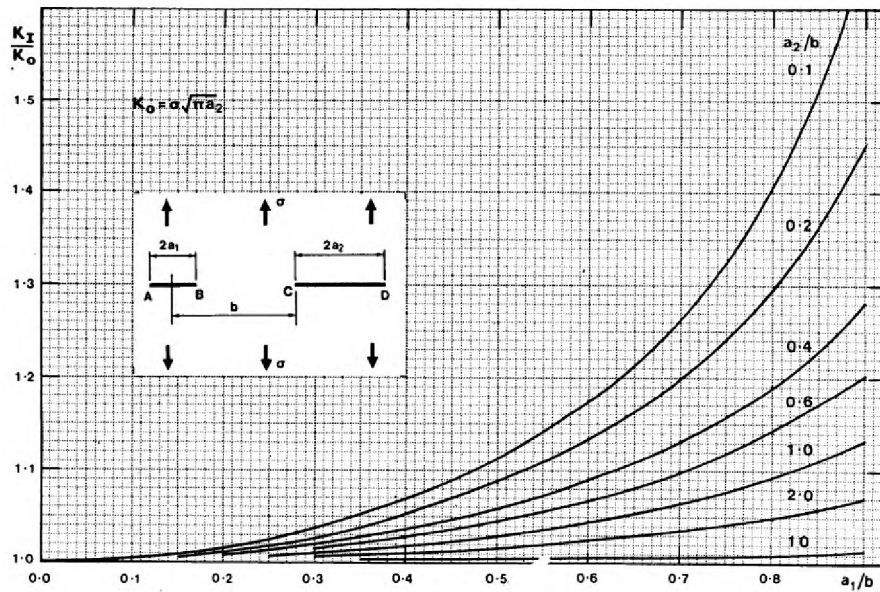


Figure 3-21 SIF for Two Unequal Cracks Subjected to Remote Stress Tip D [65].

After stress intensity factors were calculated, the next step was to perform the crack growth assessment. Experimental results of fatigue crack propagation presented a statistical variability, or scatter, as discussed by Garcia [6] and Liao [25]. A randomized crack growth model, used by Garcia [6], was applied in this work. The basic idea was placing a normally distributed variable Z ($0, \sigma^2_z$) into the crack growth constant C used in the Paris equation. Taking log on both sides of Paris Law and adding the variable Z , leads to:

$$\log\left(\frac{da}{dN}\right) = \log(C) + n\log(\Delta K) + Z \quad (46)$$

By assuming the properties of lognormal distribution with zero mean and standard deviation equal to one, $N(0, 1)$, the probability of a experiment falls in the range $Z \leq Z_p$ is given by $P(Z \leq Z_p) = p$ [6]. Where Z_p is calculated by:

$$Z_p = \alpha_p \sigma_z \quad . \quad (47)$$

The probabilistic model described in Equation 46 can be simplified if constant n is assumed as a mean value, and the stochastic nature of crack propagation is accounted for by constant C , where normal distribution was assumed. This simplification is a common practice, and it was employed in different crack growth probabilistic models [6, 66]. Therefore, Equation 46 can be re-written as:

$$\log\left(\frac{da}{dN}\right)_p = \log(C)_p + n \log(\Delta K) \quad , \quad (48)$$

where,

$$\log(C)_p = \log(C) + \alpha_p \sigma_z \quad . \quad (49)$$

where α_p is random number following Normal distribution $N\{(0, 1)\}$, that was generated using Box-Muller transformation, as described in section 3.1.1, and σ_z is the crack propagation curve standard deviation.

Crack increment sizes were determined for each crack tip along the MSD model, which required the following sequences to be applied: The first step was to calculate the number of cycles ΔN required to grow a pre-defined crack increment Δa , which was done by integrating the da/dN versus ΔK expression. It was assumed the stress intensity factor remained constant during the crack growth period (from a to $a+\Delta a$). To satisfy this condition, a small crack increment was required, and a typical $\Delta a = 0.00127$ mm was used in this work. That yields:

$$\frac{dN}{da} = \frac{1}{C(\Delta K)^n} \quad , \quad (50)$$

therefore

$$\Delta N = \frac{1}{C} \int_{a_i}^{a_i+\Delta a} \frac{1}{(\Delta K)^n} da \quad . \quad (51)$$

Equation 51 was solved using Simpson (3-Points) numerical integration, as described in [67]:

$$\int_{x_0}^{x_2} f(x) dx = \frac{h}{3} [f(x_0) + 4f(x_1) + f(x_2)] - \frac{h^5}{90} f^{(4)}(\xi) \quad . \quad (52)$$

The fourth derivative term $f^{(4)}(\xi)$ represents the error, which can be neglected because the integral gives the exact solution when a polynomial of degree three or less is applied. Therefore, the following expressions were obtained:

$$y = f(x) = \frac{1}{(\Delta K)^n} \quad (53)$$

$$\Delta N = \frac{\Delta a}{3} [y_0 + 4y_1 + y_2] \quad . \quad (54)$$

when Equation 54 was performed for each crack tip along the MSD model, it was possible to determine the shortest interval, or fastest-growing tip, defined as ΔN_{min} . By assuming ΔN_{min} as the integration limit, it was possible to determine the increment sizes for all other crack tips, as:

$$\Delta a_i = C \int_N^{N+\Delta N_{min(j)}} (\Delta K)^n dN \quad . \quad (55)$$

Using the Equation 52 integration, and the assumption that stress intensity factor remained constant, the increment sizes were determined to be:

$$\Delta a_i = \frac{3\Delta N_{min(j)}}{6(C\Delta K_i^n)} \quad , \quad (56)$$

where

j = fastest-growing crack tip

i = all other crack tips ($i \neq j$).

3.1.3. Failure Criterion. Plastic Zone Touch (PZT) criterion proposed by Swift [42] was employed as the failure criterion for the MSD model. According to Swift [4], the link-up takes place when the plastic zones in front of the crack tips touch each other (Figure 3-22). The plastic zones (plane stress) were calculated based on Irwin's 2nd order estimate in [51];

$$r_{p(i)} = \frac{1}{\pi} \left(\frac{K_{I(i)}}{\sigma_Y} \right)^2, \quad (57)$$

where $K_{I(i)}$ is the opening mode SIF for the i^{th} crack, and σ_Y is the material yielding strength, where $i = 1$ (lead crack) and $i = 2$ (MSD crack). The following algorithm was implemented in the MSD model as a failure criterion check:

$$A_{\text{net}} = (L - d - a_1 - a_2 - r_{p1} - r_{p2}) \quad (58)$$

If $A_{\text{net}} \geq 0.0001$, then

$\Delta a_1 \rightarrow$ lead crack increment crack size

$\Delta a_2 \rightarrow$ MSD crack increment size

Else

Stop crack propagation;

Go to the Next Scenario.

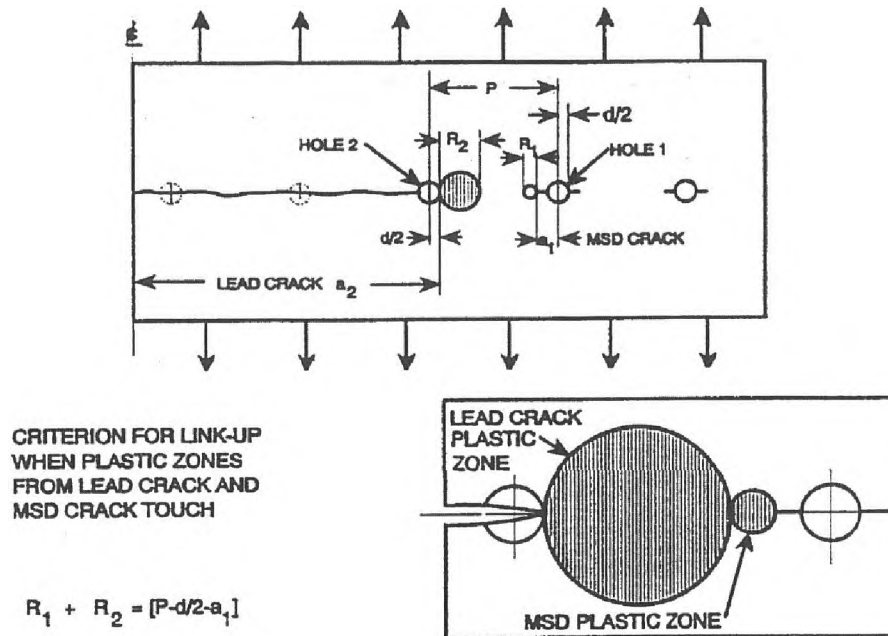


Figure 3-22 Plastic Zone Touch or Link-Up Model Suggested by Swift [4].

The first link-up as a failure criterion was demonstrated to be adequate from an engineering safety standpoint, which was corroborated by fatigue tests performed with lap joint panels, as shown in Figure 3-23. As presented in [16], after the first link-up occurrence at 106,217 cycles, the panel reached final failure after accumulating 1,241 cycles. Therefore, adopting the first failure criterion as a first link-up was conservative, and it was validated by experiments.

In addition to the link-up failure check, fracture toughness criterion was also employed in the MSD automated tool. If any crack tip stress intensity factors exceeded the fracture toughness for plane strain condition (K_{IC}), the crack growth was interrupted, and the program moved to the next Monte Carlo simulation scenario. The SIF of any crack tip, defined as K_i , was checked using for the following criteria:

$$K_i \leq K_{IC} \quad (59)$$

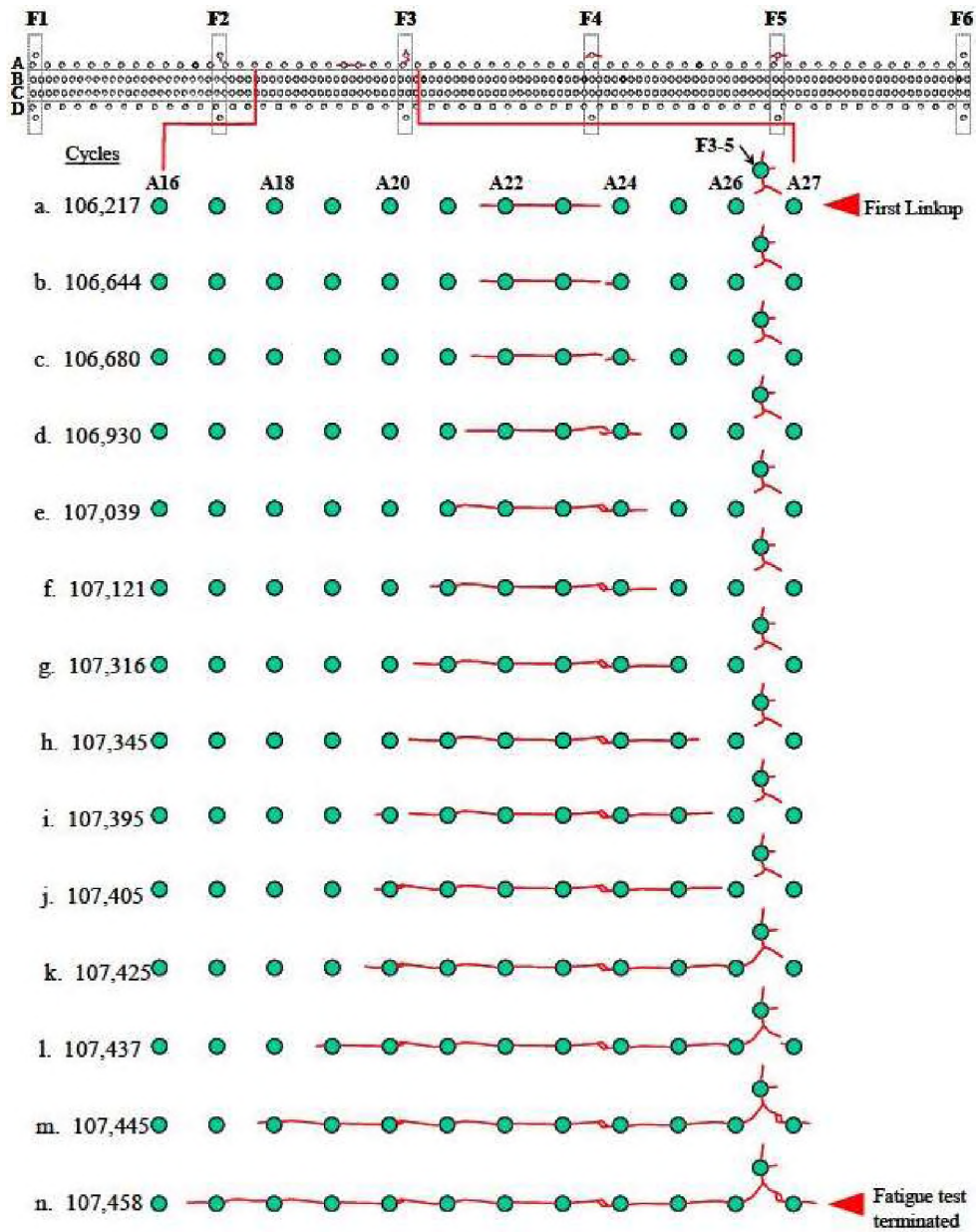


Figure 3-23 Example of Lead Crack Propagation after Link-Up [16].

4. RESULTS AND DISCUSSIONS

In this section, the results of MSD methodology discussed in Section 3 were presented. To validate the employed methods and assumptions, the Monte Carlo simulation results were compared against other numerical methodologies and experimental results published by other researchers. A typical fuselage structure lap joint analyzed by Garcia [6] was reproduced in Figure 4-1. The skin panel was made of Aluminum 2024-T3 alloy, 1.6mm thick, and had three rivet rows with nine fasteners per row, yielding eighteen PCIS. Outer and inner panels were attached with solid rivets with diameters of 4.0 mm and installed 20 mm apart (pitch). The structure was subjected to a remote tensile stress of 100 MPa, and the stress ratio $R = 0$. Geometrical details are:

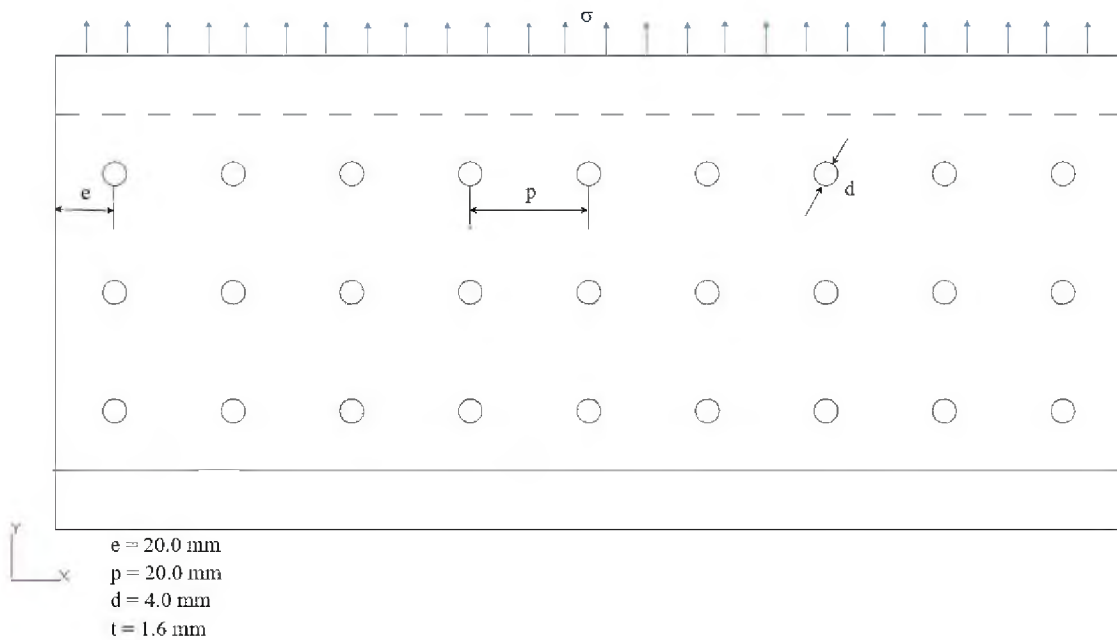


Figure 4-1 Analyzed Lap Joint.

The material properties used were outlined by [6], with Yielding Strength $\sigma_y = 331$ MPa and fracture toughness (plane strain) $K_{IC} = 1012 \text{ MPa}\cdot\text{mm}^{1/2}$. As described in Section 3, the Paris model was used for crack growth analysis, where the following constants were assumed: $C = 6.09\text{E-}11 \text{ mm/cycle}$, and $n = 2.6$. Stochastic nature of crack growth curve was accounted by assuming $\sigma_z = 0.043$ (log-scale), as suggested by Garcia [6]. The mean life for fatigue crack initiation (S-N) curve, and the respective standard deviation are required input data for a MSD model, and they were extracted from [6], as shown:

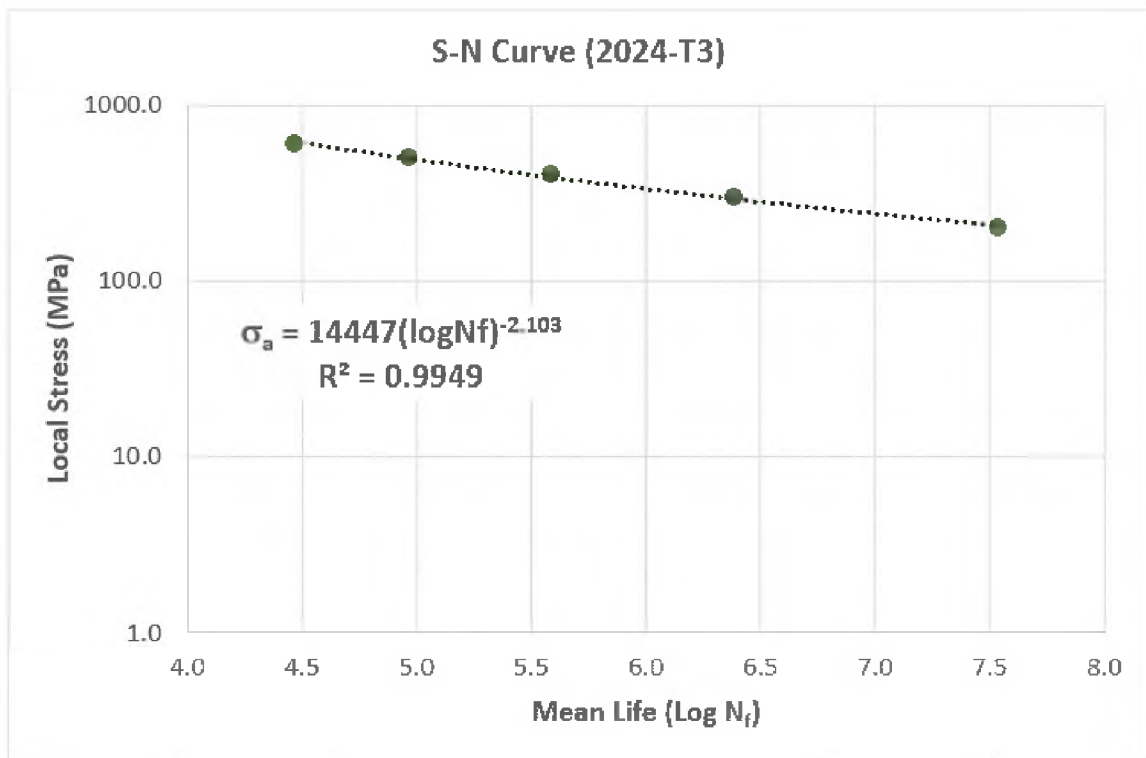


Figure 4-2 2024-T3 Mean Life ($\log N_f$) for Fatigue Crack Initiation.

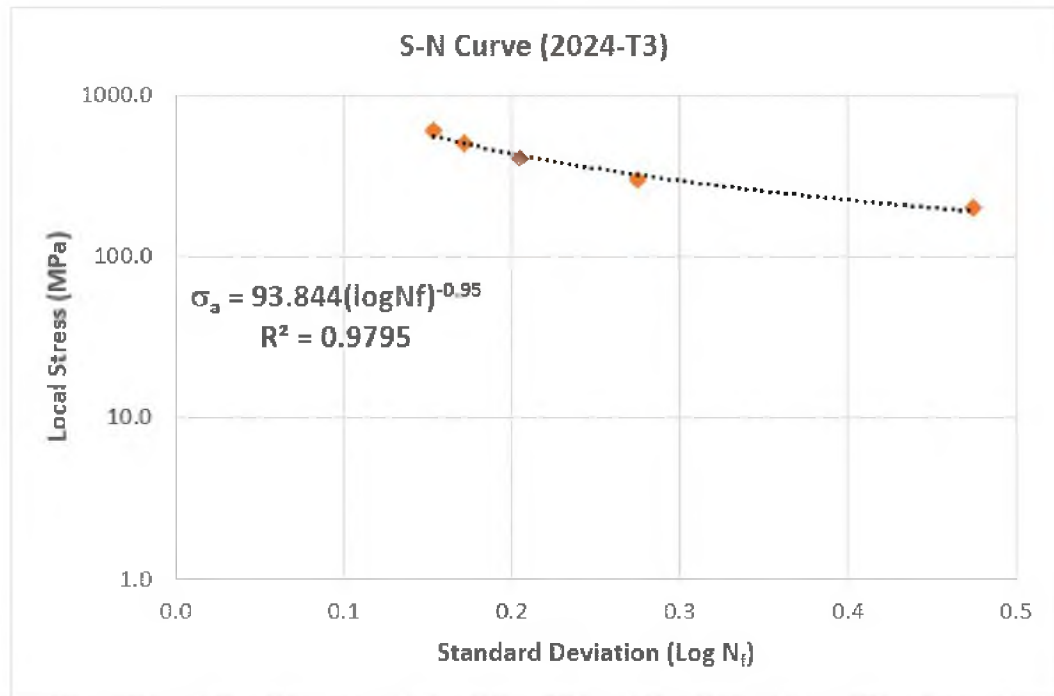


Figure 4-3 2024-T3 Standard Deviation ($\log N_f$) for Crack Initiation.

The equations shown in Figure 4-2 and Figure 4-3, were re-written to solve for mean life (μ) and standard deviation (σ) as a function of alternate stress (σ_a), and they were applied in the present MSD assessment methodology along with Equation 1:

$$\mu = \log(N_f) = 10^{\frac{\log\left(\frac{\sigma_a}{1447}\right)}{-2.103}} \quad (60)$$

$$\sigma = 10^{\frac{\log\left(\frac{\sigma_a}{93.844}\right)}{-0.95}} \quad (61)$$

The number of cycles to initiate a fatigue crack (log-scale) was presented in Figure 4-2 as a function of local stress, and not remote stress as usually found in classical fatigue textbooks [45,67], and material database. Garcia [6] used DBEM to calculate the local stresses for each PCIS when a remote stress of 100 MPa was applied. The model also

included the effect of the fastener bearing load acting on each PCIS. The obtained stresses for each PCIS were reproduced in Figure 4-4.

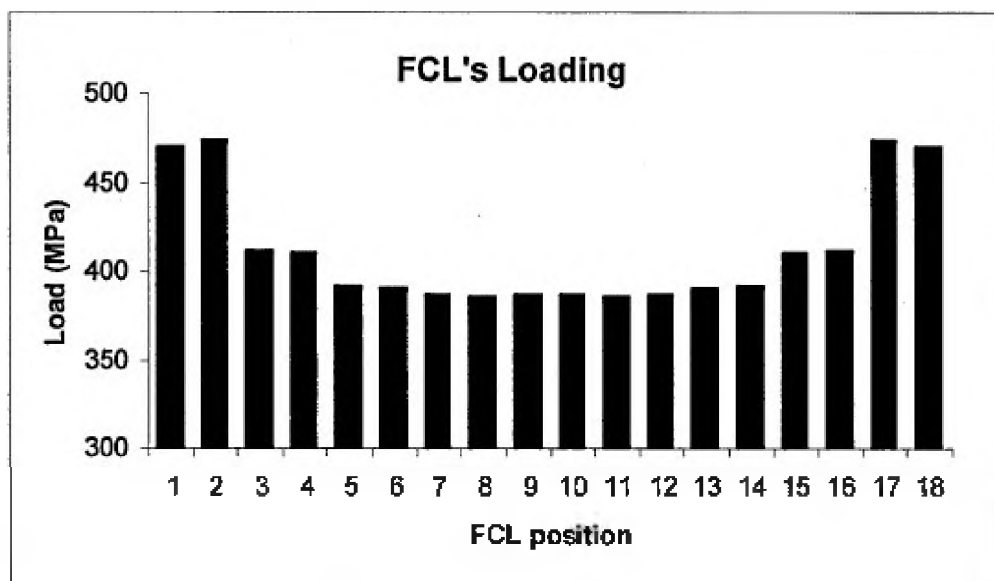


Figure 4-4 Local Stresses as a Function of PCIS [6].

The current work used 392.88 MPa, which represents the average stress of 18 FCLs presented in Figure 4-4 as an input for the MSD assessment. The rationale for this simplification was based on the fact that the stresses acting on real fuselage lap joint structures, constructed with skin, stringers and frames can be considered as uniform.

Fastener loads (N/mm) for the external row were determined via NASTRAN FEA, which represented the lap joint configuration by employing shell elements (CQUAD4) connected via fastener elements (CBAR and CBUSH), are shown in Table 4-1.

It was observed from Table 4-1, that an initial crack size of 1.0 mm was used for the lead crack. This differed from what was proposed in Section 3, and it was required to compare MSD results against the results published by Garcia [6].

Table 4-1 MSD Model Input Data.

N° Simulations	400	
N° Randon	7200	
N° Fasteners	9	
Stress	392.88	MPa
Panel Geometry		
Width	200.00	mm
Thickness	1.60	mm
Fastener Pitch	20.00	mm
Edge Margin	20.00	mm
Fastener Diameter	4.00	mm
Initial Crack Sizes		
Lead Crack	1.000	mm
Opposite Crack	0.127	mm
MSD cracks	0.127	mm
Crack Growth		
Remote Stress	100	MPa
C	6.09E-11	
m	2.6	
Kc	1012	Mpa.mm ^{1/2}
σ_y	331	MPa
Fastener # Load (N/mm)		
1	726.00	
2	726.00	
3	565.00	
4	565.00	
5	512.00	
6	512.00	
7	498.00	
8	498.00	
9	495.00	
10	495.00	
11	498.00	
12	498.00	
13	512.00	
14	512.00	
15	565.00	
16	565.00	
17	726.00	
18	726.00	

A total of 400 Monte Carlo simulations were performed, during which fatigue Total Time to Crack Initiation (TTCI) and its subsequent crack growth phase up to link-up, Total Time to Crack Propagation (TTCP) were calculated for all 18 Potential Crack Initiation Sites (PCIS). Simulation results and discussions are presented.

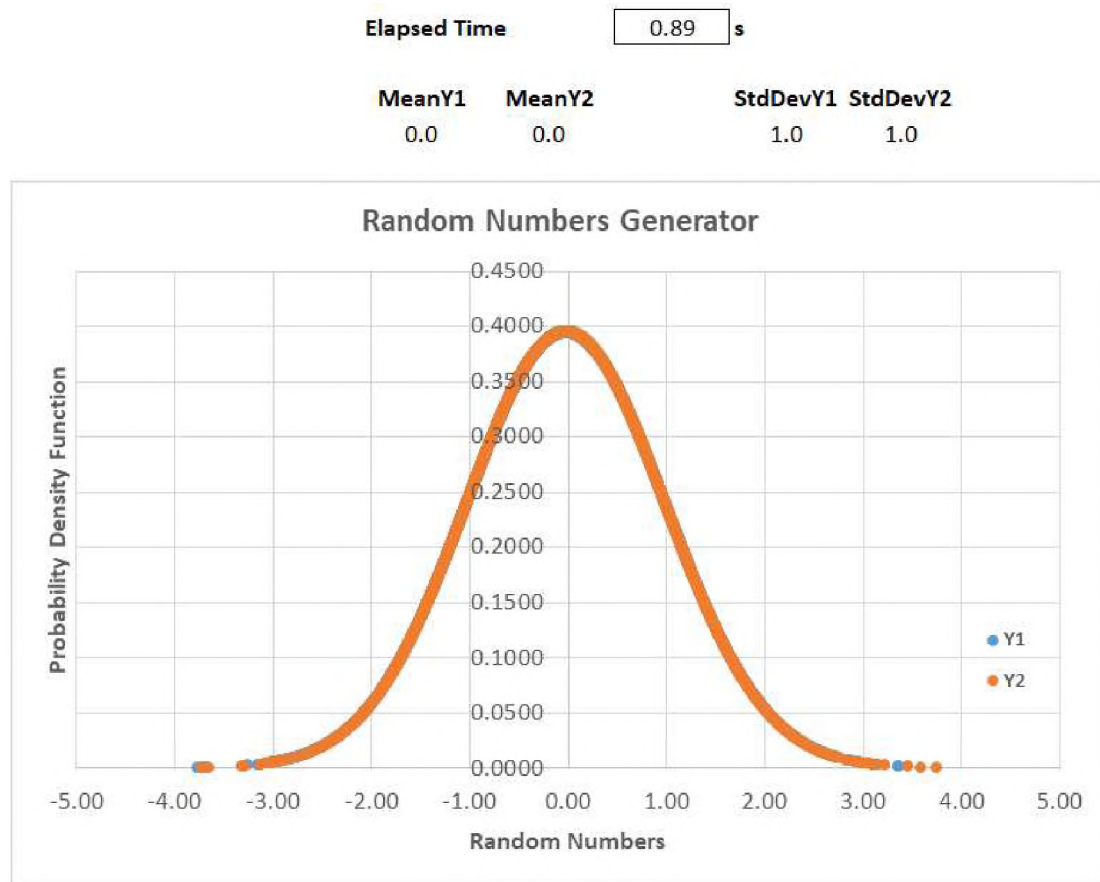


Figure 4-5 7,200 Pairs of Random Numbers Generated for the MSD Model.

As presented in Figure 4-5, 7,200 pairs of random numbers were generated following a Gaussian distribution with a mean of zero and standard deviation of one $\{0,1\}$ as proposed in Section 3. The elapsed time to generate the random numbers was 0.89 seconds, thus demonstrating the MSD tool efficiency for this step.

An unique random number was placed in each PCIS from #2 to #17 for each Monte Carlo simulation performed, therefore, accounting for the stochastic nature of fatigue crack initiation. This generated 400 different damage scenarios, as presented:

Table 4-2 Example of Damage Scenarios Generated via MSD Model.

MCS PCIS	1	2	3	4	5	6	7	8	9	10
	Cumulative Damage									
2	0.50	0.26	0.47	0.48	0.42	0.25	0.14	0.23	0.30	0.14
3	0.72	1.00	0.93	0.35	0.30	0.63	0.56	0.71	0.73	0.30
4	0.38	0.38	0.55	0.55	0.47	0.46	0.36	0.58	0.27	0.21
5	0.70	0.72	0.24	0.41	0.51	0.66	0.54	0.68	0.44	0.22
6	0.82	0.42	0.47	0.95	0.59	0.43	0.41	0.90	0.58	0.17
7	0.24	0.41	0.39	0.98	1.00	0.77	0.26	0.43	0.18	0.29
8	0.39	0.22	1.00	0.99	0.58	0.32	0.37	0.31	0.57	0.15
9	0.59	0.13	0.31	1.00	0.84	0.44	0.25	0.53	0.36	0.24
10	0.34	0.74	0.38	0.56	0.61	0.22	0.24	0.25	0.16	0.42
11	0.49	0.17	0.24	0.61	0.38	0.69	0.42	1.00	0.19	0.32
12	0.45	0.34	0.20	0.52	0.35	0.30	0.44	0.88	0.62	0.16
13	1.00	0.57	0.73	0.47	0.50	0.37	0.28	0.83	0.52	1.00
14	0.64	0.33	0.22	0.65	0.37	0.71	0.41	0.54	0.42	0.46
15	0.46	0.42	0.17	0.61	0.86	0.36	0.61	0.32	0.11	0.09
16	0.36	0.45	0.44	0.68	0.42	0.55	0.82	0.63	1.00	0.09
17	0.86	0.42	0.33	0.73	0.39	1.00	1.00	0.27	0.25	0.31

Table 4-2 presents the cumulative damage (D_i) obtained using the MSD automated tool for each PCIS. The rows numbered from #2 to #17 represented the PCIS. Note that for positions #1 and #18, the cumulative damage was not calculated, because random numbers were not assigned for these positions. This was meant to avoid single lead crack scenarios, which are addressed by traditional damage tolerance analysis, as explained in Section 3. Columns numbered from #1 to #400 (first 10 showed for simplicity) represented the number of Monte Carlo simulations performed. When fatigue damage is equal to 1.00 (highlighted in red), an initial lead crack of 1.0 mm is assigned, and an initial damage scenario was created. It was observed in Column 4, that PCIS #9 has cumulative damage equal to 1.00 (lead crack), while PCIS #8 has damage equal to 0.99. Position #8 was conservatively assigned with an initial crack of 0.127 mm, even before reaching damage equal to 1.00.

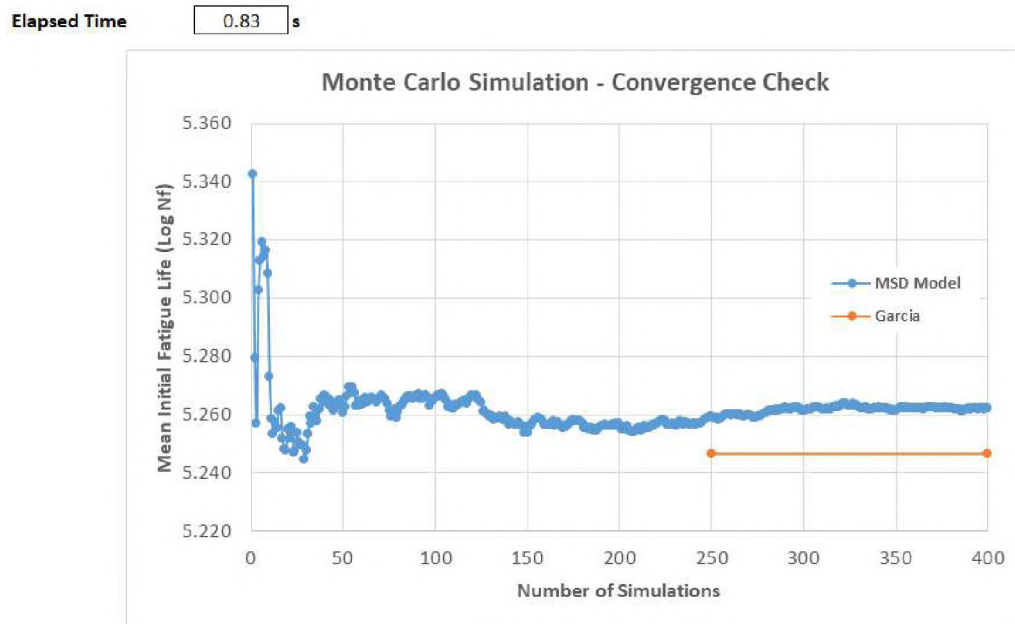


Figure 4-6 Mean Fatigue Life (TTCI) Convergence Check – 400 MCS.

Figure 4-6 presents the convergence check of fatigue mean life (TTCI) as a function from the number of Monte Carlo simulations performed. The difference in mean life obtained via the MSD model, when compared to Garcia's work [6], was attributed to the stress level applied to each PCIS. This work assumed a uniform stress of 392.88 MPa, while Garcia used non-uniform stress for each PCIS that ranged from 386.3 MPa, to 410.40 MPa, as shown in Figure 4-4

When a different stress was used, for example 396.00 MPa, the results obtained by the proposed MSD model were in 100% in agreement with ones obtained by Garcia, as demonstrated in Figure 4-7. Therefore, this study concluded that the proposed MSD assessment methodology presented accurate and reliable results for fatigue crack initiation life (TTCI) compared with other numerical methodologies [6].

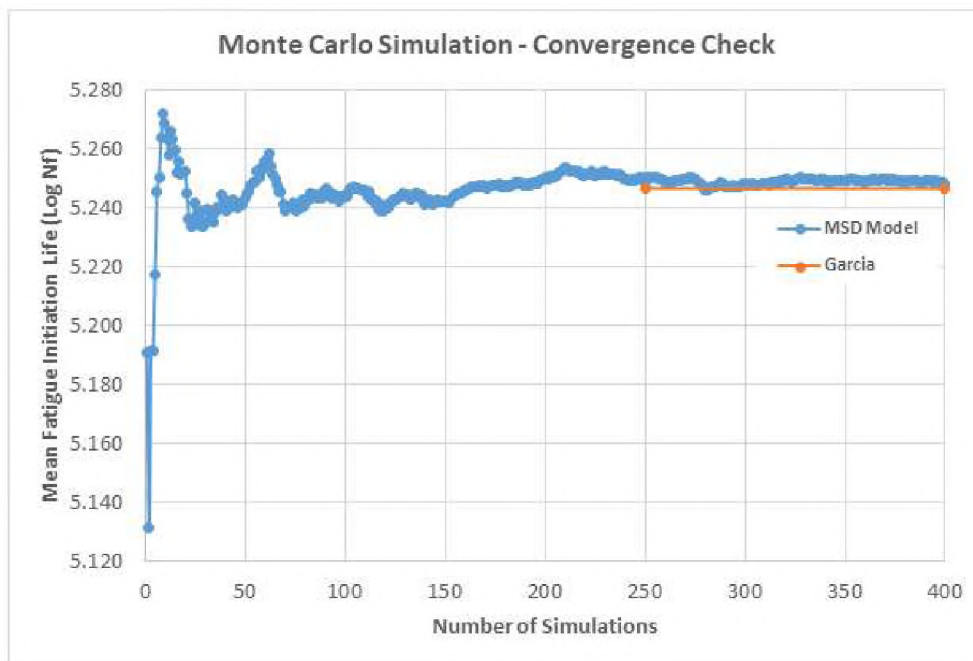


Figure 4-7 Mean Fatigue Life (TTCI) – 400 MCS for a Local Stress of 396 MPa.

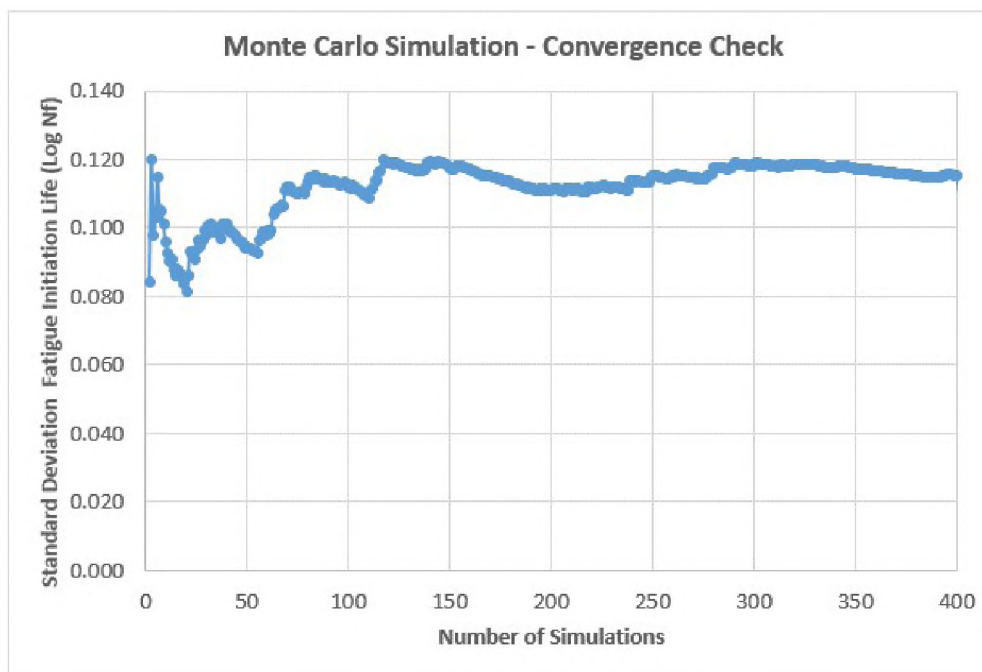


Figure 4-8 Standard Deviation (TTCI) Convergence Check – 400 MCS.

Figure 4-8 presents the standard deviation associated with mean life (TTCI) in Figure 4-7, as a function of the Monte Carlo simulation numbers. It was concluded from Figure 4-7 and Figure 4-8 that the Monte Carlo simulation converged when 300 simulations were performed.

In Figure 4-9, the numerical results for total fatigue life (TTCI+TTCP) are presented for 400 Monte Carlo simulations. The abscissa corresponded to total time to crack initiation, and the ordinate defined the total time to crack propagation. The numerical simulation results obtained via MSD model were compared against experimental data (TTCI) described in [6], which was reproduced in Table 4-3.

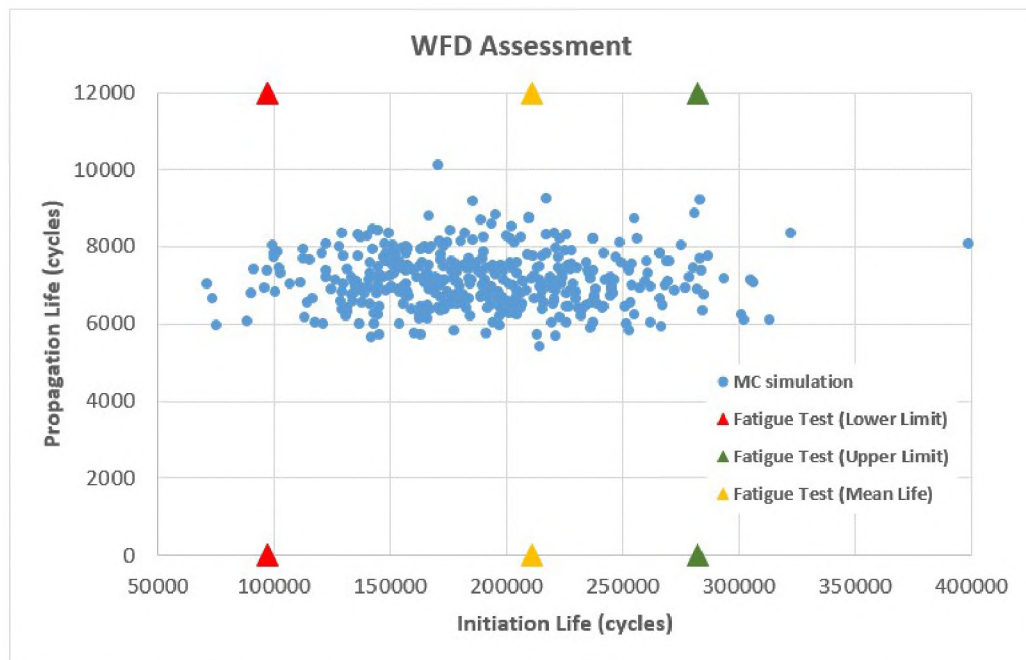


Figure 4-9 Distribution of Total Lives Compared with Fatigue Test Data.

To validate the proposed MSD assessment methodology, the TTCI obtained via the Monte Carlo simulation were compared to fatigue crack initiation life (TTCI) obtained from experiments, as shown in Table 4-3. Regarding the TTCP, direct comparison with experimental data presented in Table 4-3 was not possible because Garcia did not use first link-up as failure criterion; therefore, the number of cycles for crack growth from experiments averaged 67,642 cycles (Table 4-3), while numerically obtained ones averaged 7,148 cycles.

It was concluded that the numerical results from the MSD probabilistic methodology for TTCI predicted the fatigue scatter well, and most of data points were distributed between fatigue test lower limit (97,000 cycles) and upper limit (281,950 cycles).

Table 4-3 Experimental Fatigue Test Data Presented by Garcia [6].

Specimen no.	TTCI (cycles) $a_0 = 1.0 \text{ mm}$	TCP (cycles)	$N_f = \text{TTCI} + \text{TCP}$ (cycles)
1	280,900	85,200	366,100
2	281,950	85,111	367,061
3	201,700	36,200	237,900
4	201,950	68,150	270,100
5	200,000	85,368	285,368
6	97,000	45,827	142,827
Mean	210,583	67,642	278,226

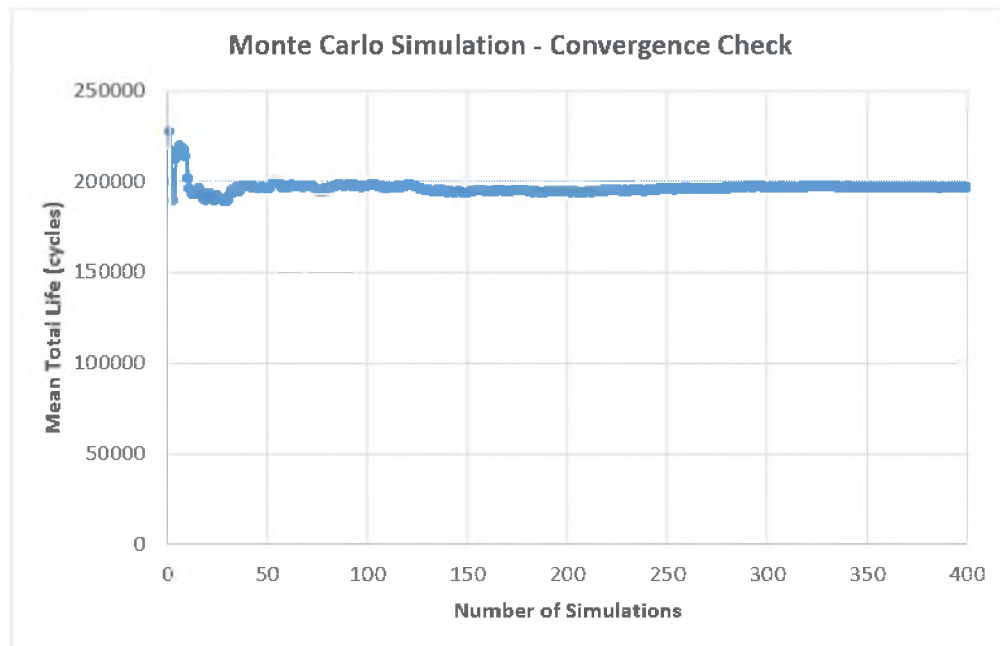


Figure 4-10 Fatigue Life (TTCI+TTCP) Convergence Check – 400 MCS.

Crack propagation life (Figure 4-9) ranged from 5,402 to 10,097 cycles. Convergence check for the total life (TTCI+TTCP) was performed and is shown in Figure 4-10. The life of 196,542 cycles was obtained via MSD model, and that was demonstrated to be a realistic number compared to that presented by Garcia [6] in Table 4-3, column TTCI+TCP, in which the first link-up was not used as failure criterion for the MSD model.

To validate crack growth life (number of cycles from crack nucleation to first link-up), MSD results were compared to previous data [26]. Wang [26] performed crack growth tests on five Al2024-T3 lap joints containing 3 fastener rows with 8 solid rivets per row, rivet diameters of 4.96 mm, installed 25.4 mm apart (pitch), plate thickness was 2.29 mm. Specimen #2 in Figure 4-11 was selected for comparison because 97 MPa was used as applied stress, which was closest when compared to proposed methodology. Initial crack lengths for each PCIS were presented in Table 4-4.

Crack growth tests were conducted by Wang [26] using dogbone test specimen which represented a lap joint configuration attached by 3 rows of fasteners, with 8 countersunk rivets per row. Saw blade was used to create an average 0.015 inches small notch at each side of all rivet holes. After cyclic load was applied to initiate cracks from saw-cut notches. The pre-cracking was performed at a frequency of 5Hz. Crack growth test results were presented in Figure 4-11.

Table 4-4 Initial Crack Length - Lap Joint Specimen #2 [26].

PCIS #	Fastener Number #	Initial Crack Length (mm)
1	1	0.127
2		0.127
3	2	0.127
4		0.551
5	3	0.851
6		0.953
7	4	2.837
8		2.344
9	5	3.264
10		1.956
11	6	0.010
12		0.272
13	7	0.041
14		0.124
15	8	0.127
16		0.127

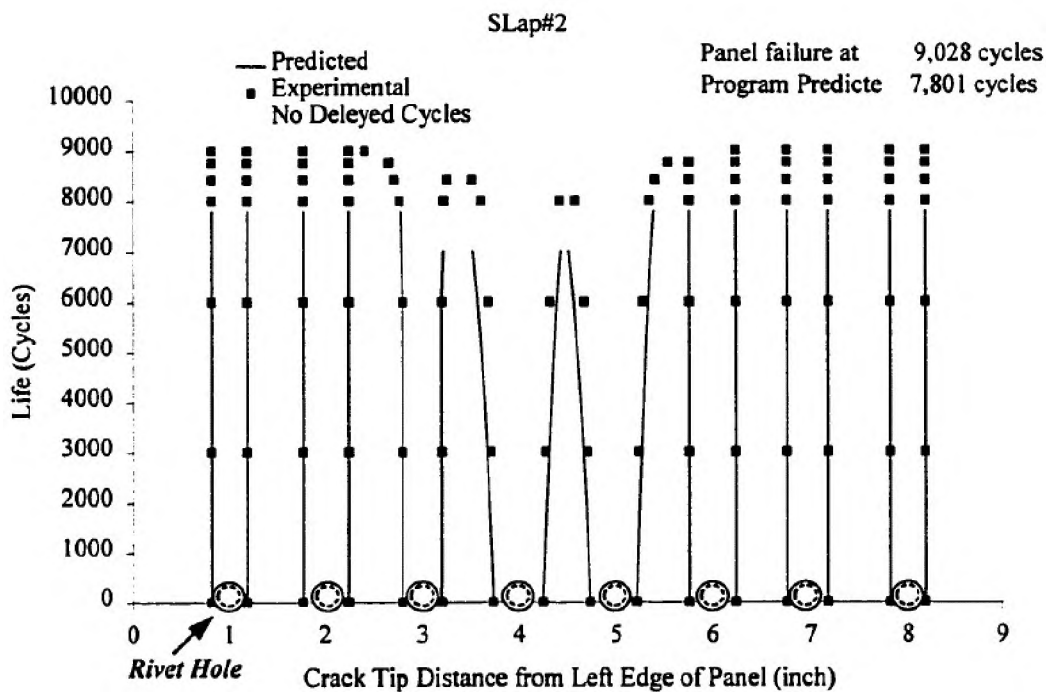


Figure 4-11 Experimental Results – Crack Propagation Test – Lap Joint #2 [26].

Figure 4-11 shows the crack growth experimental results in each fastener hole. The abscissa represents the fastener holes (1,2, ... 8), where each fastener has two crack fronts, one from the left and one from the right. The ordinate represents the number of cycles to grow the cracks. The black dots are experimental data and solid lines are numerical data obtained by Wang [26] simulations.

It was concluded from Figure 4-11 that first link-up occurred at 8,000 cycles, and final panel failure occurred at 9,028 cycles. Another evidence that the first link-up as failure criterion was an acceptable choice by the practical and safety standpoints.

The initial crack lengths for PCIS #8 and #9 (Table 4-4) were higher than the 1.27 mm used in the MSD model, as seen in Table 4-4. Panel 2.29 mm thick for specimens used for experiments versus 1.6 mm used in the numerical simulations. Experimental results

presented in Figure 4-11 were compared against Monte Carlo simulation scenario #133 results, where the lead crack was placed at PCIS #9, similar to specimen #2 presented in [26]. Only crack tips at fastener #5 and #6 were plotted because the MSD model accounted for primary, opposite, and adjacent secondary cracks only, as shown in Figure 4-12.

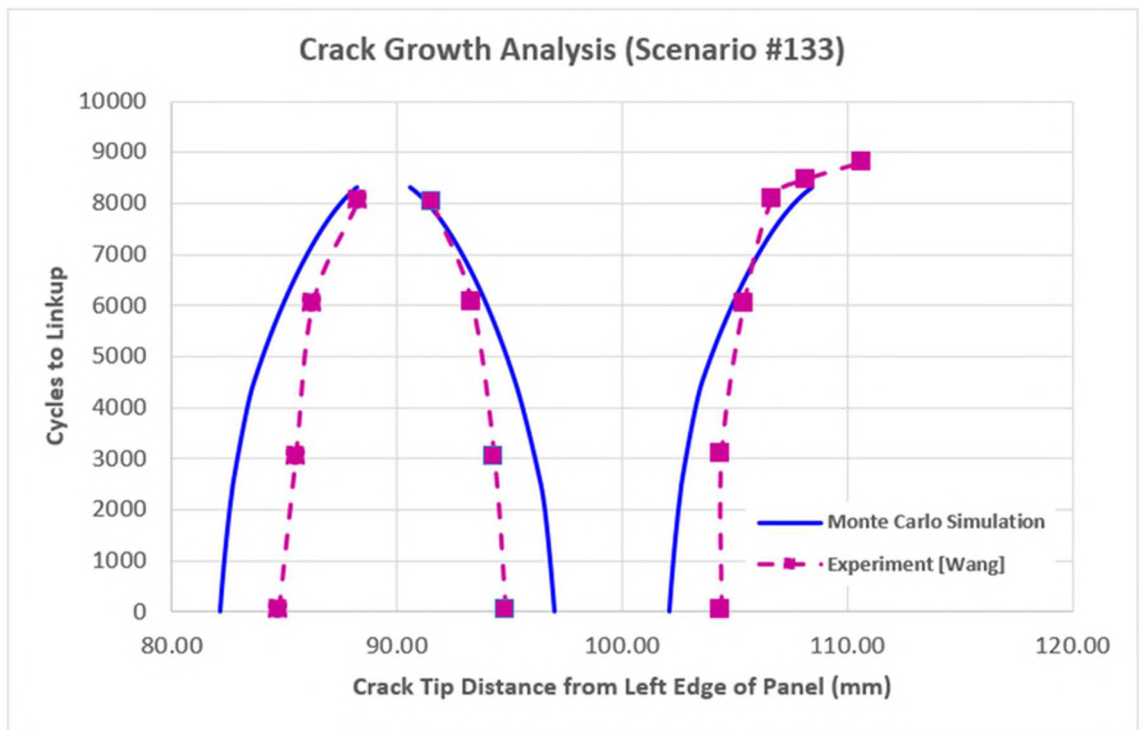


Figure 4-12 Crack Growth Analysis Compared to Experimental Data.

The cumulative density function (CDF) was computed considering the mean life presented in Figure 4-10 and its respective standard deviation. Results are presented in Figure 4-13.

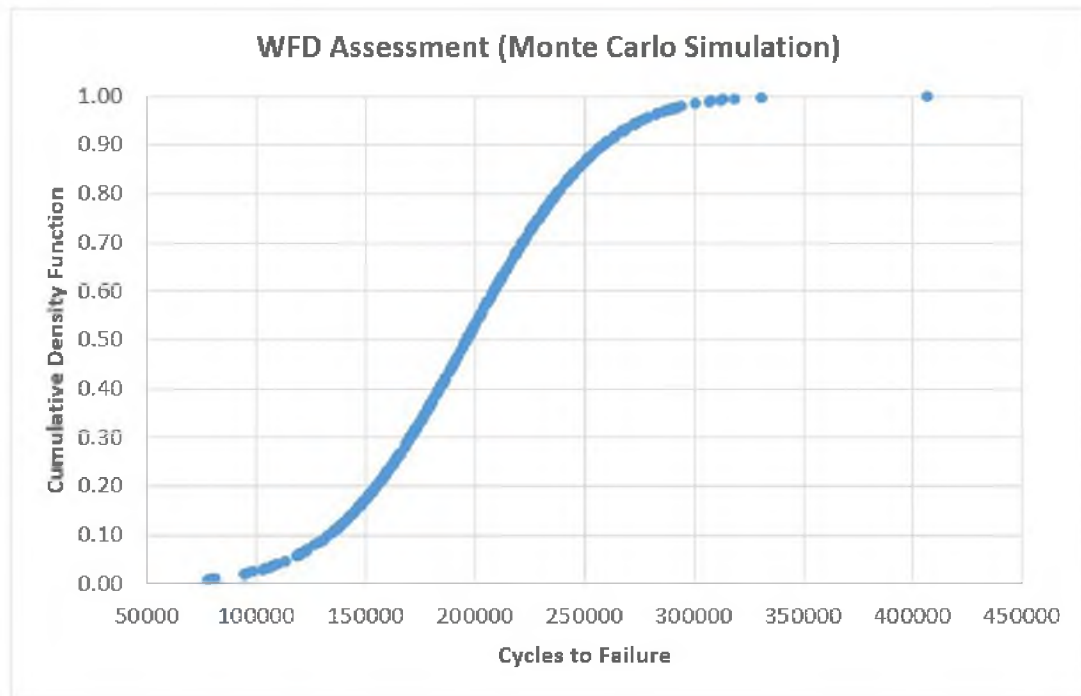


Figure 4-13 Widespread Fatigue Damage (WFD) – Cumulative Density Function.

The WFD parameters, Inspection Start Point (ISP) and Structural Modification Point (SMP), were calculated by considering 50% probability of failure, defined as $WFD_{(avg)}$ point. When 0.5 was considered on the ordinate, 196,542 cycles were obtained in the abscissa. According to the recommendations of Advisory Circular AC 120-104 [3], the ISP is determined by dividing the $WFD_{(avg)}$ by 3, and SMP by dividing $WFD_{(avg)}$ by 2. Therefore the following is true:

$$ISP = \frac{196,542}{3} = 65,514 \quad (62)$$

$$SMP = \frac{196,542}{2} = 98,271 \quad (63)$$

The obtained SMP was within the typical commercial aircraft Limit of Validity (LOV) that ranges from 20,000 to 100,000 flight cycles, as shown in Table 4-5 and Table 4-6. Recurring inspections dedicated to preclude the MSD onset were expected to be started at 65,514 cycles. Table 4-5 shows LOV for Airbus 300 series, which ranges from 30,000 to 48,000 flight cycles, and Table 4-6 presented typical LOVs for different aircraft manufacturers, including Bombardier, Embraer, Fokker, Lockheed and McDonald Douglas commercial models.

Table 4-5 Limit of Validity (LOV) for Airbus Models [68].

Airplane model	Compliance date—months after January 14, 2011	Default LOV (flight cycles (FC) or flight hours (FH))
Airbus—Existing ¹ Models Only:		
A300 B2-1A, B2-1C, B2K-3C, B2-203	30	48,000 FC
A300 B4-2C, B4-103	30	40,000 FC
A300 B4-203	30	34,000 FC
A300-600 Series	60	30,000 FC/67,500 FH
A310-200 Series	60	40,000 FC/60,000 FH
A310-300 Series	60	35,000 FC/60,000 FH
A318 Series	60	48,000 FC/60,000 FH
A319 Series	60	48,000 FC/60,000 FH
A320-100 Series	60	48,000 FC/48,000 FH
A320-200 Series	60	48,000 FC/60,000 FH
A321 Series	60	48,000 FC/60,000 FH
A330-200, -300 Series (except WV050 family) (non enhanced)	60	40,000 FC/60,000 FH

Table 4-6 Limit of Validity (LOV) of 4 Different Manufacturers [68].

Bombardier—Existing ¹ Models Only:		
CL-600: 2D15 (Regional Jet Series 705), 2D24 (Regional Jet Series 900)	72	60,000 FC
Embraer—Existing ¹ Models Only:		
ERJ 170	72	See NOTE.
ERJ 190	72	See NOTE.
Fokker—Existing ¹ Models Only:		
F.28 Mark 0070, Mark 0100	30	90,000 FC
Lockheed—Existing ¹ Models Only:		
L-1011	30	36,000 FC
188	30	26,600 FC
382 (all series)	30	20,000 FC/50,000 FH
McDonnell Douglas—Existing ¹ Models Only:		
DC-8, -8F	30	50,000 FC/50,000 FH
DC-9 (except for MD-80 models)	30	100,000 FC/100,000 FH
MD-80 (DC-9-81, -82, -83, -87, MD-88)	30	50,000 FC/50,000 FH
MD-90	60	60,000 FC/90,000 FH
DC-10-10, -15	30	42,000 FC/60,000 FH
DC-10-30, -40, -10F, -30F, -40F	30	30,000 FC/60,000 FH
MD-10-10F	60	42,000 FC/60,000 FH
MD-10-30F	60	30,000 FC/60,000 FH
MD-11, MD-11F	60	20,000 FC/60,000 FH

The numerical results obtained via MSD model (400 MCS) were compared to experimental data, as shown in Figure 4-9 and Figure 4-12. It demonstrated the abilities of the proposed MSD model and developed automated tool to accurately and efficiently predict the WFD behavior of real structures. It was concluded that the developed MSD automated tool represents a potential tool with practical aeronautical engineering applications, such as the design of new aircraft structures, the designs of repairs and alterations, and the study of future academic problems.

The proposed MSD model was also compared to the work of Galatolo and Lazzeri [69], who performed fatigue and crack growth experiments on Al2024-T3 lap joint structures with thickness of 2.0 mm, width of 300 mm, and 11 rivet rows spaced at 20.0 mm apart. The following material properties were taken from Galatolo and Lazzeri [69], $\sigma_y = 331$ MPa, $K_{IC} = 1423$ MPa.mm^{1/2}, $C = 5.0 \times 10^{-12}$ mm/cycles and $m = 2.94$. The applied remote tensile stress was 120 MPa. Fatigue mean life (μ) and standard deviation (σ) were assumed to follow [28], as described below:

$$\mu = 10^5 \left(\frac{S-58}{176-58} \right)^{-2.28} \quad (64)$$

$$\sigma = \frac{2169}{S^2} + \frac{1.299}{S} + 0.028 \quad (65)$$

Table 4-7 MSD Model Input Data – 400 MCS 120 MPa.

N° Simulations	400	
N° Random	9000	
N° Fasteners	11	
Stress	120	MPa

SN Curve		
S _{endurance}	58.00	MPa
FQI	176.00	MPa
p	-2.28	
A	2169.90	
B	1.299	
C	0.028	

Fastener #	Load (N/mm)
1	726.00
2	726.00
3	565.00
4	565.00
5	512.00
6	512.00
7	498.00
8	498.00
9	498.00
10	498.00
11	495.00
12	495.00
13	498.00
14	498.00
15	498.00
16	498.00
17	512.00
18	512.00
19	565.00
20	565.00
21	726.00
22	726.00

Panel Geometry		
Width	300.00	mm
Thickness	2.00	mm
Fastener Pitch	20.00	mm
Edge Margin	40.00	mm
Fastener Diameter	4.80	mm

Initial Crack Sizes		
Lead Crack	1.270	mm
Opposite Crack	0.127	mm
MSD cracks	0.127	mm

Crack Growth		
Remote Stress	120	MPa
C	5.00E-12	
m	2.9327	
Kc	1423	Mpa.mm ^{1/2}
σ_y	331	MPa

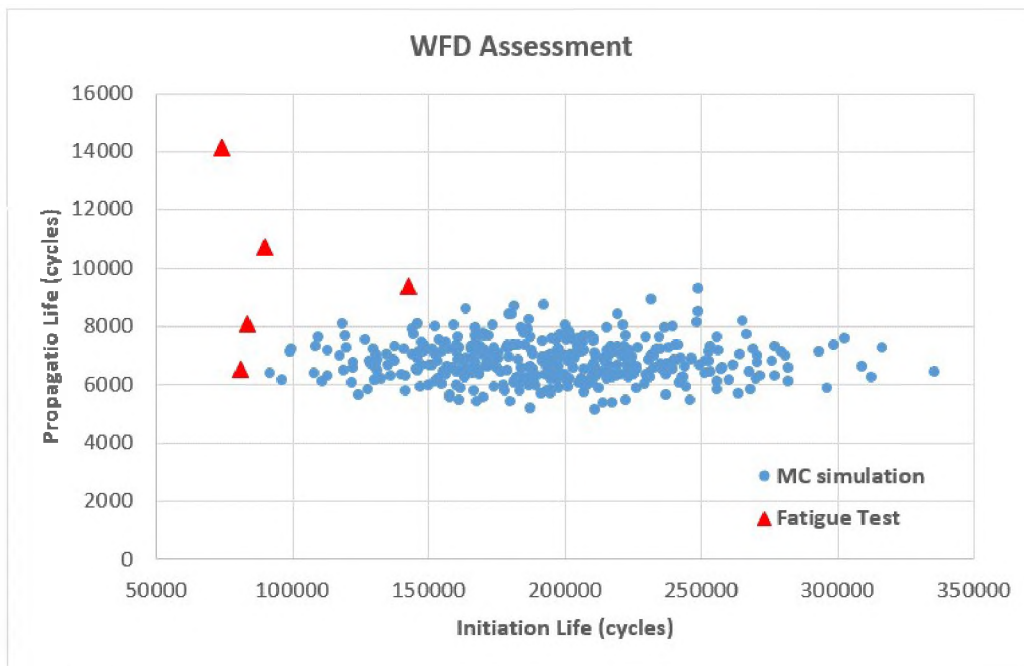


Figure 4-14 Distribution of Total Lives Compared with Fatigue Test Data.

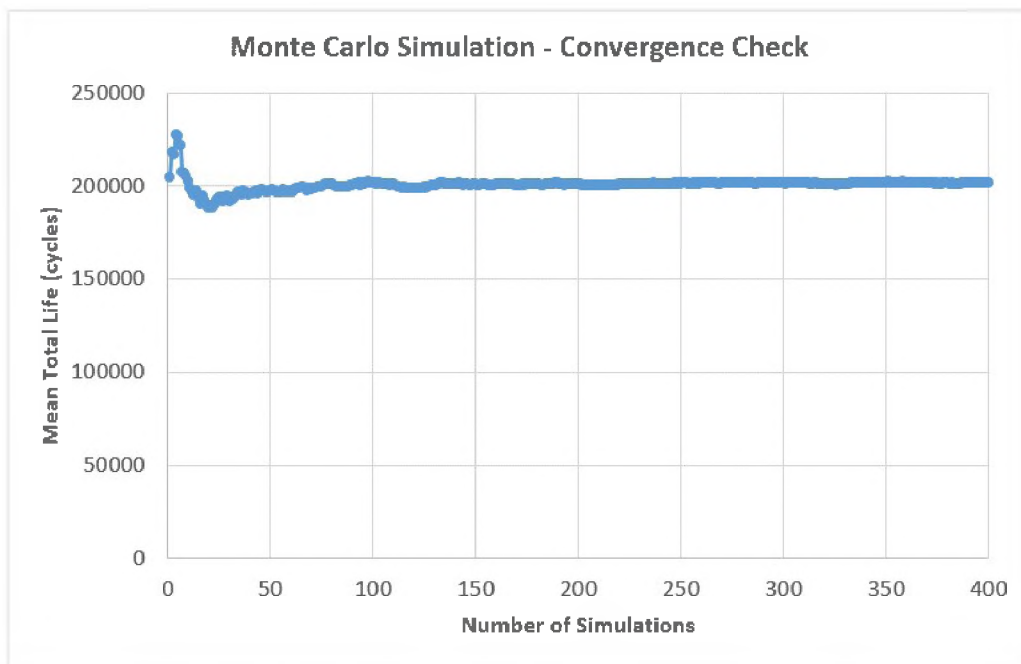


Figure 4-15 Fatigue Life (TTCI+TTCP) Convergence Check – 400 MCS.

Table 4-7 presented the MSD model input data based on Galatolo and Lazzeri [69], which employed 400 Monte Carlo simulations to represent a 300 mm width, 2.0 mm thick lap joint made of 2024-T3 Aluminum alloy, containing 11 fasteners of 4.80 mm diameter, subjected to 120 MPa remote stress. As shown in Figure 4-14, the MSD assessment methodology presented a good agreement compared to experimental data, especially regarding crack propagation life. As observed in the same figure, the fatigue initiation lives predicted via simulation presented a higher scatter when compared to experimental data.

This may be explained because only 5 specimens were tested. Another point to explain the difference was the S-N curve used for numerical simulation, which was assumed to be the same as [28], since Galatolo and Lazzeri [69] did not present the S-N data on their work. Crack propagation lives predicted by Monte Carlo simulation presented a good agreement when compared to experimental data. Predicted lives range from 5,132 cycles to 9,279 cycles; and experiments ranged from 6,528 to 14,150 cycles.

Crack growth life obtained via MCS in Scenario #14, was compared to specimen BJ6 [69], as shown in Figure 4-16. The abscissa represents the crack tip distance from the left edge of the panel. The ordinate shows the number of cycles to grown an initial crack flaw up to first link-up. The dots represented experimental data and solid lines were obtained using MSD model. Predicted crack growth via MSD model presented an excellent agreement compared to experimental data. Therefore, model accuracy and efficiency was demonstrated by comparing simulation results against experimental data performed by different researchers. Figure 4-15 shows that Monte Carlo simulation convergence was achieved at 150 simulations with total life average equal to 201,000 cycles.

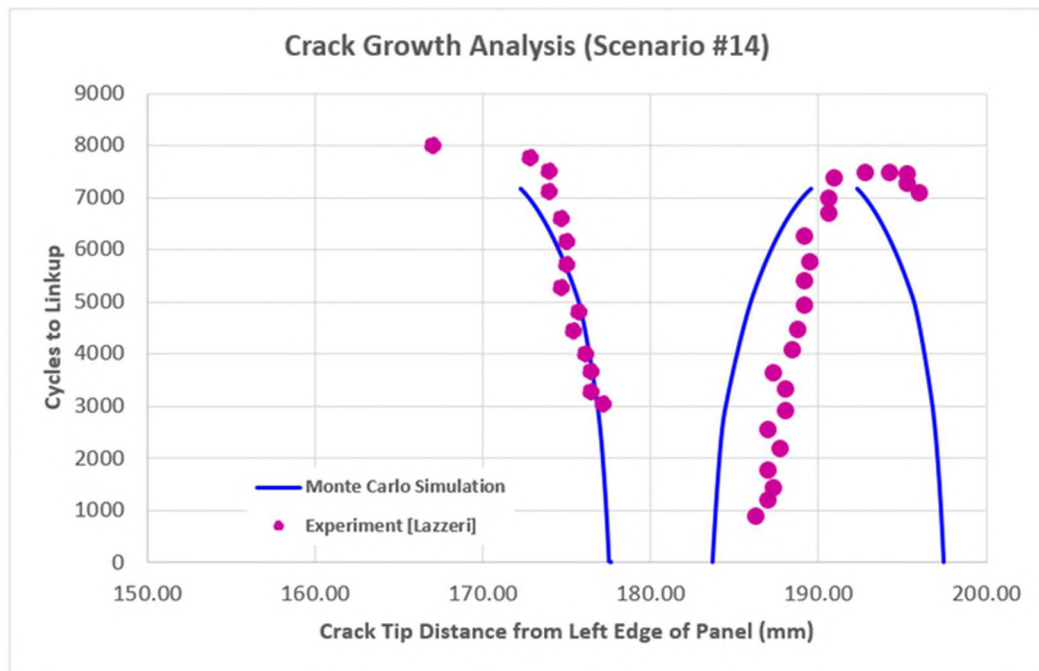


Figure 4-16 Crack Growth Analysis Compared to Experimental Data.

Finally, a typical commercial aircraft fuselage structure made of Al2024-T3 operating with a cabin differential pressure of 5.93×10^{-2} MPa (8.6 psi) equivalent to flying at 12,801 m (42,000 feet), skin thickness of 0.91mm (chemical milled pockets), and a fuselage diameter of 1880 mm was considered. This operational condition associated with geometrical configuration led to a remote tensile stress of 122 MPa as presented in Table 4-8. This section presented the results of 400, 600, and 800 Monte Carlo simulations in terms of WFD parameters.

This trade study was intended to verify the influence of different number of Monte Carlo simulations and its impact in total mean fatigue life (crack initiation and propagation) and the respective standard deviation, and therefore impact on final WFD assessment, by keeping all other input data. MSD model input data and results were:

Table 4-8 MSD Model Input Data 400 MCS 122 MPa.

N° Simulations	400
N° Random	9000
N° Fasteners	11
Stress	122 MPa

SN Curve		
S _{endurance}	58.00	MPa
FQI	176.00	MPa
p	-2.28	
A	2169.90	
B	1.299	
C	0.028	

Panel Geometry		
Width	300.00	mm
Thickness	0.914	mm
Fastener Pitch	25.00	mm
Edge Margin	25.00	mm
Fastener Diameter	4.76	mm

Initial Crack Sizes		
Lead Crack	1.270	mm
Opposite Crack	0.127	mm
MSD cracks	0.127	mm

Crack Growth		
Remote Stress	122	MPa
C	6.09E-11	
m	2.6	
Kc	1012	Mpa.mm ^{1/2}
σ _y	331	MPa

Fastener #	Load (N/mm)
1	1164.55
2	1164.55
3	906.29
4	906.29
5	821.28
6	821.28
7	798.82
8	798.82
9	798.82
10	798.82
11	794.01
12	794.01
13	798.82
14	798.82
15	798.82
16	798.82
17	821.28
18	821.28
19	906.29
20	906.29
21	1164.55
22	1164.55

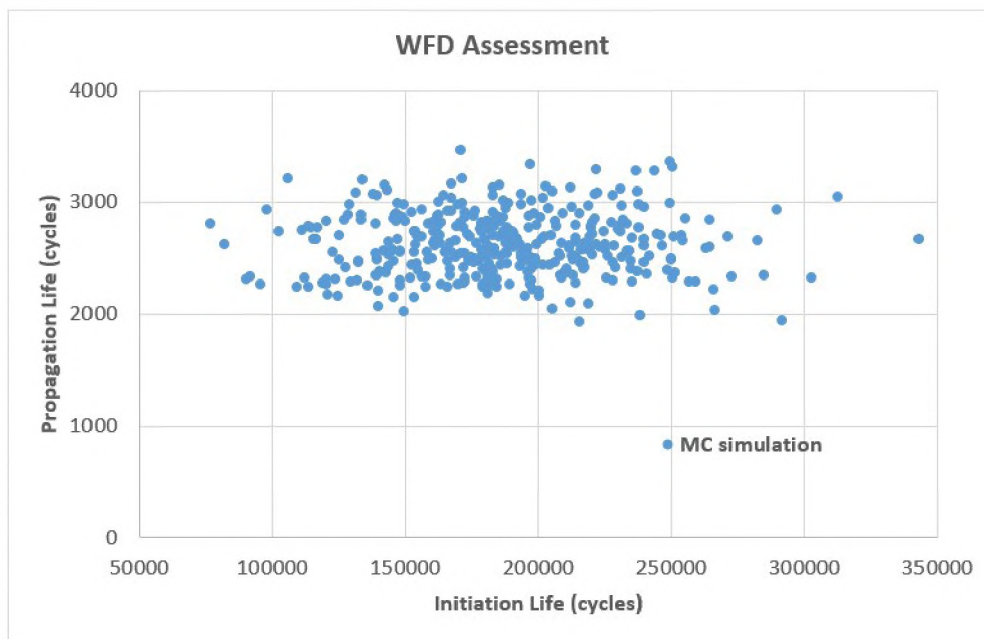


Figure 4-17 Distribution of Total Lives – 400 MCS.

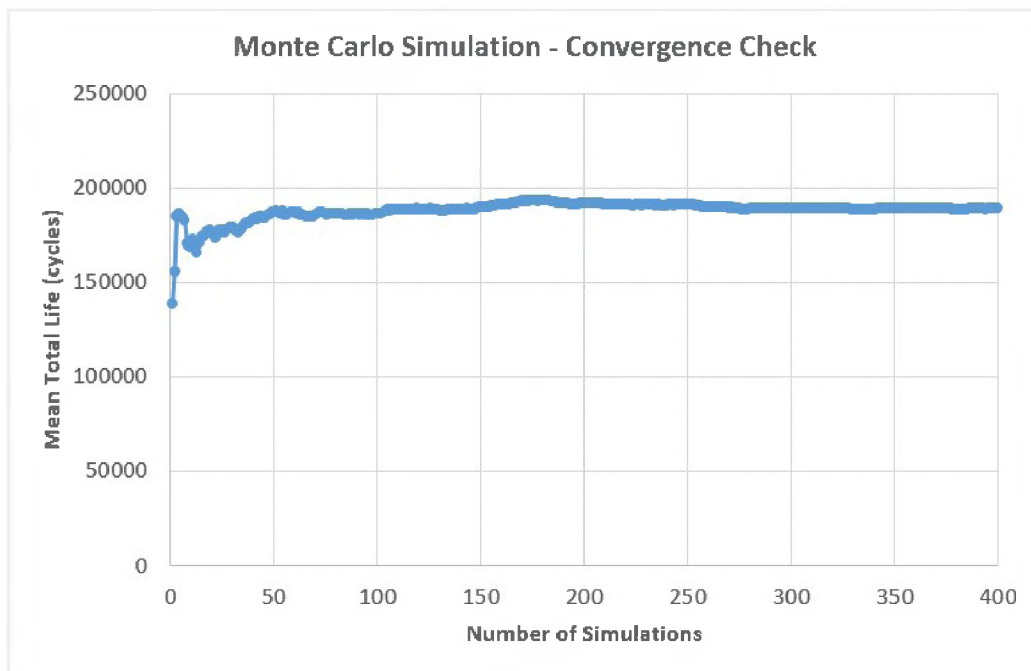


Figure 4-18 Fatigue Life (TTCI+TTCP) Convergence Check – 400 MCS.

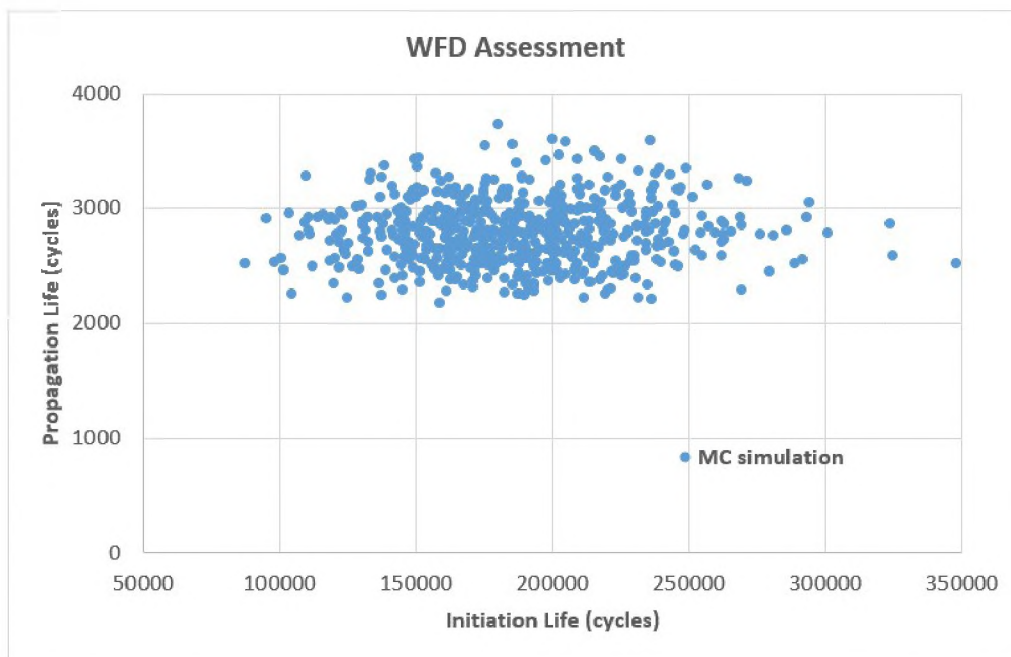


Figure 4-19 Distribution of Total Lives – 600 MCS.

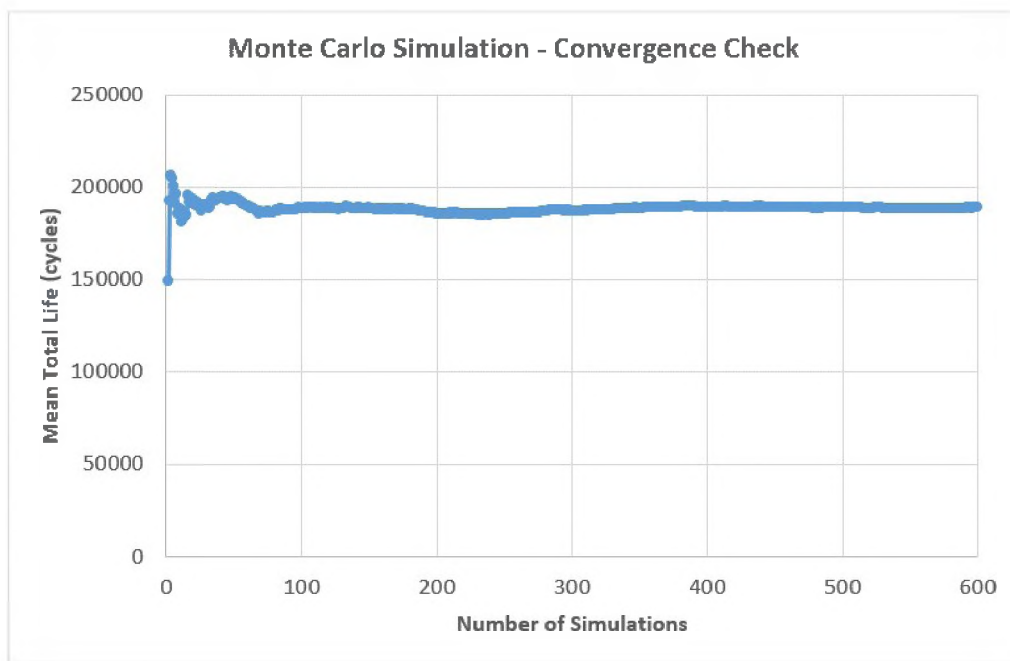


Figure 4-20 Fatigue Life (TTCI+TTCP) Convergence Check – 600 MCS.

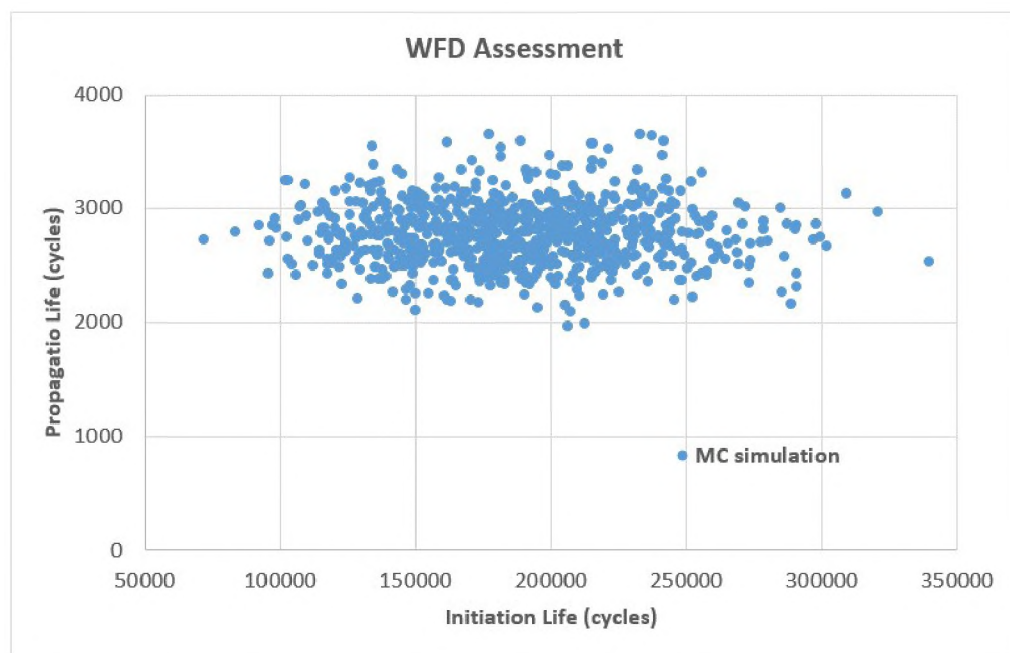


Figure 4-21 Distribution of Total Lives – 800 MCS.

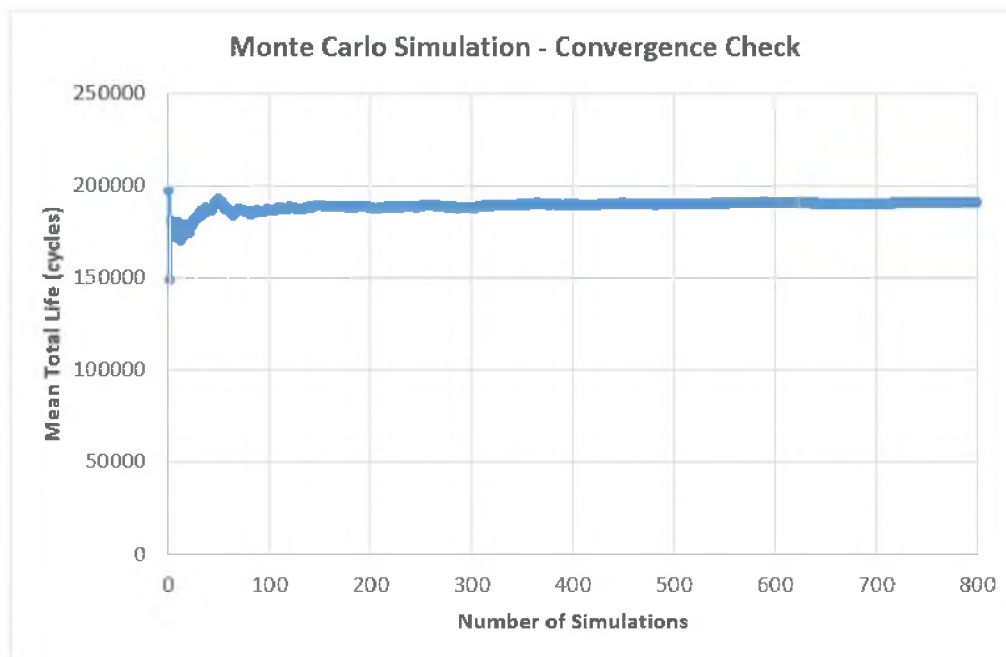


Figure 4-22 Fatigue Life (TTCI+TTCP) Convergence Check –800 MCS.

Table 4-8 presented the MSD input data for 400 MCS, analyzes were performed for 600 and 800 simulations keeping all other MSD model inputs. Distribution of total lives are presented in Figure 4-17, Figure 4-19, and Figure 4-21 for 400, 600 and 800 simulations respectively, while convergence checks were shown in Figure 4-18, Figure 4-20 and Figure 4-22. It was observed that by increasing the number of Monte Carlo simulations from 400 to 800, there were no significant changes to WFD parameters, as shown in Table 4-9. Convergence was achieved using simulations from 200 and on for all MSD assessments performed. The WFD parameters were calculated as follows: ISP by dividing $WFD_{(avg)}$ by 3, SMP by dividing $WFD_{(avg)}$ by 2, and the $I_{(WFD)}$ is the difference between SMP and ISP divided by safety factor. According to the AAWG recommendations [15], several opportunities must be given to detect fatigue crack before reaching WFD point. Advisory

Circular AC120-104 [3] presented safety factor of 4. Safety factor of 5 was assumed in this work to be conservative, due to the short period of first crack initiation and first link-up.

It was concluded that 400 simulations yielded appropriate numbers that provided reliable and consistent results when combined with computational efficiency.

Table 4-9 Influence of Number of MC Simulation on WFD Parameters.

N° of MC Simulations	WFD(avg) (Cycles)	ISP (Cycles)	SMP (Cycles)	I _(WFD) (Cycles)	Elapsed Time
400	189,104	63,035	94,552	6,303	12.66
600	189,328	63,109	94,664	6,311	20.19
800	190,127	63,376	95,063	6,338	28.56

This section presented the results of the probabilistic multiple site damage methodology to assess structural integrity of riveted panels by employing Monte Carlo simulation technique. Results obtained via Monte Carlo simulations were compared with published test data. Fatigue crack initiation lives and crack propagation lives demonstrated good agreement with experimental data. Monte Carlo simulation convergence check was performed considering 400, 600 and 800 simulations. The results showed that convergence was achieved around 200 simulations. The proposed methodology presented to be a useful and efficient source of predicting MSD behavior in aeronautical riveted joints.

5. CONCLUSIONS AND FUTURE WORK

5.1. CONCLUSIONS

A methodology and computational code to assess multiple-site fatigue cracking in riveted panels was developed and presented. Probabilistic fatigue crack initiation was performed by employing the Monte Carlo simulation technique and by assuming lognormal distribution of fatigue lives. Numerical results obtained from Monte Carlo simulations were compared with experimental data from previously published research. The results were consistent and presented to be accurate from the practical standpoint.

The probabilistic crack growth was performed assuming different damage scenarios via fatigue initiation life simulation. Stress Intensity Factors for multiple cracks were computed using compounding method with combinations of known solutions that were previously published. Crack propagation first link-up lives were compared with experimental data published. Predicted numerical results agreed well with the experimental data. Therefore, crack growth model was validated. The compounding method used to compute the stress intensity factor was an acceptable method based on model accuracy and efficiency.

Finally, fatigue crack initiation and fatigue crack propagation lives were added to determine the total life for each simulated scenario. The results of Monte Carlo simulations were compared with published test data, and the results were found to be in good agreement with MSD observed in real structures.

Statistical treatment was performed to find WFD average behavior, which means the point in time when 50% of the entire population was expected to develop WFD due to

multiple fatigue cracking. Maintenance actions required to preclude WFD were determined by calculating the Inspection Start Point (ISP) and the Structural Modification Point (SMP). The results were consistent with real aircraft inspection intervals published by different manufacturers. The influence of 400, 600, and 800 Monte Carlo simulations and the impact on WFD parameters were checked. It was concluded that 400 simulations were appropriate number to obtain accurate results while keeping computational efficiency.

The proposed methodology and program were demonstrated to be powerful sources to predict MSD behavior and to calculate statistical points to precluding its occurrence. The employed SIF solutions and the compounding method were relatively simple to numerically implement, when compared to more complex methods, thereby providing an efficient method to predict fatigue crack initiation life and fatigue crack propagation life for 400, 600 and 800 simulations when compared to the Finite Element Method or the Dual Boundary Element, as employed by previous authors in the study of MSD.

Based on the accuracy of the obtained results and the low computational time to perform the Monte Carlo simulations, the proposed methodology was deemed useful to predict the MSD behavior of real aircraft structures, especially riveted joints widely employed in the aircraft industry.

5.2. RECOMMENDATIONS FOR FUTURE WORK

Future students and researchers can use this material and expand upon it. Suggested research includes validating the proposed methodology by performing fatigue and crack propagation tests using riveted joint coupons, and, if possible, using component testing. It

is important to correctly account for the effect of average life and its respective standard deviation regarding fatigue crack initiation and crack propagation lives.

As previously discussed, pressurized fuselage structures are most prone to develop MSD; however, this type of damage was identified in different structures, such as wing lower skin panels and empennage. These last two examples operate under variable amplitude loading, therefore $R \neq 0$. From this researcher's best knowledge, no previous MSD methodologies accounting for variable amplitude loading have been proposed. Therefore, the current work could be expended to incorporate more complex stress history typical in aircraft service life.

The improvement of existing SIF solutions is another research topic that could be explored by future researchers; they could include variables such as fastener expansion and contact (typically found during cold work process), geometrical effects (countersink), parameters associated with fastener installation process (squeeze force), as well as considering the influence of arresting features (stringers, frames and tear straps).

The inclusion of Multiple Element Damage assessment via probabilistic analysis and its potential interaction with MSD scenario has not been discussed in previously published works, and it is recommended for future research.

The current work demonstrated a valuable tool to predict WFD behavior, and it can be used in future research to build design practices to preclude WFD in future structural designs. It can also be used to perform parametric studies considering geometric factors, such as fastener diameter, fastener spacing, and fasteners numbers. Load transferring and how it can provide better Inspection Start Point and Structural Modification Point values are valid focal points in future work.

Finally, the implementation of the Equivalent Initial Flaw Size (EIFS) by applying statistical distribution, instead of using pre-defined initial crack sizes, while performing the crack growth stage is suggested. This combination of Probability of Detection (POD) and probabilistic loading spectra could turn the proposed methodology into a powerful risk assessment tool, which seems to be the future of aircraft structural analysis.

BIBLIOGRAPHY

1. Aircraft Accident Report: Aloha Airlines, Flight 243, Boeing 737-200, N73711, near Maui, Hawaii, April 28, 1988. U.S. National Transportation Safety Board, Washington, 1989.
2. R.J.H. Wanhill, L. Molent, S.A. Barter and E. Amsterdam, Milestone case histories in aircraft structural integrity, National Aerospace Laboratory NLR Report NLR-TP-2015-193, Amsterdam, Netherland, 2015.
3. Advisory Circular AC120-104, Establishing and implementing limit of validity to prevent widespread fatigue damage, U.S. Department of Transportation, Federal Aviation Administration, 2011.
4. T. Swift, Widespread fatigue damage monitoring issues and concerns, Proceeding of the 5th International Conference on Structural Airworthiness of New and Aging Aircraft, Hamburg, Germany, June 1993.
5. Aircraft Accident Report: Southwest Airlines, Flight 812, Boeing 737-3H4, N632SW, Yuma, Arizona, April 1, 2011. U.S. National Transportation Safety Board, Washington, 2013.
6. Garcia, A. N., Multiple Site Damage of Aeronautical Riveted Joints, Ph.D. Thesis, Cranfield University, Cranfield, U.K., September 2005.
7. Swift, T., Damage tolerance in pressurized fuselages. 11th Plantema Memorial Lecture. Presented at the 14th Symposium of the International Committee on Aeronautical Fatigue, Ottawa, Canada, June 1987.
8. Schijve, J., Multiple-site damage in aircraft fuselage structures, Fatigue and Fracture of Engineering Materials & Structures. Vol.18, No. 3, pp.329-344, 1995.
9. Garcia, A. N., Irving, P. E., Lap joint MSD assessment using a probabilistic model, 11th International Conference on Fracture (ICF 11), Turin, Italy, March 20-25, 2005.
10. Santgerma, A., Developpement d'une methodologie de prevision du comportement des strutures d'avions civils en presence de dommages multiples de fatigue, Doctorate Thesis, Department of Mechanical Engineering, Toulouse, 1997.
11. Liao, M., Shi, G., Xiong, Y., Analytical methodology for predicting fatigue life distribution of fuselage splices, International Journal of Fatigue 23, SI 77- S185, 2001.

12. Newman, J.C., Fracture Analysis of Stiffened Panels Under Biaxial Loading with Widespread Cracking, NASA Technical Memorandum, NASA-TM-110197, Hampton, USA, October 1995.
13. Newman, J.C., Harris, Jr.C.E., Piascik, R.S., Dawicke, D.S. Methodology for predicting the onset of widespread fatigue damage in lap-splice joints, Technical Report NASA /TM -1998-208975, NASA Langley Research Center, Hampton, Virginia, 1998.
14. Proppe, C., Probabilistic analysis of multi-site damage in aircraft fuselages. Computational Mechanics, Vol. 30, pp. 323-329, 2003.
15. AAWG, Recommendations for regulatory action to prevent widespread fatigue damage in commercial airplane fleet, a Report of the Airworthiness Assurance Working Group (AAWG) for the Aviation Rulemaking Advisory Committee Transport Aircraft and Engine Issues, March 11, 1999.
16. DOT/FAA, Development of Multiple-Site Damage in Fuselage Structure, Technical Report AR-05/38, September 2005.
17. US Code of Federal Regulation, Title 14 – Aeronautics and Space, PART 25 – Airworthiness Standards: Transport Category Airplanes, Subpart C – Structure, 25.571 Damage tolerance and fatigue evaluation of structure, Federal Aviation Administration.
18. Mosinyi, B.R, Fatigue damage assessment of high-usage in-service aircraft fuselage structure, Ph.D. Thesis, Drexel University, 2007.
19. Niu, M. C. Y., Airframe structural design: practical design information and data on aircraft structures, Hong Kong: Conmilit Press, 1999.
20. USAF, Airplane Damage Tolerance Requirements, Military Specification, MIL-A-83444, 1974.
21. Aircraft Accident Report No. 9/78 (EW/A267), Dan Air B707 near Lusaka, May 14, 1977. Accidents Investigation Branch, London, 1979.
22. Swift. T., Verification of methods for damage tolerance evaluation of aircraft structures to FAA requirements. Presented at the 12th Symposium of the International Committee on Aeronautical Fatigue, Toulouse, France, May 1983.
23. US Code of Federal Regulation, Title 14 – Aeronautics and Space, PART 26 – Continued Airworthiness and Safety Improvements for Transport Category Airplanes, Subpart C – Aging Airplane Safety – Widespread Fatigue Damage, 26.21 Limit of validity, Federal Aviation Administration.

24. Schijve, J., Stress Intensity Factors of Hole Edge Cracks. Comparison Between One Crack and Two Symmetric Cracks, Delft University of Technology, Department of Aerospace Engineering, Memorandum M-458, Netherlands, March 1983.
25. Swift, T., Repairs to Damage Tolerant Aircraft - International Symposium on Structural Integrity of Aging Airplanes - Atlanta, Georgia, 1990.
26. Wang, H. L., Evaluation of Multiple Site Damage in Lap Joint Specimens, PhD Thesis, Perdue University, USA, October 1998.
27. Grandt, A.F., Wang, H. L., Analysis of widespread fatigue damage in lap joints, SAE Technical Paper Series, 1999-01-1585, General, Corporate and Regional Aviation Meeting and Exposition (GCRAM), Wichita, USA, April 20-22, 1999.
28. Kebir, H., Roelandt, J. M., Gaudin, J., Monte Carlo simulations of life expectancy using the dual boundary element method, Engineering Fracture Mechanics 68, pp. 1371-1384, 2001.
29. Garcia, A.N., Mello Jr., A.W.S., On the MSD assessment of real aircraft fuselage panels, Aircraft Structural Integrity Program (ASIP), San Antonio, USA, November 28-30, 2006.
30. Lincoln, J.W., Overview of widespread fatigue damage risk assessment methodology, AGARD Conference Proceeding 568, Widespread Fatigue Damage in Military Aircraft, Netherlands, May 10-11, 1995.
31. Tan, P. W., Bigelow, C. A., Bakuckas Jr., J. G., Widespread fatigue damage assessment approach, Applied Vehicle Technology Panel, Life Management Techniques for Aging Air Vehicles, Manchester, U.K., October 2001.
32. Lazzeri, R., The PISA code, Aerotecnica Missili e Spazio, Vol. 8 1 - 1, Italy, 2002.
33. Basso, V. B. Q., Garcia, A.N., Establishing structural repair life by means of Monte Carlo simulation, 3rd CTA-DLR Workshop on Data Analysis & Flight Control, S. J. Campos, Brazil, September 14-16, 2009.
34. Tong, Y. C., Literature review on aircraft structural risk and reliability analysis, DSTO Aeronautical and Maritime Research Laboratory, DSTO-TR-1110, Melbourne, Australia, February 2001.
35. Renaud, R., Liao, M., Calculation of equivalent initial flaw size distributions for multiple-site damage, 55th AIAA/ASME/ASCE/ASC Structures, Structural Dynamics, and Material Conference, Maryland, USA, January 13-17, 2014.

36. Akpan, U.O., Rushton, P.A., Koko, T.S., Development of a fuzzy probabilistic methodology for multiple-site fatigue damage, *Journal of Aircraft*, Vol. 41, No.3 pp.628-635, May-June 2004.
37. Gallagher, J.P., Giessler, F.J., Berens, A.P., USAF Damage Tolerant Design Handbook: Guidelines for Analysis and Design of Damage Tolerant Aircraft Structures, Technical Report AFWAL-TR-82-3073, Ohio, May 1984.
38. Horst, P., Schmidt, H., A concept for evaluation of MSD based on probabilistic assumptions, AGARD Conference Proceedings 568, Neuilly-Sur-Seine, France, 1995.
39. Dai, J., Creager, M., Odian, K., Safarian, P., Significance of Local Multiple Crack Growth Consideration on Aging Aircraft Structural Damage Technology.
40. Sanches, R.F., de Jesus, A.M.P., Correia, J. A.F.O., Silva, A.L.L, Fernandes, A.A., A probabilistic fatigue approach for riveted joints using Monte Carlo simulation, *Journal of Construction Steel Research*, Vol. 110, pp. 149-162, July 2015.
41. Park, J.H., Singh, R., Pyo, C.R., Atluri, S.N., Integrity of aircraft structural elements with multiple-site fatigue damage, *Engineering Fracture Mechanics*, Vol. 51, Issue 3, pp. 361-380, June 1995.
42. Swift, T., The effects of stress level, geometry, and material on fatigue damage tolerance of pressurized fuselage structure. Proc. 14th ICAF Symp., Ottawa, EMAS, pp. 1-77.
43. Ma,L., Lam, P.W.,Kokaly, M.T., Kobayashi, A.S., CTOA of a stable crack in a thin aluminum fracture specimen. *Engineering Fracture Mechanics*, p.427-442, 2003 Research Laboratory, DSTO-TR-1110, Melbourne, Australia, February 2001.
44. Ciliato, G.D. Análise da Resistência Residual e da Tensão de Ligamento em Chapas de Alumínio com Múltiplas Trincas, Tese de Mestrado – Instituto Tecnológico de Aeronáutica – ITA, São José dos Campos, Brasil, 2004.
45. Dowling, N., *Mechanical Behavior of Materials, Engineering Methods for Deformation, Fracture, and Fatigue*, 3rd ed., ISBN 0131863126, Prentice Hall PTR, 2006.
46. Schutz, W., A History of fatigue, *Engineering Fracture Mechanics*, Vol. 54, No. 2, pp. 263-300, 1996.
47. Basquin, O.H., The exponential law of endurance tests. Proc. Annual Meeting, American Society for Testing Materials, Vol. 10, pp. 625-630, 1910.

48. Stephens, R.I., Fatemi, A., Stephens, R. R., Fuchs, H.O., Metal Fatigue in Engineering, 2nd ed., Wiley Inter-Science, 2001.
49. Bruhn, E. F., Analysis and Design of Flight Vehicle Structures - 1973 Edition.
50. Griffith, A. A., The phenomena of rupture and flow in solids, Phil. Trans. Roy. Soc., Series A, Vol. 221, pp. 163-198, 1921.
51. Anderson, T.L., Fracture Mechanics Fundamentals and Applications, 3rd ed., Taylor & Francis Group, 2005.
52. Perez, N. Fracture Mechanics, ISBN 1-4020-7745-9, Kluwer Academic Publishers, 2004.
53. Paris, P. C., The fracture mechanics approach to fatigue, Fatigue – an interdisciplinary approach, edited by J. J. Burke, N. L. Reed and V. Weiss, pp. 107-132, Syracuse University Press, 1964.
54. <http://www.pages.drexel.edu/~tantm/faa/aging.htm>
55. Press, W. H., Teukolsky, S. A., Vetterling, W. T., Numerical recipes in FORTRAN: the art of scientific computing, Cambridge University Press, 2nd ed., 1992.
56. Military Specification Airplane Damage Tolerance Requirements, 1974, MIL-A-83444, United States Air Force, The Pentagon, Virginia.
57. Cartwright, D.J., Rooke, D.P., Approximate stress intensity factors compounded from known solutions, Engineering Fracture Mechanics, Vol. 6 pp. 563-571, 1974.
58. ESDU 78036, The compounding method of estimating stress intensity factors for cracks in complex configurations using solutions from simple configurations, ISBN 0-85679-240-3, November 1978, amendment A, December 1980.
59. Newman Jr, J.C., Prediction Failure of Specimens with Either Surface Cracks or Corner Cracks at Holes, NASA Technical Note TN D-8244, NASA Langley Research Center, Hampton, June 1976.
60. Rooke, D.P., Coveney, D.P., Stress Intensity Factors for a Cracked Hole in a Row of Holes, Royal Aircraft Establishment, Technical Report 77073, May 1977.
61. Rooke, D.J., Tweed, J., Opening Mode Stress Intensity Factors for Two Unequal Cracks at a Hole, Royal Aircraft Establishment, Technical Report 79105, August 1979.
62. Schijve, J. Fatigue of Structures and Materials, 2nd ed., ISBN 978-4020-6807-2, Springer 2009.

63. NASGRO® 9.2 – Southwest Research Institute
64. NASGRO Manual
65. Rooke, D.P., Cartwright, D.J., Compendium of Stress Intensity Factors, ISBN 0 11 771336 8, 1976.
66. Liao, M., Yang, Q-X., A probabilistic model for fatigue crack growth, Engineering Fracture Mechanics, Vol. 43, No. 4, pp. 651-655, 1992.
67. Buden, R.J., Faires, J.D., Numerical Analysis, 9th ed., ISBN 978-0-538-7351-9, Brooks/Cole, 2011.
68. US Code of Federal Regulation, Title 14 – Aeronautics and Space, PART 121 – Operating Requirements: Domestic, Flag, and Supplemental Operations, Subpart AA – Continued Airworthiness and Safety Improvements, 121.1115 Limit of Validity, Federal Aviation Administration.
69. Galatolo, R., Lazzeri, R., Experiments and model predictions for fatigue crack propagation in riveted lap-joints with multiple site damage, Fatigue & Fracture of Engineering Materials & Structures, Vol. 39, Issue 3, pp. 307-319, March 2016.

VITA

Haroldo Chacon obtained his Bachelor degree in Mechanical Engineering from FEI, Brazil, 2004. In December 2021, he received his Master of Science in Aerospace Engineering from Missouri University of Science and Technology. He worked in the aviation industry as a structural analysis engineer for the past 15 years, where he performed and led fatigue and damage tolerance analysis (F&DTA) of primary aircraft structures, including Boeing models 737-700/800; 737-MAX, 747-400/8; 767; 777 and KC-46 Tanker. In 2020, he received delegation privilege to act as an Engineering Unit Member (EUM) for The Boeing Company in Seattle, to perform aircraft certification and finding of compliance activities. Before joining Boeing he worked for Embraer in Brazil for 7 years as structural analysis engineer and damage tolerance subject matter expert, providing consultation to different programs including commercial aviation, business jets and defense. He taught fatigue and damage tolerance classes at Embraer for 6 years, and Fatigue and Fracture Mechanics II – AE237 at Instituto Tecnológico de Aeronáutica (ITA), as guest speaker. Haroldo's professional interests were: fracture mechanics, damage tolerance, aviation safety, structural integrity of aircraft structures and continued airworthiness.